Institut de physique
Université de Fribourg (Suisse)

Gamma-ray spectroscopy using the (n,γ) and (α,2nγ) reactions

THESE

présentée à la Faculté des Sciences de l'Université
de Fribourg (Suisse) pour l'obtention du grade de
Doctor rerum naturalium

Laurent Genilloud
de Villarepos (FR)

Thèse No 1314

Edition privée
Septembre 2000

Acceptée par la Faculté des Sciences Naturelles de l'Université de Fribourg (Suisse) sur la proposition de:

Prof. Dr. Hubert Schneuwly, Université de Fribourg, Président du Jury,
Prof. Dr. Jan Jolie, Université de Fribourg, Directeur de Thèse,
Prof. Dr. Jean-Claude Dousse, Université de Fribourg, Rapporteur,
Prof. Dr. Till von Egidy, Technische Universität München, Rapporteur .

Fribourg, le 1er septembre 2000.

Le Directeur de thèse : Le Doyen :

Prof. Dr. Jan Jolie Prof. Dr. Alexander von Zelewsky

à Jean Kern

Contents

Résumé en Français

Un des buts de la spectroscopie gamma est d'étudier la structure des noyaux atomiques. Pour ce faire, les noyaux doivent être amenés à des états excités à l'aide d'une réaction nucléaire. L'étude de la désintégration électromagnétique subséquente de ces états par la mesure des rayons γ qui la compose permet ensuite de reconstruire le schéma des niveaux excités de noyaux atomiques. La comparaison de ce schéma avec un modèle théorique permet une meilleure compréhension du système quantique qu'est le noyau atomique. Un test sensible des fonctions d'ondes prédites par les modèles peut être réalisé en mesurant les probabilités de transition entre les états excités. Ceci explique l'importance de connaître les temps de vie en physique nucléaire. Les différentes techniques utilisées dans ce travail pour parvenir à de tels résultats sont présentées dans le première partie de cette thèse.

Les noyaux atomiques, composés d'un nombre fini de nucléons, montrent des mouvements collectifs. Le noyau ^{100}Ru présente une structure vibrationnelle claire et peut être décrit par la symétrie dynamique U(5) du modèle IBA. Nous avons montré que pour cet isotope, cette limite s'est avérée reproduire de manière très satisfaisante presque tous les niveaux jusqu'aux états 4-phonons. Cependant, la comparaison avec la théorie des énergies d'excitation et des taux de transitions réduits est améliorée par l'ajout d'une perturbation SU(3) à la symétrie dominante U(5). De plus, les quelques états non-décrits par cette extension du modèle IBA ont été identifiés sur la base de leur mode de désintégration. Un ensemble complet de temps de vie d'états excités en dessous de 2.2 MeV dans un noyau déformé peut former une base de donnée unique pour l'étude de la structure nucléaire. Un bon candidat est le ^{168}Er, l'un des noyaux déformés le mieux connu. En continuation de travaux précédents, les temps de vie des états excités appartenant à quelques bandes-K de parité négative ont été mesurés par la méthode GRID. La comparaison avec le modèle IBA permet de sélectionner les bandes ayant un caractère vibrationnel octupolaire. Les résultats concernant le ^{100}Ru et ^{168}Er sont présentés dans la deuxième partie de cette thèse.

L'analyse par PGA (Prompt Gamma-ray Activation) est une excellente technique pour déterminer la présence et quantité d'éléments contenus dans un échantillon en l'irradiant continûment par des neutrons thermiques ou froids. Cependant, la complexité des spectres mesurés par des détecteurs germanium de haute pureté requiert l'utilisation d'un logiciel adéquat pour l'identification des éléments de l'échantillon. La troisième partie de cette thèse présente les bases théoriques de la technique PGA et décrit le programme d'analyse *PEGASE*.

Abstract in English

One of the goals of gamma-ray spectroscopy is to study the structure of the atomic nuclei. To this aim, the nucleus has to be brought into excited states by a nuclear reaction. The study of the subsequent electromagnetic decay via the measurement of γ rays then allows one to establish the level scheme of the atomic nucleus. The comparison of this scheme with a theoretical model allows a better understanding of the quantal system formed by the atomic nucleus. A sensitive test of the wave functions predicted by the model can be realized by measuring the transitions probabilities inbetween excited states. This emphasizes the necessity of measuring lifetimes in nuclear physics. The different techniques used in this work are described in the first part of this thesis.

The atomic nuclei, consisting of a finite number of nucleons, show collective motion. The nucleus ^{100}Ru presents a clear vibrational structure and can be described by the U(5) dynamical symmetry of the IBA model. We showed that for this isotope, this limit proved to yield a very good description of nearly all levels up to the 4-phonons states. However, the comparison with theory of excitation energies and reduced transition rates could be improved by an admixture of SU(3) breaking terms to the dominant U(5) symmetry. Moreover, the few states not described by this extension of this IBA model have been identified on the basis of their absolute decay strengths. A complete set of lifetimes of nuclear excited states below 2.2 MeV in a well deformed nucleus could form a unique database for the study of nuclear structure. A good candidate for such a nucleus is ^{168}Er, one of the best known deformed nuclei. In a continuation of prior works, the lifetimes of excited states pertaining to several low-K negative parity bands have been measured using the GRID method. The comparison with the IBA model allows to select the bands having a octupole vibrational character. The result on ^{100}Ru and ^{168}Er are presented in the second part of this thesis.

The analysis using Prompt Gamma-ray Activation (PGA) is an excellent tool to determine the presence and quantity of elements in a sample irradiate continuously with cold or thermal neutrons. However, the complexity of the spectra measured with high-purity germanium detectors requires the use of adequate software for the identification of elements contained in the sample. The third part of this thesis deals with the presentation of the theoretical basis of the PGA technique and the developed analysis program *PEGASE*.

Part One

Basic concepts

1 Introduction

"The atomic nucleus is one of the most interesting quantum systems found in nature" [1], it is formed by a finite number of nucleons (1 to 250) that interact primarily through the strong nuclear and electromagnetic forces. The exact theoretical description of an atomic nucleus is not a possible task, this for principally two reasons:

- The number of constituents is big while being finite,
- the strong nuclear interaction is relatively well known but is too complex to be implemented in an exact theory of the nucleus.

However, it is possible to describe an atomic nucleus by a relatively small number of parameters. The work of the experimenter is to measure these properties whereas the theoretician is responsible to build up theoretical models that can describe them. As this represents a broad field of investigation, different research tools have been elaborated. Amongst them is γ-ray spectroscopy which aims to study the structure of nuclear excited states. These states can be classified by a few basic quantum numbers, in particular the energy E, spin and parity J^{π}. In this introduction I will present in a concise way part of the different instruments used to measure and determine these quantities. My point is not to describe their functioning but to simply expose a few of their characteristics. The second part of this thesis consists of a selection of the articles written during my Ph.D. work. In the third part, I included the internal report describing the PEGASE program used to determine elemental quantities through the measurements of γ-ray yields following a cold neutron capture.

2 Construction of level schemes

To study nuclear structure, the nucleus has to be brought into excited states by a nuclear reaction; one deduces information by measuring the electromagnetic decay of these states via γ rays emission following the reaction. The level scheme is constructed by the placement of the observed γ rays; the two techniques we used for this task in our study of ^{100}Ru are presented in the following paragraphs.

Figure 1: estimated spin-ranges and γ decays following different nuclear reactions.

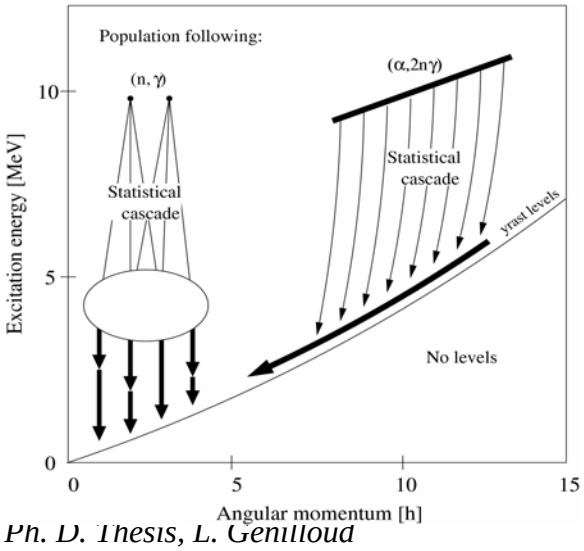

The use of two different nuclear reactions to construct the level scheme of ^{100}Ru is motivated by the fact that the γ rays following these reactions do not populate exactly the same levels. Figure 1 illustrates schematically the γ decay flow following ^{99}Ru(n,γ) and ^{98}Mo(α,2nγ) reactions. One notices, that a broad region of levels are populated through these two mechanisms. The entry states correspond to levels populated after the evaporation of particles. The entry states decay mainly by transition of E1 nature, the most favoured for statistical decay; as the possible different ways is enormous, this

radiation is quasi continuous and populates lower lying levels in a statistical way. It is only after several steps that the transitions connect clearly different excited states.

2.1 γγ-coincidences

A nucleus in a excited state below the particle emission threshold will de-excites to the ground-state via intermediate levels by emitting a cascade of γ rays. As long as the lifetimes of the intermediate levels are short in comparison with the acquisition time of the whole system, the γ rays in a cascade appear to be emitted simultaneously. The systematic analysis of the coincident relations allows to reconstruct the γ-ray cascade and thus to determine the level scheme.

An apparatus system, developed in Fribourg [2] consisting of five high-purity germanium (HPGe) detectors equipped with BGO-NaI(Tl) Compton shields, was used for the acquisition of the coincidence measurement. The germanium semi-conductors are the most appropriate detectors for such an acquisition. As a matter of fact they present the best efficiency/energy resolution compromise. High detection efficiency is required because events are recorded only when two or more γ rays arrive in different detector within a narrow time window. The data is recorded in list-mode and the coincident matrix can be built off-line by introducing more constraints on the time windows.

2.2 Ritz combinations

Most of the excited levels de-excite by more than one transition. It is then possible to establish the level scheme by using energy sums (known as Ritz combinations). A γ spectrum from an in-beam measurement contains a few hundreds of peaks; the typical γ energy precision given by an HPGe detector is of the order of 0.1 ‰. If one applies Ritz combinations to such data, this will give a much bigger amount of spurious levels than genuine ones. The solution is to use a detector with a better precision on the photon energy. Curved crystal spectrometers have an excellent resolution and consequently allow a very precise determination of the energy of photons. Rather than measuring the energy deposition of the photon in a medium (as with semi-detectors), the crystal spectrometers diffract the γ rays at precisely measured diffraction angles. This process is described by the Bragg law:

$$E_\gamma = \frac{nhc}{2d\sin(\theta)} \qquad (1)$$

where n is the refraction order, h Planck's constant, c the speed of light, d the lattice constant and θ Bragg's angle. By measuring accurately the Bragg's angle, as it is done with the GAMS23 spectrometer [3], the precision in the determination of the γ-ray energies is enhanced by a factor 10. This high resolution is paid at the price of a strongly reduced efficiency detection. As a consequence, the activation of the target must be done with a strong particle source. The high flux reactor of the Institut Laue-Langevin (ILL) in Grenoble, where the GAMS23 curved crystal spectrometer [3] is installed, produces a neutron flux of $5 \cdot 10^{14}$ ncm^2s^{-1} at the target position. The Figure 2 shows a portion of the spectrum from the $^{99}Ru(n,\gamma)^{100}Ru$ reaction measured with an HPGe detector and GAMS23 crystal spectrometer. One notices the difference of resolution of these two instruments.

Figure 2: Part of the spectrum from the $^{99}Ru(n,\gamma)^{100}Ru$ reaction measured with an HPGe detector and the GAMS23 crystal spectrometer

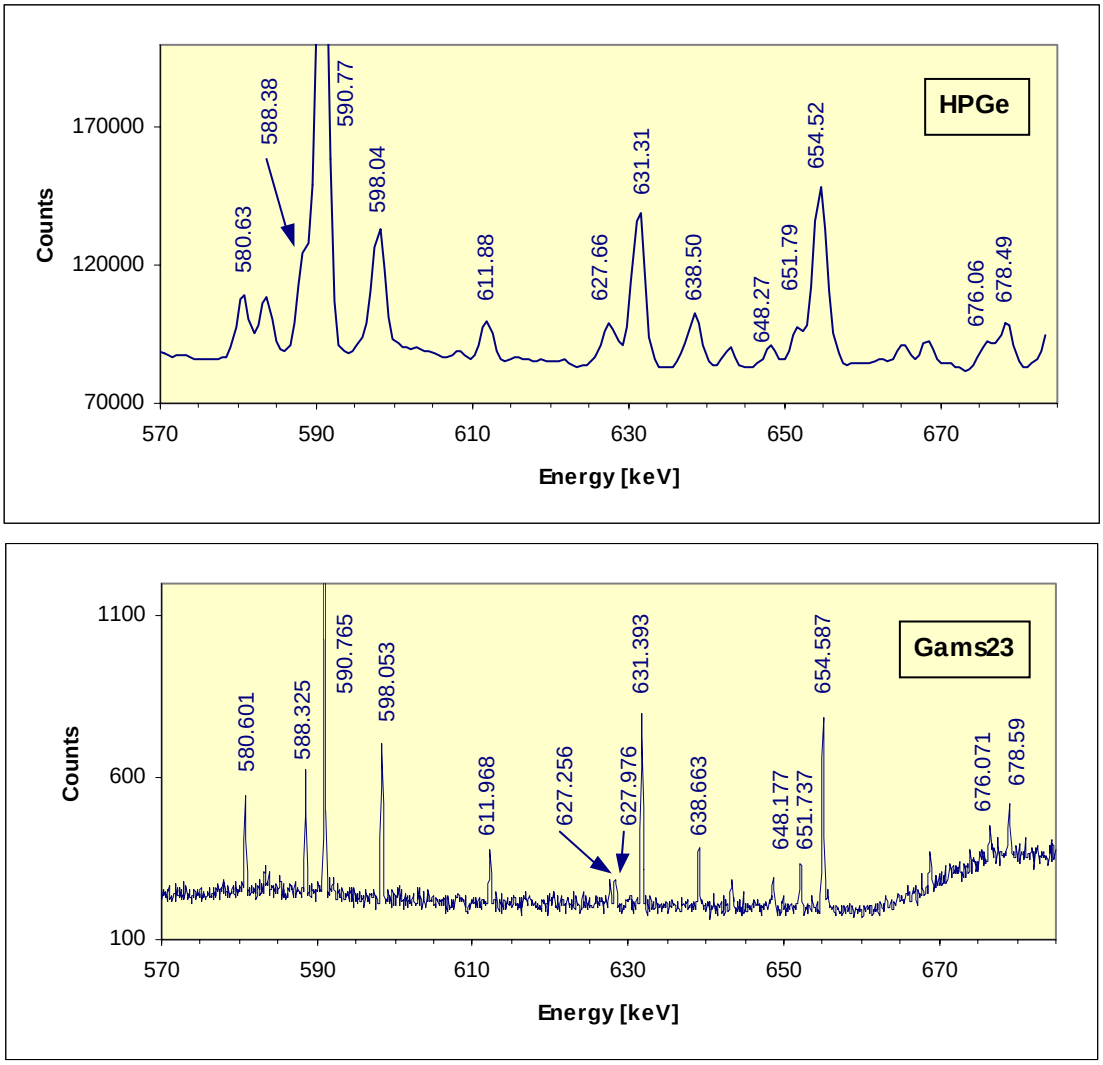

2.3 Primary transitions from the neutron capture state

A nucleus capturing a low-energy neutron forms a compound nucleus at an excitation energy $E_c=S(n)+E_n$ where $S(n)$ is the neutron separation energy. The capture state de-excites either by high-energy γ rays (called primary transitions) to low-lying levels or by statistical transitions that populate a region of high-density levels. So, by subtracting the capture state energy with the measured primary transition energies one discloses specific low-lying levels.

However, as the spin of the capture state is well defined and the primary transitions are dipolar in nature[a], it is clear that some of the low-lying states will nearly never be populated.

[a] Quadrupolar primary transitions also can depopulate the capture state but they are almost never observed

3 Lifetimes measurements

3.1 Motivation

The different excitation states of a nucleus corresponding to a specific excitation mechanism are not all of the same nature. One knows different collective modes where several nucleons participate to the nuclear properties (vibrations about a spherical equilibrium shape, rotations of a nonspherical system).

To disentangle the nature of the different states in the lower part of the level scheme one has to have an insight in the structure of the wave function of these states. It is possible to test the wave functions through the reduced transition probabilities. The theoretical expression of this quantity is:

$$B(\lambda L; J_i \rightarrow J_f) = \frac{1}{2J_i + 1} \left\langle J_f \left\| T(\lambda L) \right\| J_i \right\rangle^2 \tag{2}$$

where λL corresponds to the nature of the electromagnetic transition, J_i and J_f are the spins of the initial and final states, respectively. Thus, the probability of emission of radiation of a given multipole depends, among other things, on the structure of the initial and final states involved. The reduced transition probability can be deduced from measurable quantities:

$$B(\lambda L; J_i \rightarrow J_f) = \frac{C \cdot BR}{E_\gamma{}^{2L+1} (1+\alpha) \tau(J_i)} \tag{3}$$

where C is a constant that depends on the multipolarity of the transition, BR the total branching ratio, E_γ the energy of the decaying transition, α the internal conversion coefficient of the emitted radiation and $\tau(J_i)$ the lifetime of the excited state which is the most difficult quantity to determine. The order of magnitude of the experimental reduced transition probability will give an insight of the nature of a given excited state; the comparison between theoretical and experimental values helps to determine in a first step the collectivity of the states, and in a second step the validity of the applied theoretical model.

3.2 Doppler shift methods

The electromagnetic properties of the transitions that one can deduce from lifetimes measurements are of a great importance. But these lifetimes lie typically in the range of the picosecond to femtosecond region (10^{-12}-10^{-15} s) where no electronic timing techniques are applicable. So, it is necessary to use a time clock faster than one can obtain with electronic methods. Nuclear reactions can provide excited nuclei with large linear momenta; the slowing down of these nuclei in matter can give such a very fast clock.

It is well known that the radiation emitted from a moving source is Doppler shifted; as a consequence one can deduce the slowing down of nuclei through the relation:

$$E_g(\theta) = E_{g0}\left(1 + F(\tau)\frac{v}{c}\cos(\theta)\right) \quad (4)$$

where E_{g0} is the unshifted radiation energy, v the velocity of the moving source, c the speed of light and theta the angle between the emitted radiation and the observation device. As a matter of fact, in a very simplified point of view, levels with very short lifetimes will emit the γ ray promptly and thus just after the reaction when the nuclei have a large linear momentum, resulting to the measurement of Doppler-shifted γ rays. In the contrary, the levels with long lifetimes decay when the nuclei are stopped, so as no Doppler effect can be measured. In the next two sections, I will discuss the two different techniques we used to extract the lifetimes of the excited states for ^{100}Ru and ^{168}Er.

3.3 Doppler Shift Attenuation Method

A description of this method is presented in the article of T. Belgya *et al* [4], but the general idea is the following: by measuring the Doppler-shifted γ-ray energy as a function of $\cos(\theta)$, one extracts $(v/c)\cdot F_{exp}(\tau)$. If the initial velocity is well determined — for example in capture γ-ray experiments or inelastic scattering measurements — the experimental attenuation factor $F_{exp}(\tau)$ can be easily extracted from the slope of the experimental data (See figure 2 at page 76 of the present thesis). The comparison with the theoretical $F(\tau)$ provides the nuclear level lifetime τ. The best known model to calculate the theoretical attenuation factor is derived from the Winterbon formalism [5]. This theory describes the transport of the recoiled ions in a homogeneous, isotropic and infinite medium with binary collisions between the recoiling nucleus and the atoms of the medium. The DSAM experiments performed at the University of Kentucky Van de Graaff facility use the $p(t,^3He)n$ reaction to obtain neutrons with energies ranging from 1 MeV to 5 MeV. The nuclei interacting through an inelastic scattering reaction with these neutrons recoils with a typical velocity $v/c=0.001$. The Doppler shifts induced by this reaction on γ rays decaying levels with very short lifetimes are up to 5 keV. When one is only interested in the relative measurement of γ-rays energies, the precision on this value with an HPGe semiconductor detector is sufficient to detect Doppler shifts as low as 0.1 keV.

3.4 Gamma-Ray Induced Doppler Method

A complete description of the Gamma-Ray Induced Doppler (GRID) method can be found in the article of H.G. Börner and J.Jolie [6]. This method was developed in 1987 to measure lifetimes of states populated in thermal neutron capture reactions. In opposition to the DSAM discussed in the precedent section, the recoil given by the incoming neutron to the target nucleus is insignificant (the kinetic neutron energy is approximately $E_n = 0.025\ eV$). As we saw in section 2.3, the compound nucleus firstly de-excites by emitting a primary radiation of energy E_1 inducing a recoil of the nucleus with energy: $E_R=E_1/2Mc^2$, where M is the mass of the nucleus. If the nucleus emits a second γ ray of energy E_2 while still in movement, the detector will measure a Doppler shift of the energy E_2. In contrary to DSAM, there is no

privileged direction for the recoiling nucleus; as a consequence one does not measure shifted but broadened peaks. The typical recoil velocities induced by the emission of the primary photon are $v/c = 10^{-4} \rightarrow 10^{-6}$, resulting in an extra broadening of the detected peak lower than 300 eV. The resolution of an HPGe semiconductor detector (2.0 keV for photons of 1.3 MeV energy) is far too low to appreciate such a small difference in the peak's width. The sole instruments able to measure such a small broadening are two-axis flat crystal spectrometers like GAMS4 [7] built by the National Institute of Standards and Technology and installed at the high flux reactor of the Institut Laue-Langevin (ILL) in Grenoble. As for GAMS23, the measurement principle of this instrument is based on a very accurate determination of the Bragg's angle, these are measured by high precision Michelson interferometers that have a sensitivity lower than 10^{-10} rad. Figure 3 illustrates the difference of resolution for the same γ ray measured with three different types of detector. The figure at page 80 shows a few transitions measured with the GAMS4 spectrometer.

Figure 3: Resolution for a γ ray with energy 1.3 MeV measured with three different spectrometers

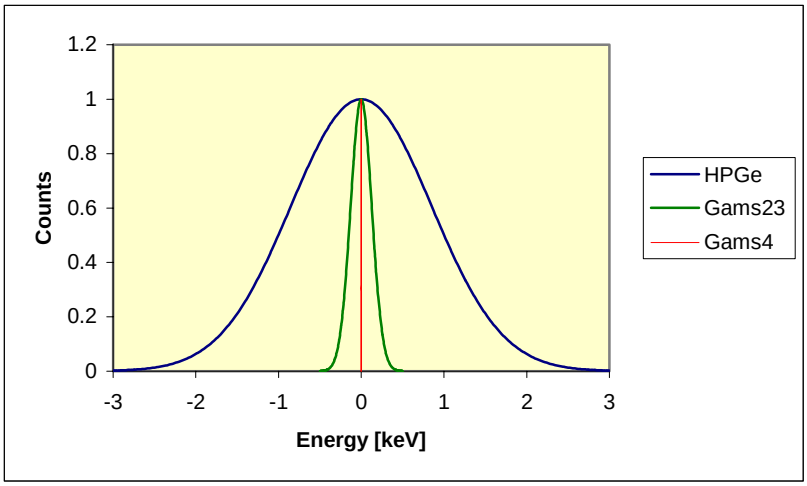

The Doppler broadening measured by the GAMS4 instrument depends on five effects: the temperature of the target, the decay pattern of the nucleus, the lifetimes of all intermediate levels encountered in the cascades that populate the level of interest, the slowing-down of the recoiling nucleus, the lifetime τ of the level of interest.

The lifetime τ can be extracted from the measured lineshape at the condition that all other phenomena are under control [7]. The major uncertainty in extracting lifetimes is not due directly to the measurement itself, but is related to the quantitative description of these phenomena. Because the complete γ-decay scheme as well as the lifetimes of intermediate levels are experimentally unknown one has to base the analysis either on extreme feeding assumptions or on a statistical decay calculation. These two approaches are described in pages 81 and following.

4 Applications of gamma-ray spectroscopy to elemental analysis

The knowledge gained with experimental techniques used for fundamental nuclear research can also be used for tasks closer to applied physics. The determination of the mass of elements contained in a sample in a non-destructive way is an example.

An object absorbing solar light will reflect a spectrum of photons characteristic of its molecular composition. Our eyes act as spectrometer which task is to measure the energy of the reflected photons, allowing us to visualize the object's colours (the colour is not only characteristic of the object and the incoming light but it is also a physiologic property of the eye itself). Similarly it is possible to *recognize* elements by analysing the characteristic γ rays emitted by a sample. The photons composing the solar lights do not have sufficient energy to excite the atomic nuclei of the sample, so one has to use a different *light*, as thermal neutrons. When one *illuminates* a sample with such particles, the atomic nuclei are excited and they release this energy by emitting γ rays. Each type of nucleus (corresponding to isotopes) emits different characteristic γ rays; as a consequence it is possible to *recognize* isotopes by measuring the emitted radiation.

Among the different techniques developed around this idea lie the Prompt Gamma-ray Activation (PGA) analysis; the principle of this method is to measure the prompt γ rays emitted by a sample irradiated by a continuous flux of cold neutrons. The Compton suppressed germanium spectrometers are the most suited instruments for the measurement of such a radiation. These detectors allow to measure hundreds of γ rays with both high energy resolution and high detection efficiency. The identification of the different elements in the sample is realized by comparing the precise measured energies to a standard; the use of adequate software is necessary to achieve this task. ***PEGASE*** is the acronym for **P**rogram **E**valuating **GA**mma-ray **S**pectra for the determination of **E**lemental compositions; I wrote this program at the request of the Paul-Scherrer Institut (PSI) for the analysis of spectra issued from a prompt γ-ray activation. The internal report describing this software forms the third part of this thesis.

As conclusion of this first part of this thesis, the Figure 4 summarizes some of the properties than one can determine with the help of the two types of γ-ray detectors I used in this thesis work.

Figure 4

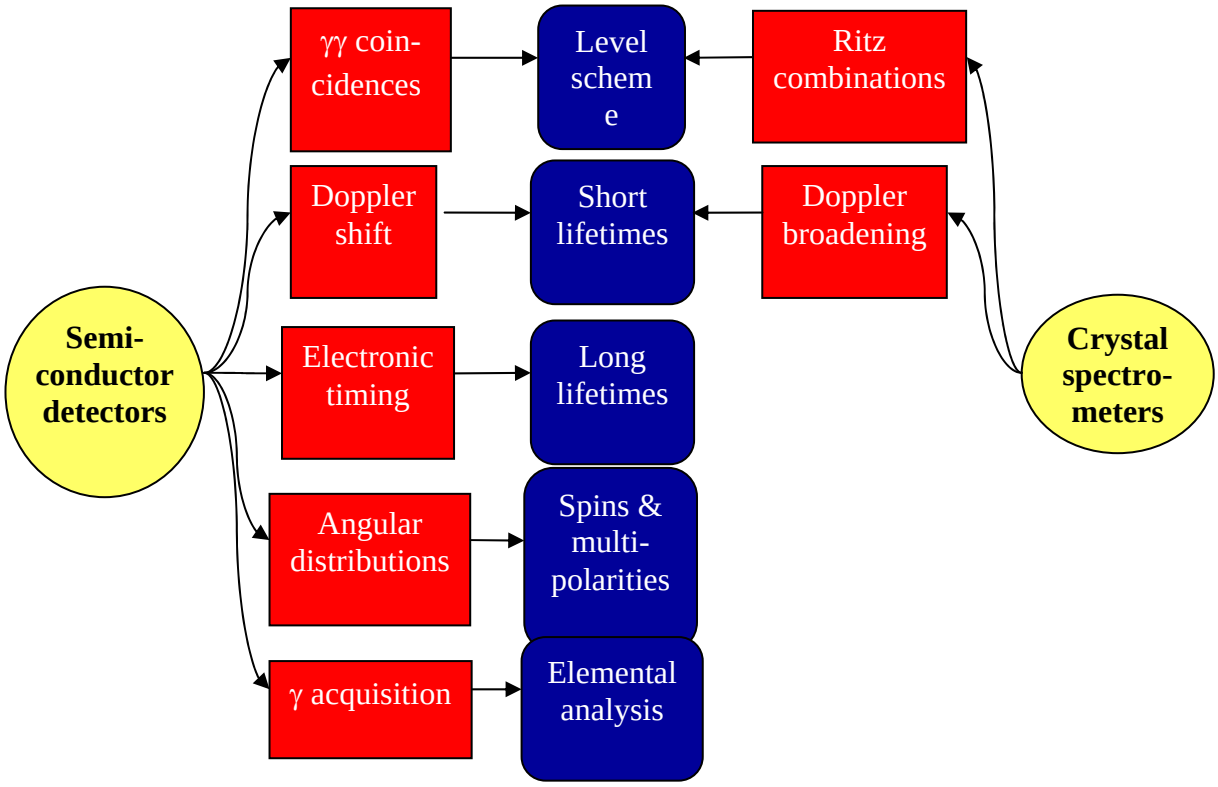

5 References

[1] H. Ejiri and M.J.A de Voigt, Gamma-Ray and ElectrSpectroscopy in Nuclear Physics, Oxford University Press, Oxford (1989).
[2] N. Warr, Ph.D. thesis work, University of Fribourg, Switzerland (1997).
[3] H.R. Koch, H.G. Börner, J.A. Pinston, W.F. Davidson, J. Faudou, R. Roussille and O.W.B Shult, Nucl. Instr. **175** (1980) 401.
[4] T. Belgya, G. Molnar, S.W. Yates, Nucl.Phys. **A607** (1996) 43.
[5] K.B. Winterbon, Nucl.Phys. **A246** (1975) 293.
[6] H.G. Börner and J.Jolie, J.Phys.**G19** (1993) 217.
[7] E.G. Kessler, G.L. Greene, M.S. Dewey, R.D. Deslattes, H.G. Börner and F. Hoyler, J. Phys. **G**14 (1988) 167.

Part Two

Publications

ELSEVIER

Nuclear Physics A 669 (2000) 407–449

NUCLEAR PHYSICS A

www.elsevier.nl/locate/npe

Study of the vibrational nucleus ^{100}Ru by the ^{98}Mo(α,2nγ) and ^{99}Ru(n,γ) reactions

L. Genilloud [a], H.G. Börner [b], F. Corminboeuf [a], Ch. Doll [b], S. Drissi [a], M. Jentschel [b], J. Jolie [a], J. Kern [a], H. Lehmann [a,b], N. Warr [a,c]

[a] *Institut de Physique, Université de Fribourg, CH-1700 Fribourg, Switzerland*
[b] *Institut Laue-Langevin, Grenoble, France*
[c] *University of Kentucky, Lexington, KY 40506-0055, USA*

Received 30 June 1999; received in revised form 13 August 1999; accepted 17 August 1999

Abstract

The nuclear structure of ^{100}Ru was investigated using the ^{99}Ru(n,γ) and ^{98}Mo(α,2nγ) reactions. In the in-beam spectroscopy study, the use of a coincidence system equipped with five Compton-suppression spectrometers allowed to place 207 transitions in the decay scheme. Spin and parity assignments of the states were determined using angular distribution analysis together with the excitation function slopes and side-feeding intensities. The photons following the neutron capture were observed using curved crystal and pair spectrometers. Using the results of both reactions, the level scheme was extended by 36 new levels. The interpretation of the resulting level scheme was performed in the framework of the *spdf* interacting boson model.

PACS: 21.10.Re; 21.60.Fw; 23.20.Lv; 27.60.+j
Keywords: NUCLEAR REACTION ^{98}Mo(α,2n), E = 21.0,24.7,28.7 MeV; measured E_γ, $I_\gamma(\theta)$, $\gamma\gamma$-coin; ^{99}Ru(n,γ), E_n = thermal; measured E_γ, I_γ; ^{100}Ru deduced levels, J,π; Enriched targets, Compton-suppressed Ge detectors; Comparison with interacting boson model

1. Introduction

In the framework of the *sd*-IBA-1 model of Arima and Iachello [1], vibrational nuclei are described by the U(5)-symmetry limit. This leads to an elegant and analytical solution of the nucleus many-body problem. Recently, the U(5) description gained new interest [2,3] because new experiments allowed one to answer two fundamental ques-

0375-9474/00/$ - see front matter
PII: S0375-9474(00)00140-8

Table 1
Summary of the γ-ray data obtained from the $^{98}Mo(\alpha,2n)$ reaction; only the transitions attributed to ^{100}Ru are listed

E_γ [keV] [a]	ΔE_γ [eV]	Angular distribution coefficients			Slope [b]		Observed multipolarities and multipole-mixing ratios				Assignments	Comments
							previous works [c]		this work		$E_i - E_f$	
		A_0	A_2/A_0	A_4/A_0	SL	ΔSL	δ	multip.	δ [d]	multip. [e]		
128.300	300	0.5(1)			−0.2	3.0					2705.6–2576.9	
129.939	100	0.4(1)									3576.5–3446.6	
148.720	14	7.0(3)	−0.158(18)		11.8	0.3	−1.5(15)	M1+E2	0.05(1)	M1+E2	3503.5–3354.7	
152.563	40	1.3(1)	0.47(8)		17.2	1.3			0.04(9)	M1	4235.9–4083.4	
155.681	40	1.3(1)	0.43(10)	−0.29(15)	−10.1	1.4					2747.5–2591.9	
166.377	150	0.3(1)									2951.6–2785.3	
175.550	60	1.3(2)									3139.3–2963.7	
175.837	60	2.3(2)			8.5	1.9					2527.3–2351.3	[f]
178.053	90	0.7(1)									4408.8–4230.6	
187.760	13	13.7(5)	0.50(28)		4.5	0.3			0.17(10)	M1+E2	3139.3–2951.6	
191.926	30	2.8(1)			4.5	1.0					5010.6–4818.7	
203.590	14	12.4(4)	0.51(4)		4.5	0.3			0.18(20)	M1+(E2)	3263.7–3060.1	
215.480	30	3.9(2)			6.1	0.6					3354.7–3139.3	
218.874	40	2.7(1)	−0.12(4)		16.8	0.7			0.078(8)	M1+E2	5010.6–4791.7	
228.100	500	0.5(3)									3139.3–2911.5	
229.686	50	1.6(1)	0.43(6)		−2.7	2.0			0.02(15)	M1	3369.0–3139.3	
238.351	16	9.8(2)	0.33(3)	−0.15(5)	3.3	0.3			0.33(3)	M1+E2	4230.6–3992.3	[g]
239.736	50	1.7(1)			10.5	1.4					3503.5–3263.7	
244.405	130	0.7(1)	0.76(16)		7.5	2.1			0.2(3)	M1+(E2)	3599.4–3354.7	
245.965	80	1.3(1)			8.1	1.8					2951.6–2705.6	
247.943	17	11.6(2)	0.48(3)	−0.06(4)	−6.3	0.3			0.6(2)	M1+E2	2775.2–2527.3	
254.486	19	8.3(2)	0.385(21)	−0.16(3)	−4.1	0.9				E2	3218.2–2963.7	
262.083	30	3.0(1)	0.44(7)		−2.7	1.0			0.17(22)	M1+(E2)	2967.6–2705.6	
270.082	80	0.9(1)									4353.4–4083.4	
288.080	110	0.7(1)			11.5	7.3					4791.7–4503.6	[g]
294.612	26	3.7(1)	0.48(4)	−0.07(5)	5.8	0.9			0.08(20)	E1	3354.7–3060.1	
301.634	28	3.5(3)	−0.08(3)	−0.09(5)			1.2(5)	[E1]	0.03(6)	E1	2167.0–1865.1	

309.524	90	0.9(1)			−13.3	4.5							2660.9–2351.3	
312.616	150	1.1(2)											3576.5–3263.7	
354.087	40	2.3(1)	−0.19(5)	−0.15(8)	10.0	1.5				0.04(6)	E1		3139.3–2785.3	
360.331	23	6.0(1)	0.43(3)	−0.20(5)	1.2	0.7					E2		2527.3–2167.0	
364.055	15	15.7(2)	0.438(17)	−0.071(26)	11.4	0.3		E2			E2		3503.5–3139.3	
371.774	19	11.8(2)	0.410(17)	−0.098(25)	3.2	0.4					E2		2963.7–2591.9	
378.809	110	1.3(1)			13.6	1.3		(E2)					1741.0–1362.2	f
381.207	180	0.8(1)			12.6	3.5							3599.4–3218.2	
384.217	30	4.8(2)	0.29(3)	−0.21(5)	−7.2	0.8							2911.5–2527.3	
390.981	14	41.9(4)	0.413(14)	−0.099(21)	7.9	0.2		(E2)			E2		3354.7–2963.7	
403.092	15	14.8(3)	0.713(14)	0.177(20)	6.3	0.3	1.7(5)	(E2 + M1)		1.58(7)	M1 + E2		$\frac{3354.7}{2569.9}$ – $\frac{2951.6}{2167.0}$	h
405.500	500	0.5(3)											3369.0–2963.7	
416.800	300	0.5(3)											3992.2–3575.6	
417.407	20	10.9(2)	0.31(4)		−0.6	0.5				−0.21(7)	M1 + E2		3369.0–2951.6	g
419.919	160	1.1(2)			11.9	6.0							4503.6–4083.4	
421.355	96	2.2(2)			9.6	4.5								
424.318	14	20.6(33)	0.32(4)	−0.07(8)	5.2	0.2		(E2)			(E2)		2951.6–2527.3	
424.826	210	9.5(22)	0.92(22)							1.2(3)	M1 + E2		2591.9–2167.0	
430.340	40	4.5(3)			−15.6	0.2							2493.0–2062.7	g, i)
433.003	150	1.0(2)			3.3	3.6							4663.5–4230.6	
436.352	18	16.2(3)	0.641(20)	0.121(28)	3.7	0.3	2.8(20)	(M1 + E2)		0.69(25)	M1 + E2		$\frac{2963.7}{3575.6}$ – $\frac{2527.3}{3139.3}$	h
438.373	330	0.8(2)											4791.7–4353.4	
443.317	16	21.5(3)	−0.156(15)		11.0	0.2	−0.11(5)	E1(+M2)		0.06(6)	E1		3503.5–3060.1	
460.013	70	2.3(2)	−0.83(7)	0.31(11)	3.3	1.8				−2.8(2)	M1 + E2		3599.4–3139.3	
465.332	150	0.8(1)											4818.7–4353.4	
477.100	500	0.5(3)											4076.0–3599.4	
478.467	22	8.2(2)	0.42(2)	−0.19(4)	5.9	0.8					E2		3263.7–2785.3	
488.671	20	15.2(2)	0.343(17)	0.033(27)	7.8	0.4	4.(2)	E2 + M1		0.37(2)	M1 + E2		3992.3–3503.5	
490.048	40	5.7(2)	0.72(3)		6.4	1.2					E2		3550.2–3060.1	
502.692	280	1.0(4)						M1,E2					1865.1–1362.2	
515.470	50	6.3(6)	−0.08(3)		6.2	1.5				0.09(12)	E1		3575.6–3060.1	
518.879	60	5.6(5)	0.22(5)		−9.9	1.7		M1,E2		0.38(6)	M1 + E2		1881.1–1362.2	
521.859	50	6.6(4)	0.32(3)		6.5	1.2				−0.25(7)	M1 + E2		4097.5–3575.6	
539.509	14	1000.0(79)	0.340(5)	−0.122(7)	0.0	0.0		E2			E2		539.5 –0.0	

(continued on next page)

Table 1 (*continued*)

E_γ [keV] [a]	ΔE_γ [eV]	Angular distribution coefficients			Slope[b]		Observed multipolarities and multipole-mixing ratios				Assignments $E_i - E_f$	Comments
							previous works [c]		this work			
		A_0	A_2/A_0	A_4/A_0	SL	ΔSL	δ	multip.	δ [d]	multip. [e]		
544.909	140	5.4(10			−6.4	1.9					2911.5–2366.6	
551.881	14	28.3(3)	0.414(21)	−0.08(3)	11.2	0.2		(E2)		E2	3503.5–2951.6	
555.689	60	2.6(1)			10.8	1.5					4791.7–4235.9	
557.976	30	5.4(1)	0.31(3)	−0.16(5)	4.6	0.7				E2	3263.7–2705.6	
564.505	150	1.9(3)									4917.9–4353.4	
565.668	650	0.5(4)									4663.5–4097.5	
567.458	90	2.0(2)			19.5	2.4					4798.2–4230.6	
572.406	130	1.0(1)	−0.27(11)		3.0	3.5			0.05(7)	DP	4076.0–3503.5	
580.515	120	1.1(1)	0.43(9)						0.62(16)	M1 + E2	2747.5–2167.0	
582.815	80	2.3(2)	0.33(9)		11.5	2.3			−0.26(20)	M1 + E2	4818.7–4235.9	
588.298	100	1.3(2)					E1				2469.4–1881.1	
590.844	20	8.6(2)			−6.0	0.6	E2				1130.4–539.5	
593.932	50	3.2(2)			−3.1	1.8					3369.0–2775.2	
598.110	73	3.7(2)									2660.9–2062.7	
598.110	73	3.7(2)									2765.0–2167.0	
605.717	40	3.5(1)			1.4	1.6					3960.4–3354.7	
608.900	500	0.5(3)									3576.5–2967.6	
612.055	18	24.4(4)	0.339(16)	−0.139(25)	4.2	0.3		E2		E2	$^{3139.3}_{2493.0}$ — $^{2527.3}_{1881.1}$	[h]
623.933	14	54.2(5)	0.379(20)	−0.108(31)	10.6	0.2				E2	3575.6–2951.6	
626.892	88	2.7(3)			−1.0	1.7						
629.793	50	7.0(3)	0.246(21)	−0.159(32)	2.1	0.9			1.00(7)	M1 + E2	2705.6–2075.7	
631.405	50	2.9(4)	0.240(23)	−0.22(4)	−5.2	1.2					2512.5–1881.1	
636.544	150	8.3(26)	0.61(19)	−0.15(31)	12.4	1.8				E2	4235.9–3599.4	
637.441	70	27.5(29)	0.40(4)	−0.02(6)	13.5	0.8	E2			E2	3992.3–3354.7	
638.807	130	1.0(2)					E2				1865.1–1226.5	
642.818	19	26.9(4)	0.343(20)	−0.169(31)	1.9	0.5				E2	2705.6–2062.7	
647.752	20	15.5(3)	−0.949(8)	0.072(13)	5.6	0.4			−0.30(2)	M1 + E2	3599.4–2951.6	
654.776	50	5.0(2)	−0.241(26)				M1,E2		2.1(3)	M1 + E2	1881.1–1226.5	
660.336	110	1.5(2)									4235.9–3575.6	

														3929.5–3263.7	
666.148	100	1.6(2)													
673.049	80	2.5(2)												4248.5–3575.6	
678.542	140	1.2(2)												2543.6–1865.1	
686.973	17	819.1(12)	0.359(4)	−0.124(6)	1.7	0.2		E2				E2		1226.5–539.5	
689.300	500	0.5(3)												2569.9–1881.1	f
695.810	330	8.9(4)	0.32(6)	−0.28(10)	4.9	3.8						E2		2576.9–1881.1	f
700.712	550	12.9(8)	0.24(3)	−0.12(4)	−4.1	1.9						E2		2062.7–1362.2	
708.500	500	0.5(3)												4791.7–4083.4	
709.431	30	26.9(6)	0.400(17)	−0.086(26)	0.1	0.7				0.54(8)		M1 + E2		2785.3–2075.7	f
710.817	50	15.7(8)	−0.16(3)	−0.21(5)	−0.4	1.2				0.05(8)		E1		2591.9–1881.1	
712.758	130	2.3(3)			−2.5	2.9								2775.2–2062.7	
722.677	22	1.8(3)	0.146(22)	−0.047(35)	6.8	0.5						E2		2785.3–2062.7	i,j)
727.340	20	27.7(4)	0.341(13)	−0.060(19)	17.5	0.5		(E2)				E2		4230.6–3503.5	
728.484	190	1.9(4)			5.1	2.6								4097.5–3369.0	
732.459	50	4.5(2)	−1.14(4)	0.27(6)	12.2	1.0				−1.05(12)		M1 + E2		4235.9–3503.5	
734.844	80	3.3(2)						(E2)				E2		1865.1–1130.4	
736.931	180	1.3(2)												2099.1–1362.2	
740.222	19	22.9(3)	0.33(4)	−0.06(7)	16.3	0.3						E2		4315.8–3575.6	
742.269	90	2.8(2)	0.62(10)							0.58(12)		M1 + E2		3960.4–3218.2	
750.800	500	0.5(3)												5066.3–4315.8	
765.037	60	4.6(2)	0.34(4)	−0.21(5)	5.5	1.0						E2		3550.2–2785.3	
772.970	190	2.0(3)			−4.7	2.1									
774.416	290	1.8(4)												5010.6–4235.9	
779.785	60	8.1(5)	0.54(10)	−0.35(16)	−2.2	1.7						E2		2660.9–1881.1	
785.696	200	1.8(3)			−0.1	1.8								3446.6–2660.9	
795.295	50	3.9(2)	0.22(6)		18.8	0.7		(E2)				(E2)		5713.2–4917.9	
803.258	60	3.2(2)	0.28(4)		13.4	1.4						(E2)		4353.4–3550.2	
806.021	20	10.0(2)	0.28(5)	−0.10(8)	18.8	0.4		(E2)				E2		4798.2–3992.3	
812.390	80	2.4(2)												4315.8–3503.5	
819.623	70	2.8(2)												4083.4–3263.7	
822.666	17	25.1(3)					3.7(4)	E2 + M1						1362.2–539.5	j
830.394	40	5.1(2)			16.6	1.0								5066.3–4235.9	

(continued on next page)

Table 1 (*continued*)

E_γ [keV] [a]	ΔE_γ [eV]	Angular distribution coefficients			Slope [b]		Observed multipolarities and multipole-mixing ratios				Assignments	Comments
							previous works [c]		this work		$E_i - E_f$	
		A_0	A_2/A_0	A_4/A_0	SL	ΔSL	δ	multip.	δ [d]	multip. [e]		
834.454	80	7.9(5)	0.21(9)	−0.07(13)	19.3	0.9				E2	4917.9–4083.4	
835.200	200	0.5(1)									5066.3–4230.6	
836.187	23	24.1(5)	0.15(3)	−0.19(4)	−2.3	0.6			1.85(21)	M1 + E2	2062.7–1226.5	
840.921	100	2.9(3)			1.0	2.4						
844.474	70	18.6(20)									3550.2–2705.6	k
846.710	90	5.0(3)									5162.5–4315.8	
849.241	15	538.1(65)	0.362(12)	−0.105(19)	4.5	0.1		E2		E2	2075.7–1226.5	
854.151	400	3.4(14)										
861.934	100	3.2(3)									4791.7–3929.5	
866.291	210	1.5(3)									2747.5–1881.1	
869.686	160	4.6(8)	0.36(4)	−0.11(7)	−1.5	1.9				E2	3446.6–2576.9	
870.988	210	3.8(10)	−0.47(12)						−0.12(7)	M1 + E2	3576.5–2705.6	
875.878	12	155.2(12)	−0.219(6)	0.009(9)	6.4	0.1		E1	−0.02(3)	E1	2951.6–2075.7	
883.800	500	0.5(1)									3851.5–2967.6	
886.500	500	0.5(3)									3661.5–2775.2	
887.981	17	42.1(6)	0.388(13)	−0.053(20)	2.8	0.2	0.4(7)	E1(+M2)	−0.08(10)	E1	2963.7–2075.7	
891.665	80	5.4(3)	0.31(3)		3.5	0.9			−0.17(8)	M1 + E2	2967.6–2075.7	
893.765	90	4.6(4)	0.56(3)		2.4	2.5			0.52(5)	M1 + E2	4248.5–3354.7	
896.785	80	4.0(3)	0.44(7)	−0.27(10)						E2	4343.5–3446.6	
904.801	50	8.8(4)			15.7	1.5					2967.6–2062.7	
927.550	500	0.5(3)									5010.6–4083.4	
931.717	30	4.7(1)	0.17(5)	−0.03(7)	22.3	0.5		(E2)		E2	5162.5–4230.6	
935.374	90	3.1(2)			9.2	1.5					4381.8–3446.6	
936.937	210	1.9(3)			19.0	1.0					4076.0–3139.3	f
943.620	160	1.2(1)									3111.1–2167.0	
946.317	150	1.5(2)	0.41(13)		8.6	2.7						
948.980	110	1.7(1)	0.46(13)	−0.19(19)	−8.4	2.8				E2	3610.0–2660.9	
953.384	30	6.2(2)	0.29(7)	−0.06(11)	14.7	0.9				E2	4503.6–3550.2	f
959.030	120	4.4(4)	0.36(5)	−0.07(7)	16.9	1.6				E2	5274.9–4315.8	
961.932	80	4.5(3)	0.32(9)	−0.10(13)	−0.3	1.6		(E2,M1)		E2	3929.5–2967.6	

966.675	150	2.3(4)			3.1	2.3						2099.1–1130.4		
969.200	500	0.5(3)										4235.9–3263.7		
972.132	60	7.4(4)	0.19(8)	−0.07(14)	14.5	0.6			E2			3060.1–2075.7		
974.723	170	2.3(4)										2877.7–1881.1	f	
984.439	12	169.5(13)	0.327(17)	−0.045(27)	9.3	0.1	E2		E2			3576.5–2576.9		
994.133	250	1.5(3)						0.05(20)	DP			4083.4–3060.1		
996.564	150	2.8(3)	0.23(9)						E2			5125.4–4083.4		
999.539	70	5.6(3)	0.26(4)	−0.09(7)	2.7	1.0			E2			5274.9–4230.6		
1023.252	15	39.3(4)	0.27(4)	−0.06(6)	14.3	0.2	(E2)		E2			4408.8–3354.7		
1036.975	200	1.6(3)										3139.3–2075.7		
1042.028	130	3.9(5)			17.1	1.1		−0.03(5)	E1			4343.5–3263.7		
1043.800	200	3.3(7)	0.42(13)	−0.35(20)					E2			2469.4–1362.2		
1051.505	58	5.0(3)	0.24(5)		−5.6	1.1						4381.8–3263.7		
1054.009	110	5.5(5)			−1.0	2.6						2351.3–1226.5		
1063.670	30	9.1(2)	−0.216(18)		4.2	0.6						3661.5–2527.3		
1067.211	150	1.6(2)										2366.6–1226.5		
1079.975	130	1.8(2)	0.48(5)	0.37(7)	9.3	2.1		2.84(8)	M1 + E2			4343.5–3263.7		
1098.946	150	1.6(2)					E1					2469.4–1362.2		
1107.103	120	1.9(2)						−0.11(7)	M1 + E2			4381.8–3263.7		
1117.985	110	2.0(2)	−0.47(10)									2351.3–1226.5		
1124.841	30	7.9(2)			−8.5	0.8						3661.5–2527.3		
1134.209	130	1.5(1)	−0.51(7)	−0.20(10)	−8.1	3.0		−0.16(6)	M1 + E2			2366.6–1226.5		
1139.772	650	1.0(8)												
1141.001	220	3.4(10)			−8.7	1.4								
1153.246	200	1.6(2)												
1160.046	70	3.8(2)	0.37(8)	−0.12(12)	11.6	1.3			E2			4663.5–3503.5		
1175.776	23	17.1(2)	0.27(4)	−0.07(6)	11.9	0.3			E2			4235.9–3060.1		
1181.425	120	1.7(1)										2543.6–1362.2		
1188.012	20	15.7(2)	0.314(15)	−0.121(23)	4.7	0.3			E2			3263.7–2075.7	f	
1201.401	290	0.6(1)			13.0	2.1						1741.0–539.5	f	
1207.700	50	3.4(2)			−4.7	1.8						2569.9–1362.2		
1224.381	76	4.0(3)			−0.5	1.5								
1238.341	120	3.1(3)												
1266.519	220	4.2(12)			−8.2	1.7						2493.0–1226.5		
1274.700	500	0.5(1)										3851.5–2576.9		

(continued on next page)

Table 1 (*continued*)

E_γ [keV] [a]	ΔE_γ [eV]	Angular distribution coefficients			Slope [b]		Observed multipolarities and multipole-mixing ratios				Assignments	Comments
							previous works [c]		this work		$E_i - E_f$	
		A_0	A_2/A_0	A_4/A_0	SL	ΔSL	δ	multip.	δ [d]	multip. [e]		
1293.303	30	15.5(3)			11.1	0.4					4353.4–3060.1	
1295.905	190	2.1(3)										
1300.792	12	110.5(10)	−0.230(7)	−0.025(13)	0.8	0.1	−0.07(3)	E1+M2	0.004(6)	E1	2527.3–1226.5	
1309.519	330	1.1(2)			−8.3	3.0					2536.3–1226.5	
1325.561	70	4.8(2)			−11.7	1.3		M1,E2	5.5(5) 0.35(2)		1865.1–539.5	
1341.601	18	39.5(5)	0.183(10)		−6.3	0.2		M1,E2		M1+E2	1881.1–539.5	
1344.323	140				3.0	0.3			−3.4(2) −0.12(4)			
1350.404	30	14.2(3)	−0.40(3)	0.12(4)	−2.2	0.6				M1+E2	2576.9–1226.5	
1362.172	23	18.4(3)	0.149(22)	−0.11(3)	−8.5	0.3		E2		E2	1362.2–0.0	
1365.401	30	11.6(3)	0.263(11)	−0.05(2)	−5.0	0.5			−0.05(12)	E1	2591.9–1226.5	
1370.952	90	3.8(2)	−0.058(24)	0.13(4)	−1.3	1.2			0.12(2)	M1+E2	3446.6–2075.7	
1376.171	160	2.1(2)										
1380.542	82	5.3(3)			−0.2	2.0						
1427.705	130	2.1(2)										
1433.662	220	5.3(16)										
1434.808	200	6.3(18)	0.297(21)		−2.0	0.7			0.38(4)	M1+E2	2660.9–1226.5	
1474.371	70	4.2(2)	0.39(6)	−0.15(9)	5.9	1.1				E2	3550.2–2075.7	
1479.143	22	18.3(3)	0.314(15)	−0.150(24)	1.0	0.4				E2	2705.6–1226.5	
1512.100	220	1.2(1)			−6.2	4.4					2051.5–539.5	
1515.543	120	2.9(2)			−1.7	1.5					2877.7–1362.2	
1520.830	120	4.0(2)	0.58(5)		−8.1	1.4			0.38(15)	E1+M2	2747.5–1226.5	
1523.199	24	27.5(4)	0.228(12)	−0.143(18)	−3.7	0.4				E2	2062.7–539.5	
1534.400	100	4.8(2)	0.52(6)	0.39(8)	−0.7	2.6			2.6(2)	M1+E2	3610.0–2075.7	
1536.230	303											
1538.310	220	2.9(2)									2765.0–1226.5	
1540.199	310	1.0(2)										
1548.698	120	2.3(2)			−5.5	2.0					2775.2–1226.5	
1552.460	94	2.5(2)	−0.65(5)		−6.8	2.0						
1558.802	84	11.1(12)	0.179(20)	−0.09(3)	−2.7	0.5				E2	2785.3–1226.5	

							M1				2099.1–539.5	
1560.079	560	2.3(3)										
1562.602	220	1.6(3)										
1627.462	22	26.0(4)	−0.173(6)	−0.103(10)	−6.8	0.3	E1		0.02(3)	E1	2167.0–539.5	
1651.753	240	1.4(2)										
1685.302	240	4.8(8)			−5.4	7.6					2911.5–1226.5	
1686.798	380	2.2(10)										
1701.297	150	1.5(1)	−0.37(7)		−10.9	2.8					2240.8–539.5	
1705.439	140	1.7(2)										
1731.668	280	0.8(1)									4791.7–3060.1	
1741.236	70	3.8(2)	0.285(19)	−0.120(29)	−3.1	1.2				E2	2967.6–1226.5	
1775.142	290	1.1(2)										
1811.793	80	4.9(2)			−7.0	1.1					2351.3–539.5	
1827.125	50	12.1(3)	0.150(21)	−0.16(3)	−7.7	0.5				E2	2366.6–539.5	
1865.123	90	4.3(2)			−11.5	1.5					1865.1–0.0	
1870.886	120	3.4(3)										
1874.703	230	1.6(2)			−9.8	2.5					2413.8–539.5	
1886.173	170	2.1(2)										
1972.829	250	1.2(3)			−6.0	3.2					2512.5–539.5	
1996.806	130	2.6(2)	−0.33(10)		−12.8	2.0			−0.2(3)	M1(+E2)	2536.3–539.5	
2004.010	130	2.5(2)			−16.3	2.6					2543.6–539.5	
2166.645	160	1.9(2)			−4.3	2.8	E3			E3	2167.0–0.0	

[a] Energy taken from the excitation function measurement.
[b] Slope computed using the definition in Section 3.1.2.
[c] Data taken from Ref. [6].
[d] Multipole-mixing ratio gained from the analysis of the angular distribution.
[e] Transition multipolarity expected from our spin and parity assignments. M1(+E2) means that δ is very small or compatible with zero. DP indicates a pure dipole transition decaying from a level of unknown parity.
[f] Imprecise slope due to the presence of a line assigned to ^{99}Ru at 21.0 MeV bombarding energy.
[g] Imprecise slope due to the presence of a line assigned to ^{101}Ru at 28.7 MeV bombarding energy.
[h] Double assignment supported by coincidences.
[i] Intensity calculated from a coincidence relation.
[j] No reliable angular distribution coefficients and slope due to the presence of a strong line belonging to ^{98}Mo.
[k] Part of an unresolved doublet with the strong 849.2 transition. No reliable A_2/A_0 and A_4/A_0 coefficients could be extracted from the analysis of the angular distribution.

tions. The first one is to know how well real nuclei are described effectively by this limit of the model and the second one is to which excitation energy such a collective description may persist. At the present moment, only a few Cd nuclei have been confirmed as good vibrators up to high excitation energy, multi-phonon states up to five phonons being identified, see e.g. [2]. Guided by these observations, a survey has been performed [3] to find other candidates which could be described by this symmetry. One of these candidates is ^{100}Ru. The interesting feature of this nucleus is that it is located rather far away from semi-closed shells. The interaction of multiphonon states with 2p2h excitations, leading to so-called intruder states, will thus be reduced. Although these excitations which imply the interplay of shell structure [4] and collectivity [5] are interesting, they obscure in general the interpretation of the data. In the hope to observe an intruder-free vibrational nucleus, we have undertaken the study presented in this work.

In recent years ^{100}Ru has been investigated by many groups using different methods. The results are compiled in Ref. [6]. Among all these works, we mention especially those by Colvin et al. [7] and Islam et al. [8] on ^{99}Ru(n_{th},γ), Coceva et al. [9] on ^{99}Ru(n_{res},γ), Kenchian [10] on the electron capture decay of ^{100}Rh (20.3 h), Babenko et al. [11] on the decay of the same element (4.6 min), Peterson et al. [12] by transfer reactions and Lederer et al. [13] on ^{98}Mo(α,2n).

A description of the different experimental techniques used in this work is given in Section 2. Section 3 is devoted to the presentation of the experimental results and to the construction of the level scheme with model-independent spin and parity assignments. Finally, Section 4 deals with the interpretation of the results in the framework of the spdf IBA-1 [14]. Our conclusions concerning the structure of ^{100}Ru are then presented in Section 5.

2. Experimental procedure

2.1. The ^{98}Mo(α,2n) measurements

For the in-beam measurements, the ^{100}Ru nuclei were produced by the ^{98}Mo(α,2n) reaction using the Philips variable-energy cyclotron at the Paul Scherrer Institute (PSI) in Villigen, Switzerland.

2.1.1. Excitation functions

The target, enriched to 97.6% in ^{98}Mo and deposited on a capton foil, was bombarded by α-particles of 21.0, 24.6 and 28.7 MeV. The γ-ray spectra were measured at 55^0 with respect to the beam line with a Compton-suppression spectrometer [15]. The central detector consisted of a 114 cm^3 high purity Ge detector with an energy resolution of about 2 keV at 1300 keV. The relative efficiency and energy calibrations of the detector were performed with ^{56}Co and ^{152}Eu sources located at the target position, using intensities and energies proposed by Firestone and Shirley [16]. The γ-ray yields were normalized to an intensity of 1000 for the 539.5 keV transition at each bombarding energy (see Table 1). The beam energy corresponding to the largest cross section for the

(α,2n) reaction was found to be approximately 25 MeV. This energy was then used for the angular distribution and $\gamma\gamma$-coincidence measurements. A singles γ-ray spectrum recorded at 24.6 MeV bombarding energy is shown in Fig. 1.

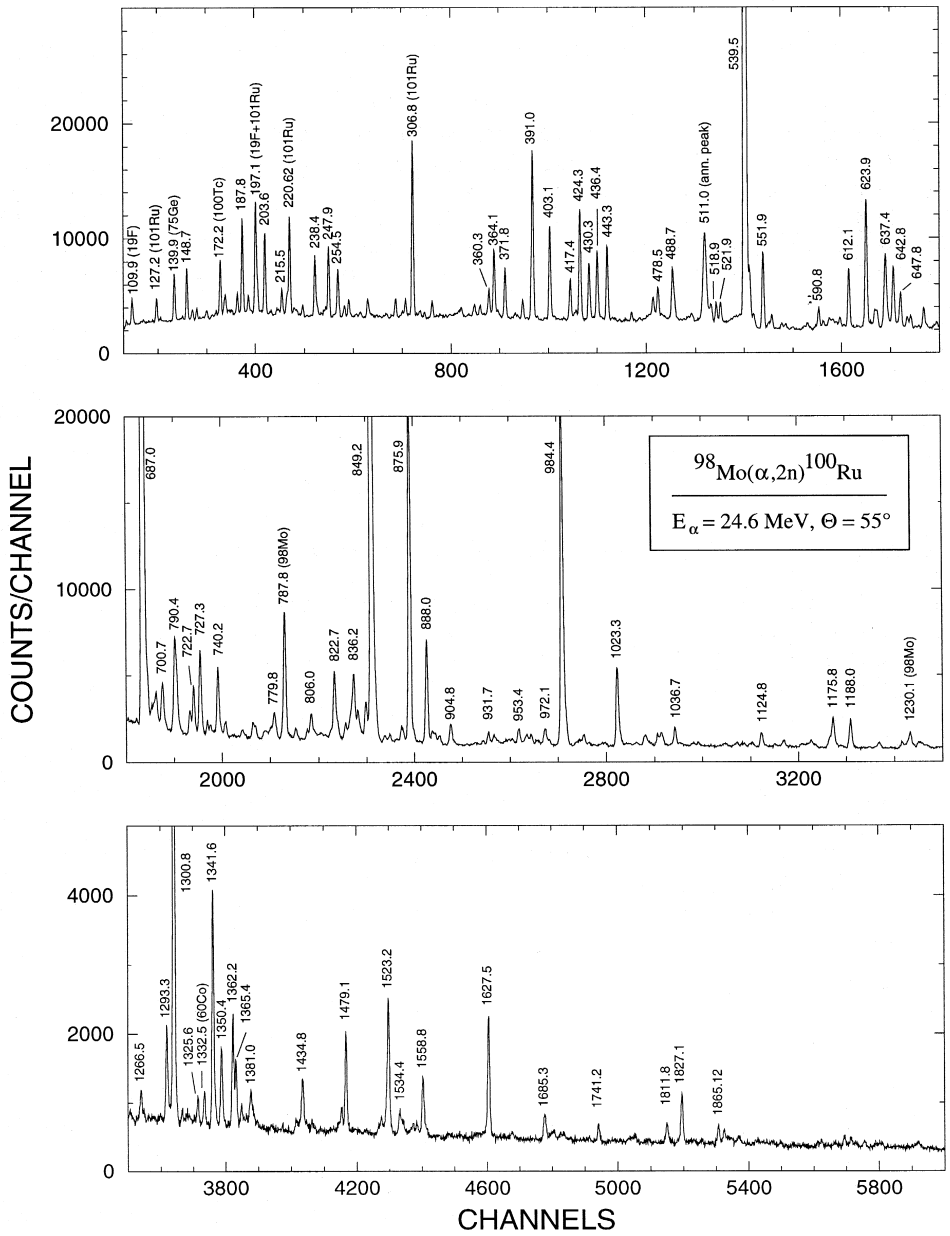

Fig. 1. Singles γ-ray spectrum resulting from the reaction ^{98}Mo(α,2n)^{100}Ru using α particles of 24.6 MeV beam energy. The strong ^{100}Ru γ-rays are labelled by their energies; transitions from other known nuclei are labelled by the name of the isotope.

Table 2
Qualitative results of selected coincidence gates

Gate [keV]	Display[a] [keV]
148.7	187.8*, **215.5***, 238.4*, **294.6***, 354.1*, 360.3*, **371.8***, **391.0***, **403.0***, 419.9*, 424.3*, **436.4***, **488.8***, **539.5***, 567.5*, 572.4*, 612.1*, **687.0***, 710.8*, **727.4***, **732.5***, 795.3*, 806.0*, 812.4*, **849.3***, **875.9***, **888.0***, 931.7*, 1043.8*, 1160.0*, 1250.5, **1300.8***, 1341.6*, 1365.4*
229.7	**187.8***, 354.1*, **539.5***, **612.1***, **687.0***, 849.2*, 875.9*, 1063.7*, **1300.8***
247.9	175.8*, 188.5+, (301.6*), **360.3***, 443.3♯, **539.5***, 593.9*, **687.0***, 724.0♯, 728.4*, 824.3♯, (886.5*), **1300.8***, 1627.5*
254.5	202.5, 231.2, 218.9*, 255.6, **371.8***, 381.2*, **436.4***, **539.5***, **687.0***, 710.8*, 742.3*, **849.2***, **888.0***, 1300.8*, 1341.6*, 1365.4*, 1627.5*
262.1	**539.5***, (608.9*), 629.8*, **642.8***, 687.0*, 700.7*, 836.2*, (883.8*), 961.9*, 1479.1*, 1523.2*
384.2	(175.8*), 360.3*, **539.5***, 545.2+, **687.0***, (1221.7+), **1300.8***
582.8	152.6*, 191.9*, **539.5***, **687.0***, **849.2***, 984.4*, **1175.8***
642.8	203.6*, **246.0***, **262.1***, (440.1), 488.7*, **539.5***, **687.0***, **700.7***, 740.2*, 757.2+, 787.4+, 822.7*, **836.2***, **844.5***, 871.0*, (905.2), 953.4*, 1362.2*, **1523.2***
695.8	306.8+, **350.1+**, 502.0+, 518.9*, **539.5***, 654.8*, 687.0*, 720.0+, 822.7*, 869.7*, 999.5*, **1341.6***, 1362.2*
709.4	(166.4*), 354.1*, 440.4, **478.5***, **539.5***, **687.0***, 765.0*
765.0	**539.5***, **687.0***, (700.7*), **709.4***, (722.7*), 803.3*, **849.2***, 953.4*, 1558.8*
830.4	148.7*, 187.8*, 364.1*, 391.0*, 424.8*, 431.9, 443.3*, 460.0*, **475.1+**, **539.5***, 551.9*, **631.4***, **636.5***, **647.8***, 660.4*, **687.0***, 722.7*, 727.3*, **732.5***, 766.8+, 849.2*, 875.9*, 1300.8*
858.1	424.8*, **539.5***, 655.5+, **687.0***, 710.8*, 727.3+, 1341.6*, 1365.4*, (1627.5*)
944.0	301.6*, 338.8*, 391.0♯, 403.1♯, 436.4♯, **539.5***, **1627.5***, (2166.6*)
999.5	**539.5***, **687.0***, **695.8***, 1341.6*, **1350.4***
1325.6	(216.3), **301.6***, **539.5***, 678.5*, (824.7), **875.9***
1371.0	129.9*, **539.5***, **687.0***, **849.2***, 896.8*, 935.4*
1479.2	(218.9*), 246.0*, **262.1***, **539.5***, 558.0*, **687.0***, 742.3♯, **844.5***, 871.0*
1627.5	247.9*, 254.5*, **360.3***, 371.7*, 391.0*, **403.0***, **424.8***, 436.4* **539.5***, 580.5* 598.1*,612.1*, 944.0*

[a] A semi-quantitative judgement about the strength of the coincidences is given: bold print means the intensity of the γ-ray in coincidence is strong or very strong, parentheses indicate questionable evidence, an asterisk signifies that the transition has been placed in the level scheme, ♯ and + mean a contaminating coincidence from another line pertaining to ^{100}Ru and to a different nucleus, respectively.

The shapes of the excitation functions were used to assign the transitions to a particular nucleus; in addition, the coincidence relations gave complementary means indentifying unambiguously the γ-rays belonging to ^{100}Ru. The slope of the excitation functions provided an indication of the spin of the levels [17] (see Section 3.1.2).

2.1.2. Angular distribution

The Compton-suppression spectrometer with the above-mentioned 114 cm^3 Ge detector was used to record γ-rays spectra at eight angles between 25° and 90° with respect to the beam direction, at a distance of about 80 cm from the target. The normalization of the angular distribution was facilitated by the presence of a relatively strong and isotropic γ-ray of 787.4 keV due to Coulomb excitation in ^{98}Mo.

The experimental angular distributions were fitted using a least-squares procedure on the expansion

$$W(\theta) = A_0 + A_2 P_2(\cos\theta) + A_4 P_4(\cos\theta), \quad (1)$$

where $W(\theta)$ is the normalized peak area and P_k are Legendre polynomials. The determined coefficients $A_0(=I_\gamma)$, A_2/A_0 and A_4/A_0 are reported in Table 1.

2.1.3. The $\gamma\gamma$-coincidence experiment

Five high-purity germanium detectors equipped with BGO-NaI(Tl) Compton shields were used. They had volumes ranging from 83 to 130 cm^3 and were placed at a distance of 15 cm from the target. A layout of the experimental arrangement is shown in Ref.

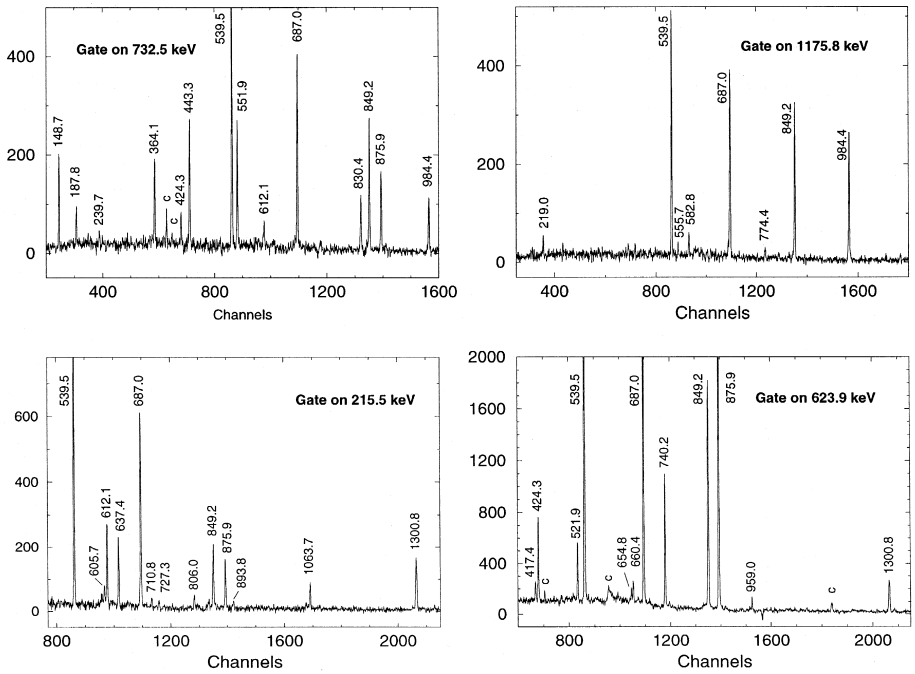

Fig. 2. Selected $\gamma\gamma$-coincidence spectra supporting parts of the proposed level scheme.

[18]. Times ($T_{i-\mathrm{RF}}$) relative to the frequency of the accelerator and energies (E_i) were recorded for each detector provided that the electronics registered coincident events within 150 ns. The data were recorded in list-mode on streamer tapes. The coincidence matrix was constructed off-line with more stringent conditions on the $T_{i-\mathrm{RF}}$ and $(T_{i-\mathrm{RF}} - T_{j-\mathrm{RF}})$ time differences.

The coincidence rate was about 250 Hz for a beam intensity of 3 nA. In total 4×10^9 events were recorded of which 8×10^8 satisfied the narrower off-line conditions. Table 2 lists results of several coincidence gates, and Fig. 2 shows a few coincidence spectra for illustration.

2.2. The thermal neutron capture experiments

2.2.1. Secondary transitions

Secondary γ-lines were measured with the curved crystal spectrometer GAMS2/3 [19] at the high-flux reactor of the Institut Laue-Langevin (ILL) in Grenoble, France.

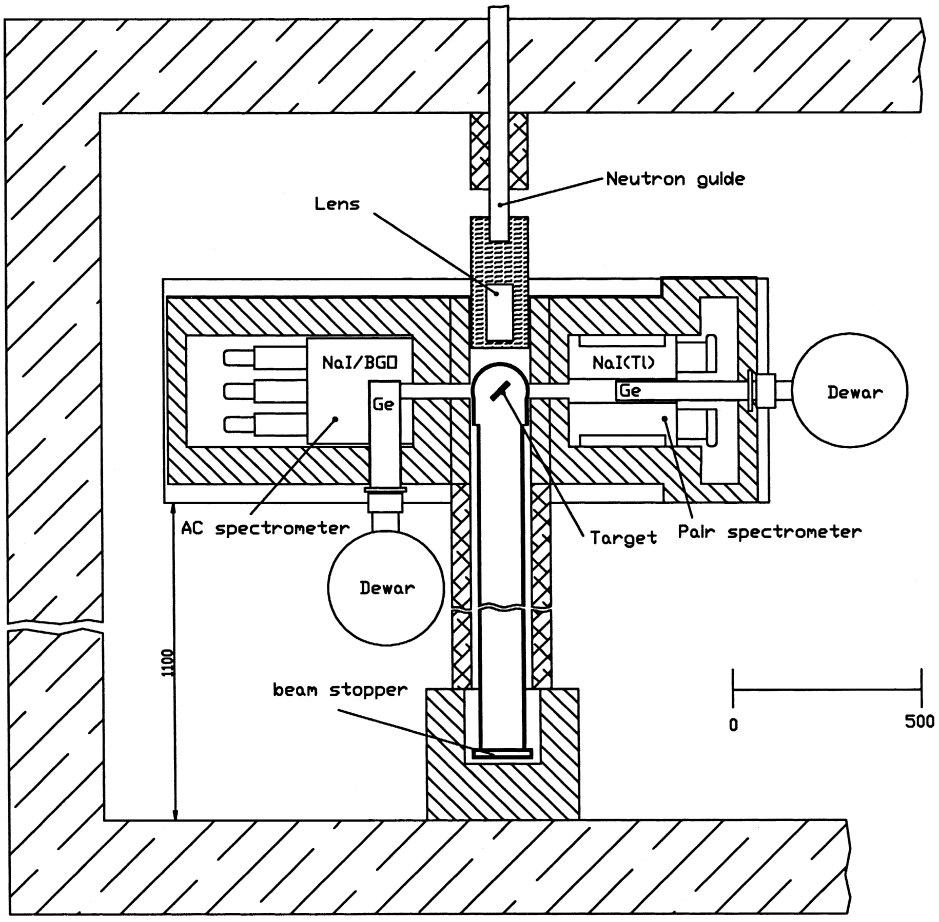

Fig. 3. Experimental arrangement of the PGAA installation at SINQ (PSI, Switzerland).

The target ($60 \times 4 \times 0.095$ mm^3) consisted of 79.9 mg ^{99}Ru enriched to 98.1%. The ruthenium powder was wrapped in an aluminium foil placed in a graphite container. The energy range from 200 keV to 2000 keV was measured stepwise. A resolution $\Delta E = 2.1 \times 10^{-6} E_\gamma^2 / n$ [E_γ in keV] corresponding to $\Delta E = 211$ eV in third order of reflection at 539 keV was obtained. In absence of trace elements in the target giving

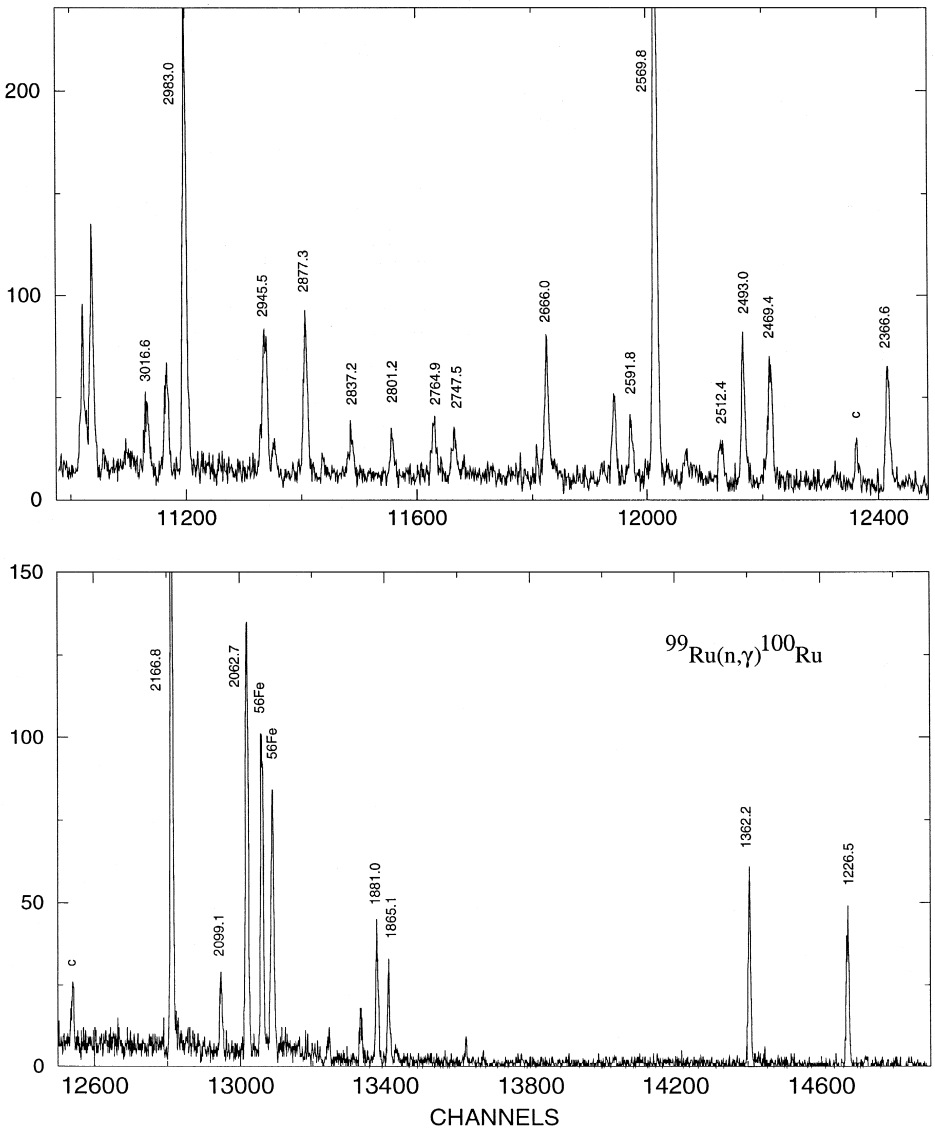

Fig. 4. Selected parts of the primary (n,γ) spectrum observed with the pair spectrometer of the PGAA installation at SINQ (Switzerland) The ^{100}Ru peaks are labelled by their corresponding level energies. Transitions from other known nuclei are labelled by the name of the isotope.

strong signals, the absolute energy calibration was performed using the 686.971(7) keV γ-line measured by Kenchian [10] in a study of the ^{100}Rh ϵ decay (20.3 h).

2.2.2. Primary transitions

This experiment was performed at the neutron spallation source (SINQ) of the Paul Scherrer Institut (PSI) in Villigen (Switzerland) which provides a cold-thermal neutron flux of 6.9×10^7 neutrons cm^{-2} s^{-1}. The target, containing 150 mg of Ru enriched to 98.1%, was pressed and encapsulated in a cylindrical teflon holder of 50 mm height and 3.5 mm in diameter. It was placed with the longer side parallel to the beam axis. The primary γ-rays were detected with a pair spectrometer consisting of a 25 cm^3 Ge detector placed inside the central hole of a cylindrical NaI(Tl) scintillator of 254 mm length and 254 mm in diameter. The scintillator was used to detect annihilation γ-rays pair; for this purpose it is divided optically into six slices. The resolution was 3.3 keV at 5 MeV and 4.2 keV at 9.1 MeV. A layout of the experimental arrangement is shown in Fig. 3; a more detailed description can be found in Ref. [20]. Portions of the spectrum are shown in Fig. 4. An absorber consisting of 6 cm thick copper and 1 cm thick lead

Table 3
List of the primary transitions from the ^{99}Ru(n,γ) reaction

E_γ [a] [keV]	I_γ [b] [$\gamma/10^4 n$]	Defined level [keV] [c]	E_γ [a] [keV]	I_γ [b] [$\gamma/10^4 n$]	Defined level [keV] [c]
9133.66(8)	18.1(4)	539.62	6926.26(18)	6.0(5)	2747.02
8446.95(8)	17.5(6)	1226.33	6908.55(15)	7.7(6)	2764.74
8311.15(7)	19.3(6)	1362.13	6871.87(20)	5.2(5)	2801.41
7808.29(11)	7.8(4)	1864.99	6835.81(19)	5.3(5)	2837.47
7792.13(9)	12.4(5)	1881.15	6811.39(61)	1.4(4)	2861.89
7610.60(7)	44.9(15)	2062.68	6795.79(9)	19.7(10)	2877.49
7574.31(16)	6.7(5)	2098.97	6768.01(27)	3.7(5)	2905.27
7506.46(6)	60.7(18)	2166.82	6757.40(34)	6.2(11)	2915.88
7432.49(82)	1.0(4)	2240.79	6690.30(6)	55.7(17)	2982.99
7306.57(9)	17.1(9)	2366.71	6673.94(11)	12.4(8)	2999.34
7259.86(50)	1.8(4)	2413.42	6656.57(15)	7.9(6)	3016.71
7203.68(9)	17.7(9)	2469.60	6639.35(43)	2.2(4)	3033.93
7180.28(9)	17.2(9)	2493.00	6608.76(7)	26.7(11)	3064.52
7160.94(19)	5.7(5)	2512.34	6562.78(14)	9.6(7)	3110.50
7136.89(46)	2.0(4)	2536.39	6554.66(41)	2.4(4)	3118.62
7129.92(26)	3.9(5)	2543.36	6496.27(23)	4.6(5)	3177.01
7103.41(5)	98.1(24)	2569.87	6441.54(16)	7.4(7)	3231.74
7081.57(15)	7.4(6)	2591.71	6407.02(31)	3.6(5)	3266.26
7066.98(26)	11.0(7)	2606.10	6401.20(28)	4.1(6)	3272.08
7056.66(61)	1.4(4)	2616.62	6372.72(7)	31.8(12)	3300.56
7013.63(46)	2.0(4)	2659.65	6365.26(13)	11.2(8)	3308.02
7007.31(9)	17.6(9)	2665.97	6347.07(7)	34.4(13)	3326.21
6934.26(51)	1.7(4)	2739.02	6340.94(5)	108.4(27)	3332.34

[a] γ-transitions energies corrected for nuclear recoil.
[b] The normalisation is based on the assumption that 95% of the ground-state population was observed; no uncertainty due to this absolute calibration is included in the intensity's error.
[c] Level defined by the primary γ-transition.

sheets was placed in front of the central detector to attenuate the lower-energy part of the γ-ray spectrum. Two different spectra were measured, one following the neutron capture of ^{99}Ru and melamine ($C_3H_6N_6$), the other from the ^{99}Ru(n,γ) reaction. Transitions following the ^{14}N(n,γ) [21] reaction and ^{100}Ru lines in the energy range from 1341 to 1865 keV were used for the energy calibration. The obtained primary γ-transition energies, corrected for nuclear recoil, are reported in Table 3, as well as their relative intensities. The intensities were normalized per 10000 captured neutrons based on an estimate that 95% of the ground-state population was observed. The excitation energies of the levels populated by primary γ transitions are also listed.

A neutron focusing lens [22] was placed before the target in order to enhance the neutron flux on the target. This lens is formed of a large number of polycapillary fibres parallel to the axis of the neutron beam at its entrance, and then curved in such a way that they converge towards a focal point. This device is primarly used in prompt gamma activation analysis to make two-dimensional scanning of samples; but it is also useful to increase the reaction rate, particularly when the cross section of the target is weak and the amount of available target material small.

The spectra were recorded over 6 h intervals for a 6 d period; the first 3 d with the focusing lens and the rest without it in order to assess the performance of the lens in standard nuclear experiments. The use of the focusing lens enhanced by a factor 6.4 the surface of the peaks while the peak to background ratio remained unchanged. Higher enhancements would be expected if the diameter of the target were smaller, i.e. closer to the size of the focused beam.

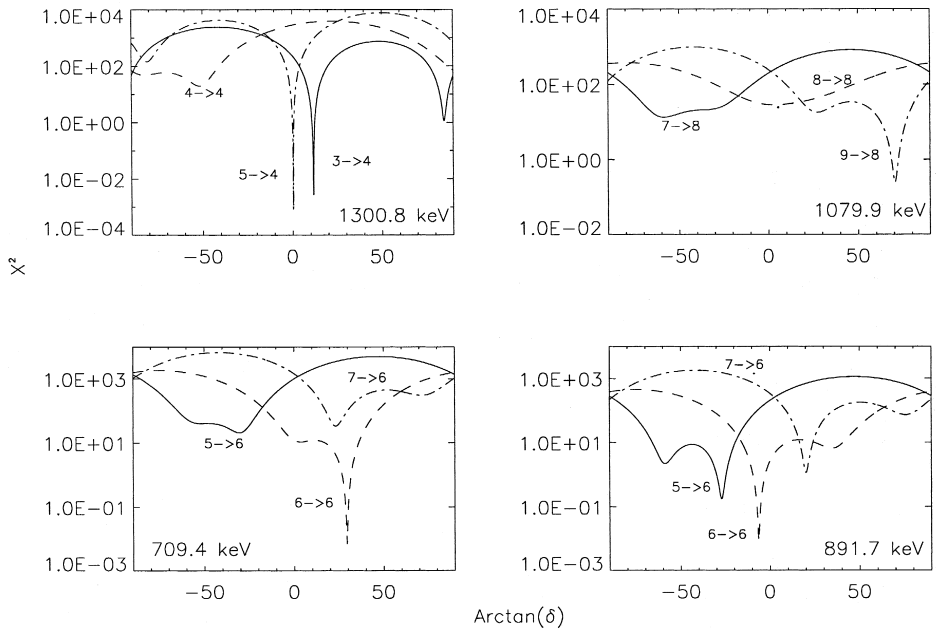

Fig. 5. Analysis of the angular distribution of a few transitions in ^{100}Ru. χ^2 is calculated for the three possible spin sequences as a function of arctan(δ).

Table 4
Levels of ^{100}Ru; above 2.7 MeV, only the levels observed in our experiments are listed

E_{exc} [keV]		Observed in experiment [c]	I^{π} [d]	Slope [e]	I^{π}_{dd} [f]	$I^{\pi}_{\alpha 2n}$ [g]	$I^{\pi}_{n,\gamma}$ [h]	I^{π} [i]	Comments
This work [a]	Previous [b]		Previous	SL				adopted	
0.0	0.0	ABCDEFGHIJKLMNO	0^+					0^+	
539.504 (12)	539.506 (5)	ABCDEFGHIJKLMNO	2^+	0.0	2^+	2^+		2^+	E2 to 0^+
1130.344 (23)	1130.297 (7)	AB DEF H JKLMN	0^+					0^+	
1226.472 (18)	1226.475 (7)	BCDEF HIJKL N	4^+	1.7 (2)	4^+	4^+		4^+	E2 to 2^+
1362.180 (16)	1362.161 (6)	ABCDEF HIJKLMNO	2^+	−8.5 (3)	2^+	2^+		2^+	E2 to 0^+
1740.98 (9)	1740.988 (11)	AB DEF KL N	0^+					0^+	
1865.12 (4)	1865.103 (6)	AB DEF H L N	2^+	−11.6 (10)	2^+	2^+	2^+	2^+	E2 to 4^+
1881.114 (20)	1881.040 (6)	BCDEF H K	$(3)^+$	−6.4 (2)	3^+	3^+		3^+	j
2051.60 (22)	2051.650 (7)	AB EF L	$0^{(+)}$					0^+	
2062.682 (34)	2062.52 (3)	C EF H	$(3^-,4^+)$	−3.3 (3)	4^+	4^+		4^+	E2 to 2^+ j,k
	2075.1 (5)	C F	(4^+)						
2075.703 (27)	2076.1 (3)	CDEFGH	6^+	4.5 (1)	6^+	6^+		6^+	E2 to 4^+
2099.11 (18)	2099.104 (8)	AB EF K	$(2)^+$				2^+	2^+	j
	2131.	KL	$2^+,3^+$						
2166.950 (22)	2166.869 (6)	B EF HIJ O	3^-	−6.7 (3)	3	3	$2^+,3^-$	3^-	
2240.80 (15)	2240.805 (9)	AB EF	$(1,2)^+$						j
	2268. (5)	K	$2^+,3^+$						
	2313.5 (3)	C	$(2^+,3,4^+)$						j,l
	2324.6 (4)	C	$3 \rightarrow 6$						j,l
2351.339 (30)	2351.4 (4)	F L	$2^+,3,4^+$	−8.0 (6)	4^+	4^+		4^+	j
2366.62 (5)	2366.50 (4)	C E L O	$(4)+$	−7.7 (5)	4^+	4^+		4^+	E2 to 2^+
	2387.17 (3)	AB E KL	$(0)^+$						
2413.72 (12)	2411.8 (2)	EF	$1 \rightarrow 4$	−6.3 (10)	$2,3,4^+$		$3^+,4^+$	$3,4^+$	j
	2438. (5)	K	$2^+,3^+$						
2469.36 (8)	2469.383 (6)	B EF	2^-		2	2	$2^-,3$	2^-	
2493.02 (4)	2492.89 (4)	E	$2^+,3,4^+$	−8.2 (17)	$3^+,4$	$3^+,4$	4^-	4^-	j
2512.52 (5)	2512.45 (5)	B E K	$(^+)$	−5.3 (11)	2,3,4	(4^+)	$3,4^+$	4^+	
2516.817 (20)	2516.820 (6)	B EF	$(1,2)^-$					$(1,2)^-$	
2527.275 (19)	2528.2 (2)	F H	5^-	0.8 (1)	5^-	5^-		5^-	E2 to 3^- j,m
2536.27 (12)	2536.17 (3)	B E	$2^+,3,4^+$	−11.4 (17)	$3^{(+)}$		$3^+,4$	3^+	

2543.59 (8)	2543.70 (3)	B E K	$(1,2^+)$	−16.3 (26)	$2,4^+$	2	1,2	2	j
2569.92 (4)	2569.91 (8)	B EF L	$(3,4^-)$				3^-	3^-	j
2576.88 (3)				−2.2 (5)	5^+	5^+		5^+	j
2591.893 (23)	2591.85 (4)	EF	$(2^+,3^-)$	−4.4 (16)	4^-	4^-		4^-	j
2606.10 (8)							(2,3,4)		
2617.33 (6)	2617.09 (4)	B K	$(1,2^+)$				$1,2^+$		
	2634. (10)	K	≤ 5						
2660.03 (3)	2660.13 (2)	E	(1,2)				1,2		
2660.93 (5)	2660.66 (4)	E	$(2^+,3,4^+)$	−2.0 (7)	5^+	5^+		5^+	E2 to 3^+
2666.15 (7)	2666.45 (6)	B EF	$(1^+,2,3^+)$				(3,4)		
2705.57 (4)	2695.	KL	$(1 \rightarrow 7)$	1.4 (3)	6^+	6^+		6^+	E2 to $4^{+\,j}$
2738.68 (3)							(3,4)		
2747.54 (5)	2747.17 (6)	dEF	$(2 \rightarrow 5)$	−9.1 (10)	3,4	$4^{(-)}$		$4^{(-)}$	j
2764.93 (3)	2764.87 (6)	dEF K	$(2^+,3^+)$	−9.6 (8)	2,3,4	$3^+,4$	4^-	4^-	
2775.21 (3)				−6.2 (3)	5,6	5^-		5^-	j
2775.48 (2)	2775.24 (9)	B dEF KL	$(2^+,3^+)$				$2^+,4^+$		
2785.25 (4)				−2.7 (5)	6^+	6^+		6^+	E2 to 4^+
2801.23 (3)	2801.49 (4)	B EF					$3^+,4^+$		
2837.24 (5)	2837.83 (10)	A E	$(0^+,1^+,2^+)$				$3,4^+$		
2861.73 (5)							$3,4^+$		
2877.45 (9)	2877.49 (10)	EF K	$(2^+,3^+)$	−1.7 (15)	3		$3^+,4$	3^+	
2905.07 (3)							$3,4^+$		
2911.50 (3)				−7.1 (7)	$5,6^+$	5^-		5^-	
2915.54 (3)	2915.54 (6)	B EF	2^-				2,3	2^-	
2951.588 (20)	2952.7 (3)	H	7^-	6.2 (1)	7^-	7^-		7^-	(E2 to 5^+) [m]
2963.682 (21)	2964.8 (3)	H	6^-	3.1 (2)	6^-	6^-		6^-	E2 to 4^- [m]
2967.60 (5)				−2.9 (8)	6^+	6^+		6^+	E2 to 4^+
2983.04 (3)	2983.25 (10)	EF K	$(1^+ \rightarrow 4^+)$				3^-	3^-	
2999.41 (3)							3,4		
3016.67 (3)	3016.67 (11)	EF					(4^-)		

(continued on next page)

Table 4 (*continued*)

E_{exc} [keV]		Observed in experiment [c]	I^{π} [d]	Slope [e]	I^{π}_{dd} [f]	$I^{\pi}_{\alpha 2n}$ [g]	$I^{\pi}_{n,\gamma}$ [h]	I^{π} [i]	Comments
This work [a]	Previous [b]		Previous	SL				adopted	
3060.118 (20)	3062.2 (3)	d GH	8^+	9.3 (1)	8^+	8^+		8^+	E2 to 6^+ [m]
3064.45 (3)							3,4		
3110.50 (3)	3110.9 (2)	EF K	$(2^+,3^+)$		2,3,4	4	3,4	4	
3118.71 (8)							$3,4^+$		
3139.32 (3)	3140.4 (3)	H	7^-	4.5 (3)	7^-	7^-		7^-	E2 to 5^- [m]
3177.24 (5)	3178. (10)	K	$2^+,3^+$				(4^-)	(4^-)	
3218.17 (3)				−4.1 (9)	$4^-,8^-$	8^-		8^-	E2 to 6^-
3263.70 (3)	3265.1 (4)	GH	(8^+)	4.7 (2)	8^+	8^+		8^+	E2 to 6^+ [m]
3300.67 (5)	3300.67 (10)	EF K	$(2^+,3^+)$				3^-	3^-	
3326.14 (4)	3326.3 (1)	EF					$3,4^+$		
3332.55 (3)	3332.6 (1)	EF					4^-	4^-	
3354.697 (25)	3356.0 (3)	H	8^-	7.4 (1)	8^-	8^-		8^-	E2 to 6^- [m]
3369.01 (5)				−0.8 (4)	7	7^-		7^-	[j]
3446.57 (5)				−1.1 (9)	7^+	7^+		7^+	E2 to 5^+
3503.43 (3)	3504.6 (3)	H	9^-	11.3 (1)	9^-	9^-		9^-	E2 to 7^- [m]
3550.15 (4)				5.9 (6)	8^+	8^+		8^+	E2 to 6^+
3575.58 (3)	3576.9 (4)	H	$(7,9)^-$	8.8 (21)	9^-	9^-		9^-	E2 to 7^- [m]
3576.44 (6)				−1.1 (15)	$6,7^+$	7^+		7^+	[j]
3599.34 (3)				5.6 (4)	8	8^-		8^-	[j]
3610.02 (8)				−4.2 (38)	$6,7^+$	7^+		7^+	
3661.48 (13)				−8.1 (30)	$4^-,6^-$	6^-		6^-	
3851.49 (35)					5,6	5,6			
3929.59 (7)				−0.3 (15)	(8^+)	(8^+)		(8^+)	(E2 to 6^+)
3960.42 (4)				1.4 (16)	7,8,9	$(8^-),9^-$		$(8^-),9^-$	[j]
3992.21 (5)	3993.8 (3)	H	$(10)^-$	8.9 (4)	10^-	10^-		10^-	E2 to 8^- [m]
4075.95 (16)				3.0 (35)	8	8		8	
4083.37 (3)	4085.2 (5)	F	10^+	14.3 (2)	10^+	10^+		10^+	E2 to 8^+
4097.47 (8)				6.2 (11)	8,9	9^-		9^-	[j]
4230.65 (4)	4232.1 (4)	H	$(11)^-$	17.5 (5)	11^-	11^-		11^-	E2 to 9^- [m]

4235.89 (3)				12.3 (9)	10^-	10^-	10^-	j	
4235.90 (5)				12.7 (10)	$9,10^+$	10^+	10^+	j	
4248.56 (7)				6.0 (13)	7,8,9	9^-	9^-		
4315.80 (3)	4317.5 (5)	H	(9,11)	16.3 (3)	(11^-)	11^-	11^-	(E2 to 9^-)[m]	
4343.44 (13)				9.3 (21)	9^+	9^+	9^+	E2 to 7^+	
4353.42 (3)	4355.0 (10)	G	(10^+)	11.3 (4)	$9,10^+$	10^+	10^+		
4381.84 (11)				9.2 (15)	$7^+,9^+$	9^+	9^+		
4408.70 (7)					$9^-,10$	10^-	10^-		
4503.53 (4)				11.9 (60)	$9^+,10^+$	10^+	10^+		
4663.50 (6)				11.6 (13)	$10,11^-$	11^-	11^-		
4791.62 (5)				10.7 (15)	$9,10^+$	10^+	10^+		
4798.23 (4)	4799.6 (5)	H	(12^-)	18.8 (2)	12^-	12^-	12^-	E2 to 10^- [m]	
4818.62 (5)				11.5 (23)	$8^+,10^+$	10^+	10^+[m]		
4917.84 (7)	4920.4 (5)	GH	(12^+)	19.3 (9)	$10,11,12^+$	12^+	12^+		
5010.53 (5)				17.6 (6)	9,11	11^+	11^+		
5066.29 (5)				16.6 (10)	$9 \rightarrow 12^-$	12^-	12^-[m]		
5125.39 (13)	5129.2 (6)	H	$(10,11^+,12^+)$	17.1 (11)	$11,12^+$	12^+	12^+		
5162.36 (4)	5164.5 (5)	H	(13^-)	22.3 (5)	$12,13^-$	13^-		13^-	m
5274.73 (15)	5279.6 (6)	H	$9 \rightarrow 13$	16.9 (16)	$11,12,13^-$	13^-		13^-	m
5713.14 (9)	5715.9 (6)	GH	(14^+)	18.8 (7)	14^+	14^+		14^+	m

[a] The excitation energies were calculated using a least-squares procedure involving all transitions placed in the level scheme.
[b] According to Ref. [6].
[c] The levels have been observed in other experiments (see Ref. [6]) denoted as: A = ^{100}Tc β^- Decay (15.8 s); B = ^{100}Rh ε Decay (20.3 h); C = ^{100}Rh ε Decay (4.6 min); D = ^{99}Tc(^{3}He,d); E = ^{99}Ru(n,γ) E = th; F = ^{99}Ru(n,γ) E = res; G = ^{76}Ge(^{34}S,2α2nγ); H = ^{100}Mo(α,4nγ), ^{98}Mo(α,2nγ); I = ^{100}Ru(α,α'); J = Coulomb Excitation; K = ^{101}Ru(p,d); L = ^{102}Ru(p,t); M = ^{103}Rh(p,α); N = ^{100}Ru(n,n'γ), (n,n'); O = ^{100}Ru(p,p').
[d] According to Ref. [6].
[e] Computed from Eq. (2).
[f] Spins and parities obtained from the angular distribution analysis.
[g] Spins and parities determined from our (α,2n) experiments (see Section 3).
[h] Spin and parity assignment deduced from the (n,γ) experiment.
[i] Adopted values resulting from the combination of all experimental information.
[j] See discussion in the text (Section 3.4).
[k] This level does not exist.
[l] Doubtful level.
[m] Level energy in disagreement with Ref. [6,16,29], see discussion for the 2527.3 keV level (Section 3.4).

3. Data analysis and results

3.1. $^{98}Mo(\alpha,2n)$ experiments

3.1.1. Analysis of the angular distributions

Taras and Haas [23] and Ionescu et al. [24] suggested that the magnetic substate population after a light ion induced reaction is not purely Gaussian. This is motivated by the fact that a state is populated by (i) discrete transitions from parent levels and (ii) by the side feeding which is of statistical nature. Consequently, the contribution of the discrete γ-rays to the magnetic substate population is taken explicitly into account using disorientation coefficients, whereas the side feeding contribution is considered to be Gaussian, the variance parameter being σ. The σ-value was determined in ^{100}Ru by considering pure E2 transitions and found to be 1.6(2). This parameter was then used for the χ^2 analysis as a function of the mixing ratio δ and the initial spin (see examples in Fig. 5). In some cases when the χ^2 analysis gives more than one acceptable solution for δ, the one with the smallest absolute value is reported in Table 1. The spins and parities deduced from the angular distribution analysis are given in Table 4.

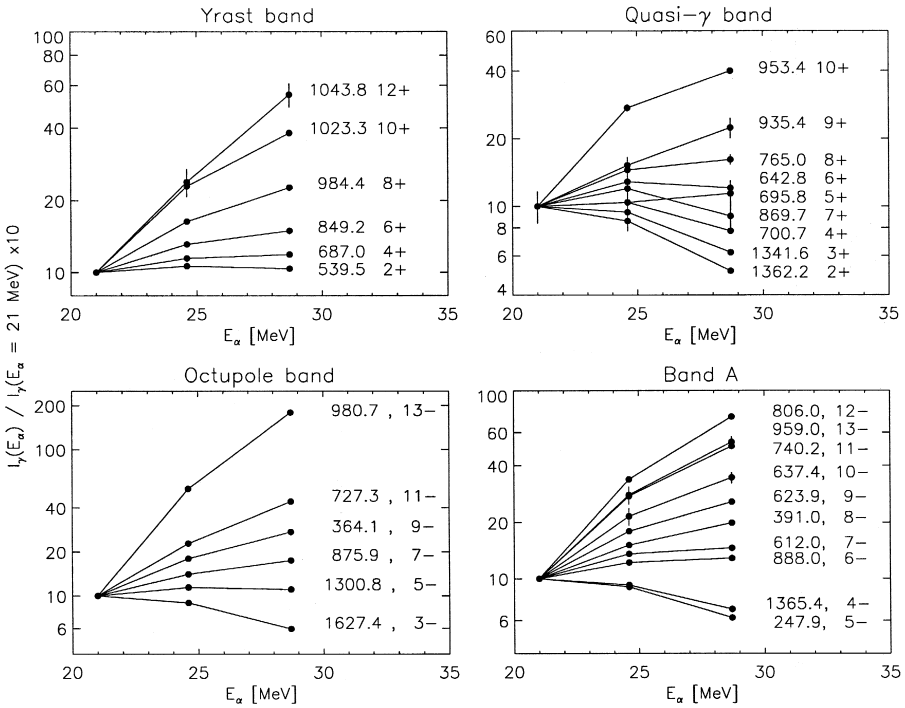

Fig. 6. Relative excitation functions of transitions pertaining to a band structure. The labels indicate the transition energy in keV and the spin and parity of the initial level.

3.1.2. Excitation function slopes

The excitation function slope *SL* is defined [17] by

$$SL = \frac{200}{E_2 - E_1}\left(\frac{I_2 - I_1}{I_1 + I_2}\right), \tag{2}$$

where I_1 and I_2 are the γ-ray intensities measured at the α-particle energies $E_1 = 21.0$ MeV and $E_2 = 28.7$ MeV, respectively.

The total feeding intensity of a particular level in a fusion reaction depends on its excitation energy and spin as well as on the beam energy. As a consequence, the excitation function slopes of the depopulating transitions vary with the spin and energy of the initial level (see Figs. 6 and 7). The measured slopes are reported in Table 1 and in Table 5 for selected levels.

3.1.3. Side-feeding intensities

The side-feeding intensity is defined as the difference between the discrete depopulation and total population of excited states. It was found empirically [17] that there is a dependence of the side-feeding intensities on the spin and level energy. Later on it was shown [25] that this finding is supported by statistical-model calculations. Therefore,

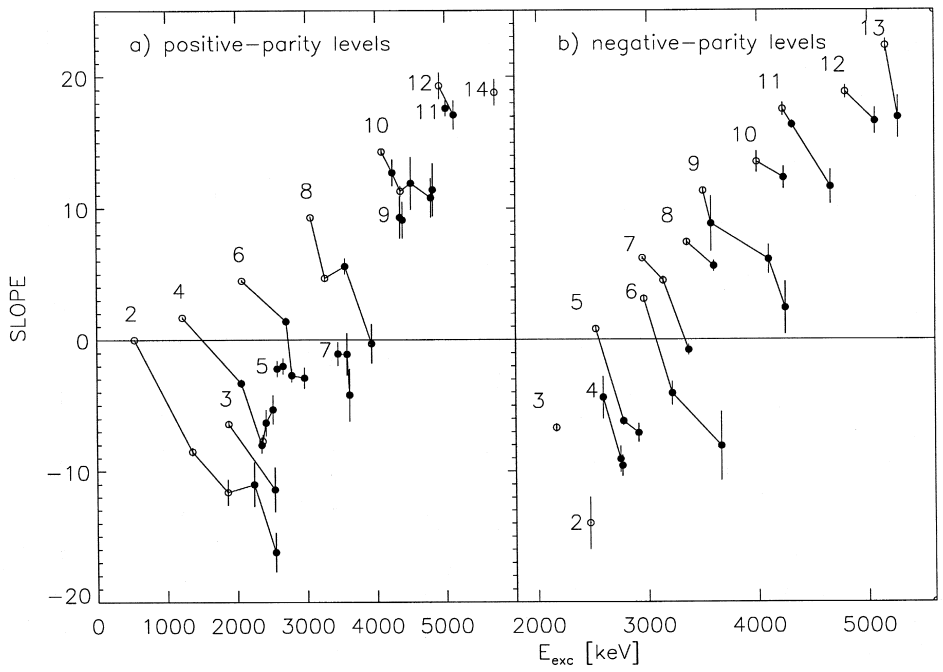

Fig. 7. Slopes of the excitation function computed using Eq. (2). The lines connect points representing levels with the same spins, indicated by the label. The open circles denote levels for which the assignment was known from previous works, the dots to levels assigned in this paper.

Table 5
Excitation function slopes of selected levels

Initial level		Transition	Slope [a]	Average slope
E_{exc} [keV]	I_i^π	E_γ [keV]	SL (ΔSL)	SL (ΔSL)
1865.1	2^+	1325.6	−11.7(13)	−11.6(10)
		1865.1	−11.5(15)	
2062.7	4^+	700.7	−4.1(19)	−3.3(5)
		836.2	−2.3(6)	
		1523.2	−3.7(4)	
2167.0	3^-	301.6	−8.4(18)	−6.8(3)
		1627.5	−6.8(3)	
		2166.6	−4.3(28)	
2527.3	5^-	360.3	1.2(7)	0.8(2)
		1300.8	0.8(2)	
2705.6	6^+	629.8	2.1(9)	1.4(3)
		642.8	1.9(5)	
		1479.1	1.0(4)	
2951.6	7^-	246.0	8.1(18)	6.2(4)
		424.3	5.2(6)	
		875.9	6.4(2)	
2963.7	6^-	371.8	3.2(4)	3.1(3)
		436.4 [b]	3.7(3)	
		888.0	2.8(2)	
3139.3	7^-	187.8	4.5(3)	4.4(2)
		612.1	4.2(3)	
		1063.7	4.2(6)	
3263.7	8^+	203.6	4.5(3)	4.7(2)
		478.5	5.9(13)	
		558.0	4.6(7)	
		1188.0	4.7(3)	
3503.4	9^-	148.7	11.8(3)	11.3(2)
		239.7	10.5(14)	
		364.1	11.4(3)	
		443.3	11.0(2)	
		551.9	11.2(2)	
3550.2	8^+	490.0	6.4(12)	5.9(6)
		765.0	5.5(10)	
		1474.4	5.9(11)	
4235.9	10^+	636.5	12.4(20)	12.4(7)
		732.5	11.0(10)	
		972.1	14.5(6)	
		1175.8	11.9(3)	
4798.2	12^-	567.5	19.5(24)	18.8(4)
		806.0	18.8(4)	

[a] The excitation function slope is calculated with the formula given in Section 3.1.2.
[b] γ-ray placed more than once.

another spin determination is obtained by comparing the measured side-feeding intensities with those of levels of known spin (see Fig. 8).

The angular distribution analysis, together with the excitation function slopes and the side-feeding intensities (ESSI-method) [17], provides a powerful method to assign the spins and parities, in most cases, unambiguously.

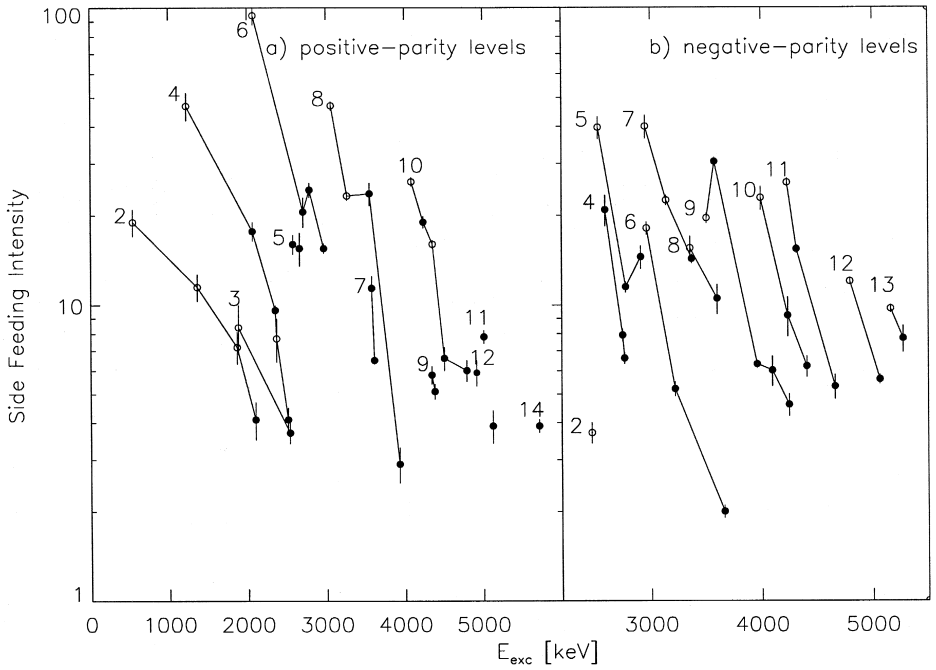

Fig. 8. Side-feeding population as defined in Section 3.1.3. The lines connect points representing levels with the same spins, indicated by the label. The open circles denote levels for which the assignment was known from previous works, the dots to levels assigned in this paper.

3.2. Neutron capture experiments

3.2.1. Data from the low energy (n,γ) experiment

Gamma rays following the ^{99}Ru(n,γ) reaction have been measured by Colvin et al. [7] using germanium detectors; the precision of the transition energies was never better than 60 eV. Through the use of a curved-crystal spectrometer the energy determination of numerous lines in the range from 170 to 1800 keV was substantially improved, resulting in a more detailed level scheme. Newly placed transitions (below 2.8 MeV) are reported in Tables 6 and 7, whereas the complete list will be published elsewhere.

3.2.2. Data from the high energy (n,γ) experiment

As this part of the spectrum has already been measured by Colvin et al. [7] and Islam et al. [8] using pair spectrometers, no new transitions were observed. However, the absolute intensity of the γ-rays listed in Table 3 differ by more than an order of magnitude with those given in Ref. [8]. In this latter paper, one can see that the summed intensity per 100 neutrons of the transitions above 6.2 MeV is larger than 100.

The separation energy of ^{100}Ru was determined using low energy (n,γ), (α,2nγ) transitions and a few strong primary transitions; it was found to be 9673.30 $\pm$ 0.03 keV which disagrees slightly with the values reported in Refs. [7,8], i.e. 9672.73 $\pm$ 0.06 keV

Table 6
Selected secondary transitions from the ^{99}Ru(n,γ) reaction with a new assignement

E_γ [a] [keV]	I_γ [b] [$\gamma/10^4 n$]	Level energy	E_γ [a] [keV]	I_γ [b] [$\gamma/10^4 n$]	Level energy
240.549(8)	5.58(45)	2591.8	778.980(14)	20.62(65)	2660.1
302.522(8)	6.07(40)	2469.4	857.621(12)	17.7 (21)	2738.7
329.058(12)	2.71(35)	2569.9	866.466(12)	24.1 (11)	2747.5
345.518(12)	4.28(65)	2512.4	872.71(5)	3.74(34)	2099.1
358.080(9)	3.98(35)	2099.1	873.66(5)	8.55(39)	2738.7
360.373(5)	14.37(91)	2527.2	878.55(9)	2.42(30)	2240.8
370.283(5)	7.85(81)	2469.4	882.63(16)	1.12(34)	2747.5
372.090(4)	8.02(36)	2738.7	968.80(5)	6.48(38)	2099.1
375.686(8)	4.59(26)	2240.8	1124.768(5)	130.1 (69)	2351.2
387.436(3)	8.85(26)	2738.7	1255.12(9)	11.9 (53)	2617.3
413.703(19)	2.67(21)	2764.9	1285.82(15)	10.7 (16)	2512.4
451.58(3)	2.98(25)	2527.2	1300.764(18)	219.5 (125)	2527.2
465.148(17)	5.39(35)	2516.8	1343.49(3)	108.8 (84)	2569.9
470.188(17)	3.04(29)	2351.2	1350.450(20)	31.9 (17)	2576.9
470.82(3)	5.93(70)	2569.9	1874.15(5)	104.8 (160)	2413.8
485.547(15)	5.94(78)	2366.7	2066.55(8)	74.2 (52)	2606.1
486.121(5)	9.82(47)	2351.2	2099.4(5)	9.6 (35)	2099.1
560.95(8)	4.80(49)	2660.1	2120.55(11)	39.3 (41)	2660.7
580.600(11)	36.3 (25)	2747.5	2543.5(3)	11.0 (23)	2543.7
655.156(12)	7.99(46)	2536.2	2617.32(12)	33.6 (32)	2617.3
676.071(21)	11.9 (11)	2738.7	2660.0(4)	8.9 (25)	2660.1
688.89(3)	7.31(58)	2569.9			
695.783(21)	25.5 (18)	2576.9			

[a] The absolute energy calibration has been performed using the 686.971(7) keV γ-transition [10]; the errors on the energy reported here do not take into account that from the reference line.
[b] The normalisation is based on the assumption that 95% of the ground-state population was observed; no uncertainty due to this absolute calibration is included in the intensity's error.

and 9673.48 $\pm$ 0.05 keV, respectively. Nevertheless, our result lies near to the weighted average of the two previous measurements.

Table 7
Set of (n,γ) transitions with precise energy values

E_γ [a] [keV]	I_γ [b] [$\gamma/10^4 n$]	Level energy	E_γ [a] [keV]	I_γ [b] [$\gamma/10^4 n$]	Level energy
301.769(1)	118.2(19)	2166.9	822.614(10)	700.4(240)	1362.1
403.013(10)	187.6(88)	2569.9	836.180(3)	159.6(26)	2062.6
424.874(18)	86.1(100)	2591.8	849.188(7)	144.1(32)	2075.7
539.508(2)	8764.(310)	539.5	1341.560(9)	640. (41)	1881.1
590.765(9)	261.1(170)	1130.3	1362.17(3)	477.3(240)	1362.1
631.393(20)	85.9(53)	2512.4	1365.416(12)	112.9(74)	2591.8
654.587(17)	90.9(54)	1881.1	1523.07(3)	153.9(81)	2062.6
686.972(3)	2982.(150)	1226.5	1627.35(4)	543. (37)	2166.9
710.771(3)	160.1(88)	2591.8	1827.16(4)	166.6(130)	2366.7
734.789(7)	125.1(31)	1865.1			

[a,b] See comments of Table 6.

3.2.3. Level scheme from the (n,γ) experiment

The level scheme established by Colvin et al. [7] was not strongly modified by our (n,γ) results. Consequently we do not list our complete results in this paper. However, the feeding by primary γ-rays from the capture state ($I^\pi = 2^+,3^+$) and the decay pattern deduced from our data allows one to restrict the spins for a few levels (see Table 1, column 8). A negative parity can be assigned when the level is populated by an intense primary transition, because this latter is then most probably of an E1 multipolarity.

3.3. Region of completeness from the present experiments

It is well known that a complete sets of levels in a restricted spin and excitation energy can be reached with the average resonance capture (ARC) method. This concept of complete spectroscopy has been extended to charged-particle fusion reactions [27]. In that paper, it was shown that the side-feeding population of all levels as a function of their excitation energy is regular and non-selective. The spin versus energy diagram for levels observed in the present experiments is shown in Fig. 9. The upper energy limit of the zone of completeness for a given spin is determined by considering the largest intensity of a transition assigned to ^{100}Ru but not placed in the level scheme [27].

From our (n,γ) measurements, a region of completeness cannot be determined, due to the well-known Porter–Thomas fluctuations.

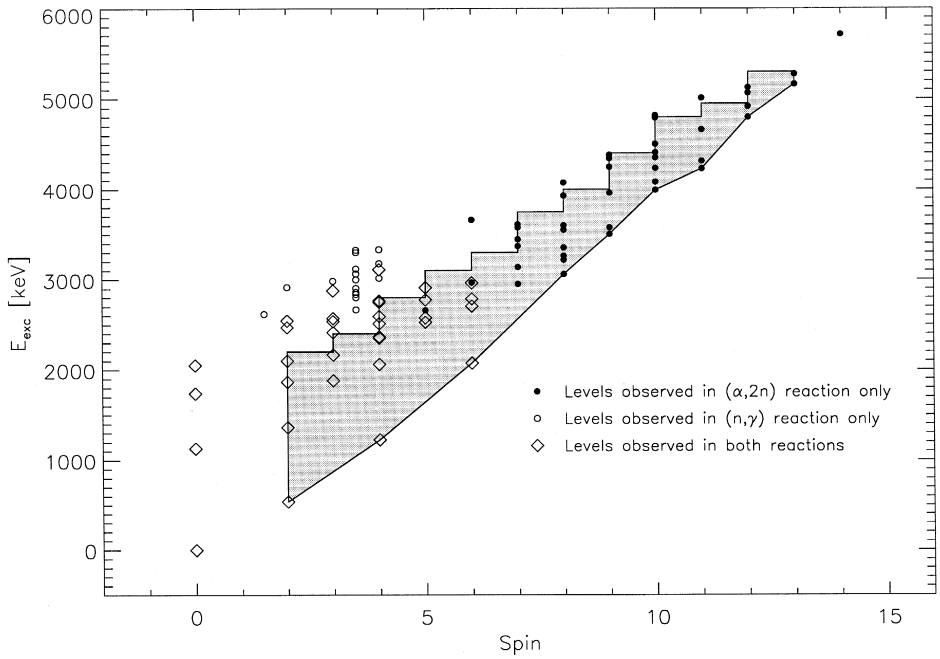

Fig. 9. Spin versus excitation energy diagram, the grey area represents the zone of completeness for ^{98}Mo(α,2n) reaction (see text).

3.4. Discussion of individual levels

In this section only those levels which present problems or where disagreements with precedent results are found will be discussed. Table 4 contains the complete list of levels established by the present experiments. Those observed in previous experiments up to 2.7 MeV are also listed for comparison. Figs. 10, 11, 12, 13 and 14 show the level scheme based on the analysis of the ^{98}Mo$(\alpha,2n\gamma)$ experiments.

1881.1 keV level: This level has been observed previously in several experiments. It decays by the following transitions: 1341.6, 654.8 and 518.9 keV. The parity was known to be positive but the spin value was not determined with certainty; Colvin et al. [7] proposed $I^\pi = 2^+$ whereas Giannatiempo et al. [28] favored the $I^\pi = 3^+$ assignment. The angular distribution analysis of each of the three transitions determines $I = 3$.

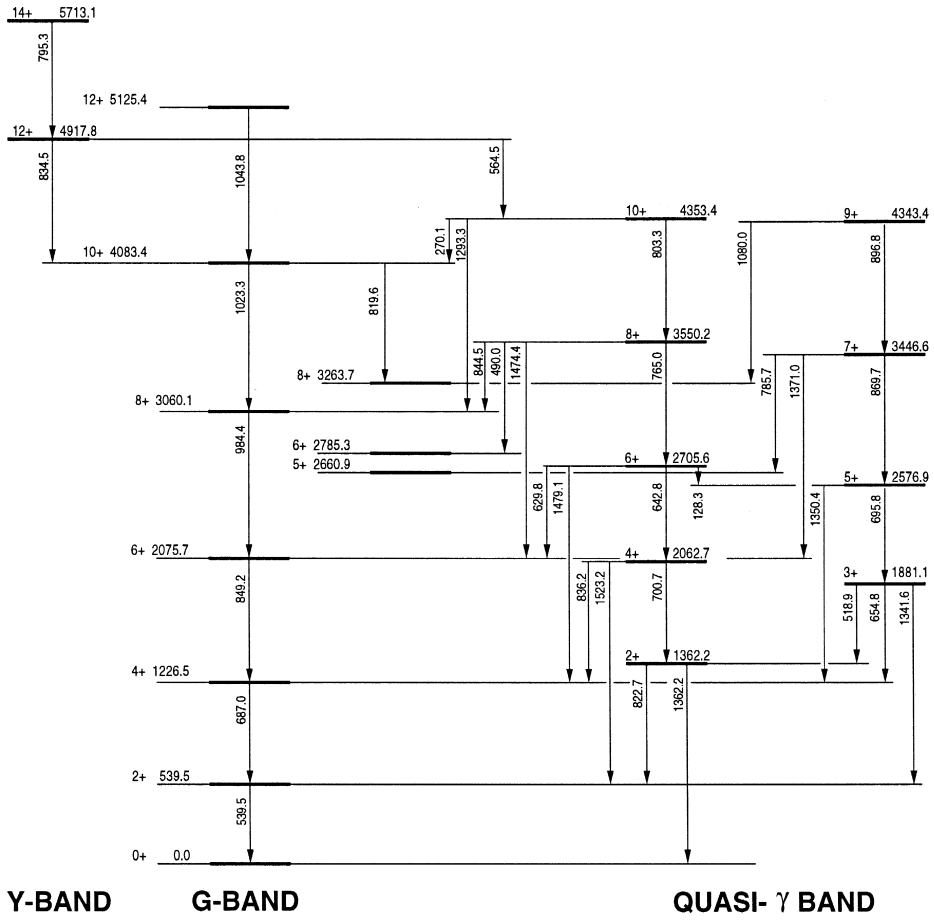

Fig. 10. Part 1 of the ^{100}Ru level scheme based on the analysis of the ^{98}Mo$(\alpha,2n\gamma)$ experiments showing states of positive parity bands. The adopted spin and parity are indicated for each level, values in parentheses indicate uncertain assignments.

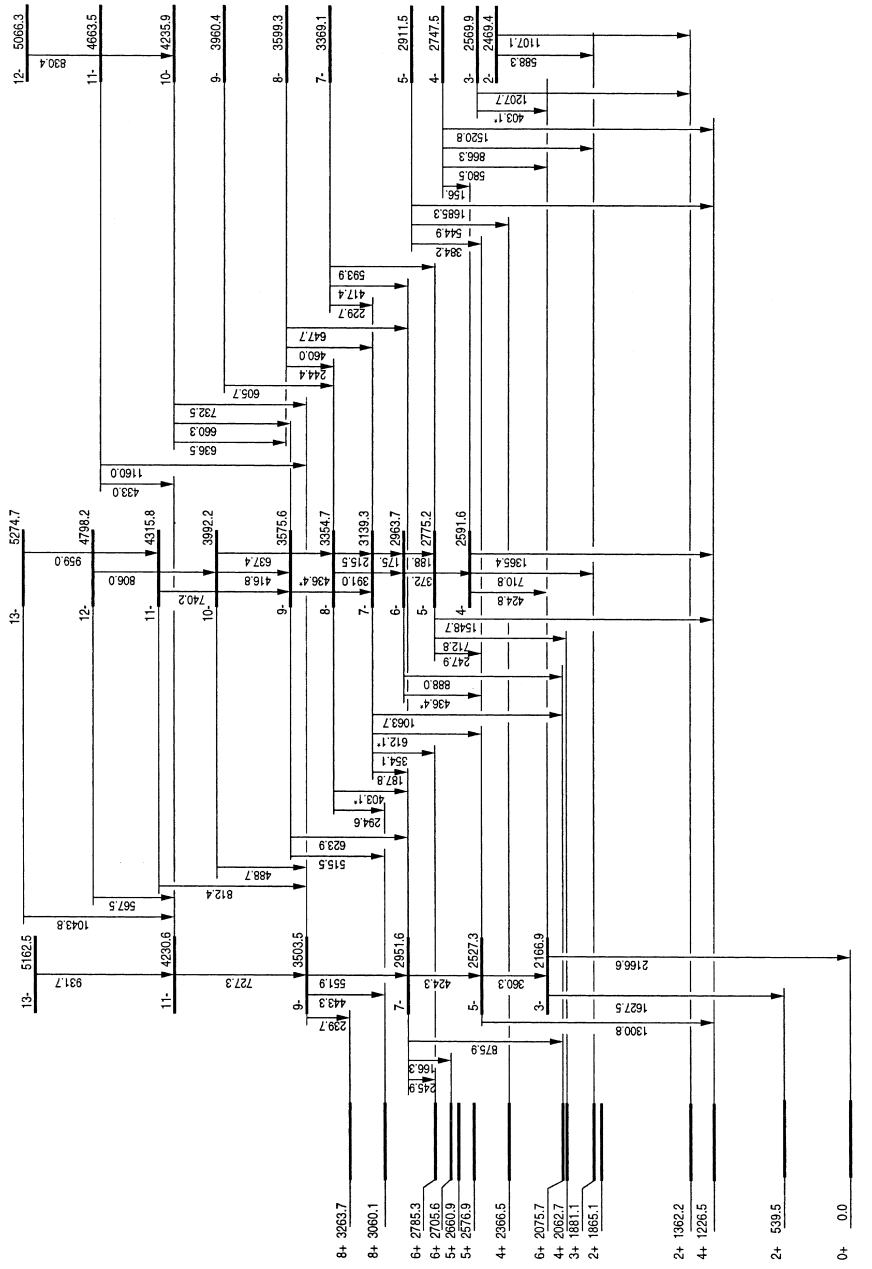

Fig. 11. Part 2 of the ^{100}Ru level scheme based on the analysis of the ^{98}Mo(α,2nγ) experiments. Same caption as for Fig. 10, but for negative-parity levels grouped in bands.

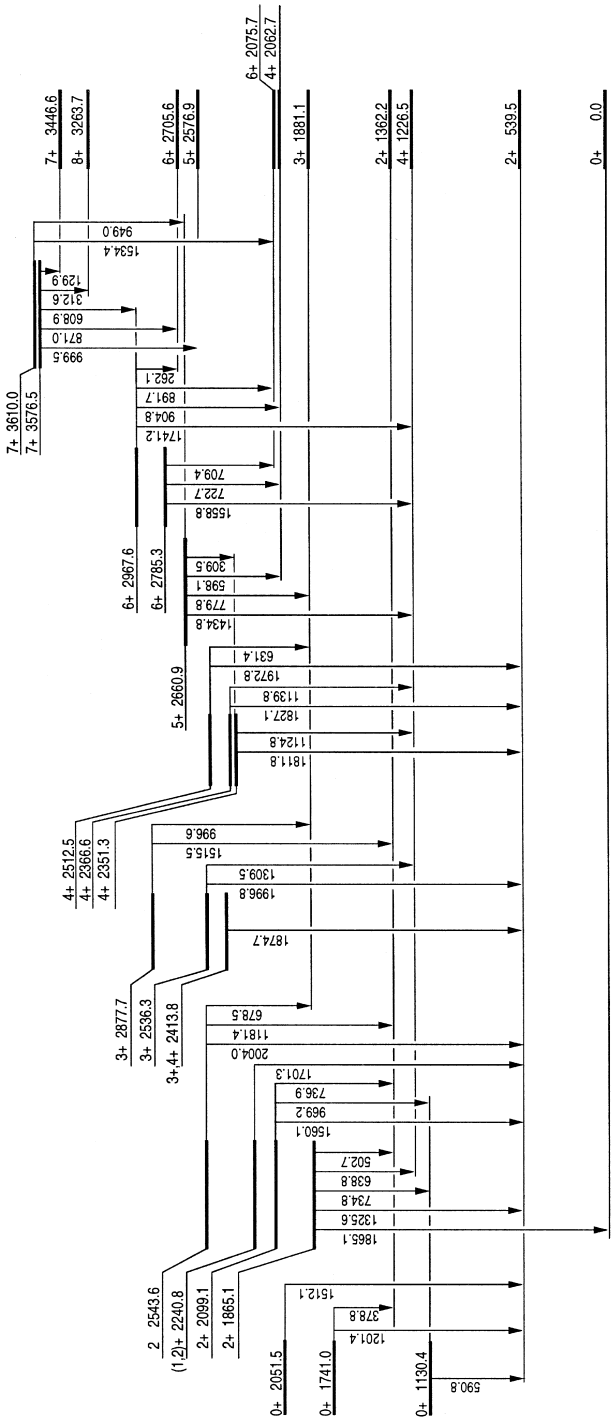

Fig. 12. Part 3 of the ^{100}Ru level scheme based on the analysis of the ^{98}Mo$(\alpha,2n\gamma)$ experiments. Same caption as for Fig. 10, but for other positive- (or presumably positive-) parity levels up to spin 7.

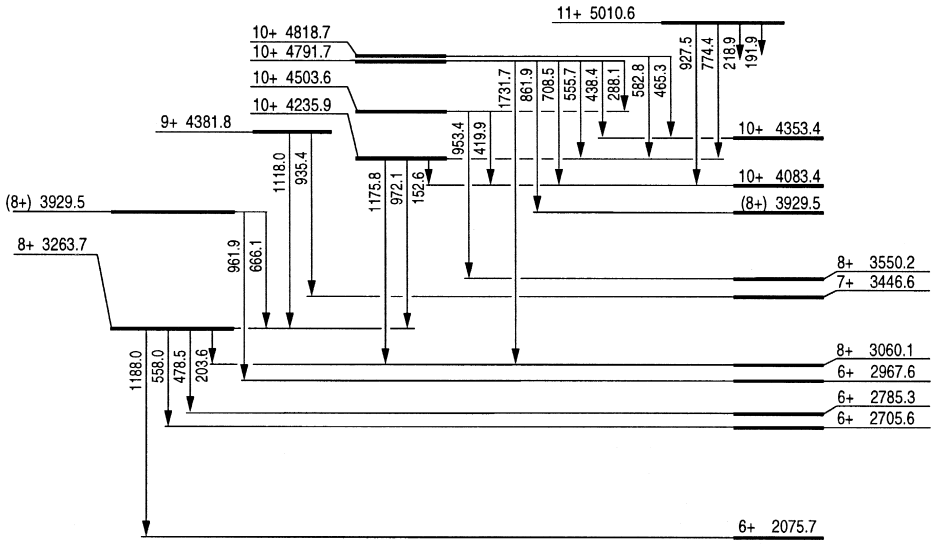

Fig. 13. Part 4 of the ^{100}Ru level scheme based on the analysis of the ^{98}Mo(α,2nγ) experiments. Same caption as for Fig. 10, but for other positive- (or presumably positive-) parity levels from spin 8.

2075.1 keV level: A tentative 2075.1 keV level, decaying by a single 1535.6(5) keV transition, has been proposed by Babenko et al. [11]. The evaluator of the compilation [6] has indentified this transition to the 1536.1(5) γ-line observed by Coceva et al. [9], which had not been placed in the level scheme. A γ-ray close to this energy shows

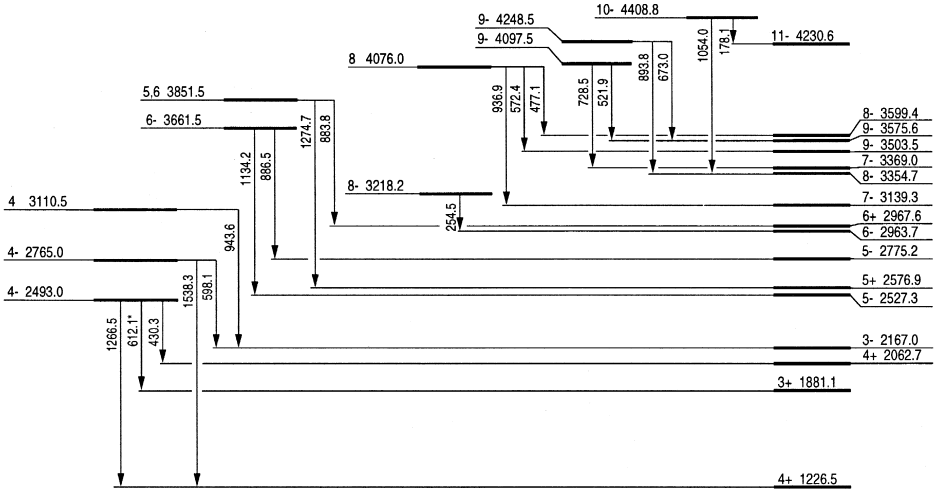

Fig. 14. Part 5 of the ^{100}Ru level scheme based on the analysis of the ^{98}Mo(α,2nγ) experiments. Same caption as for Fig. 10, but for other negative- (or presumably negative-) parity levels.

coincidence signals in the 687.0 keV gate implying its placement in the level scheme above 2760 keV. We consider this level as spurious.

2099.1 keV level: Of the six transitions known to depopulate this level, we observe all but one at 234.0 keV [10]. Its intensity is far below the sensitivity of our instruments used for both reactions. A new transition of 358.1† keV[2] can be placed, according to the Ritz principle, between the 2099.1 and 1741.0 keV levels. The decay pattern to states of positive parity and spin equal to 0,2 and 4 indicates an initial spin $I^\pi = 2^+$.

2131, 2268, 2438 keV levels: These levels were observed in pickup reactions by Peterson et al. [12] and were assigned spin 2^+,3^+. Despite our sensitivity to 2^+,3^+ states in this energy region, we have not observed these levels in the (n,γ) and $(\alpha,2n\gamma)$ experiments. We therefore consider the existence of these levels to be doubtful. It would be very interesting to redo the experiments of Ref. [12] to check whether these levels indeed do not exist.

2240.8 keV level: This level is observed to decay by three transitions of 375.7†, 878.6† and 1701.3 keV; it is fed directly by a 7432.5† keV transition. Two additional transitions of 1100.7 and 2240.1 keV were observed by Kenchian [6,10] with intensities far above and below the sensitivity threshold of our instruments, respectively. The intensity of the ground-state transition is very weak and its energy is not well determined; should this γ-ray exist and be correctly placed in the level scheme, then the spin of the state would be $I^\pi = 1^+,2^+$ [6].

2313.5 and 2324.6 keV levels: These levels were only observed in the ^{100}Rh ϵ decay (4.6 min) by Babenko et al. [11]. The five transitions proposed to depopulate these levels are either not observed in our experiments or placed elsewhere in the level scheme. Consequently they are considered as highly doubtful.

2351.3 keV level: It was observed by Coceva et al. [9]. Its decay proceeds via two γ-rays of 1124.8 and 1811.8 keV to levels of spin 4^+ and 2^+, respectively. The absence of a transition to the ground state and from the capture state together with the decay pattern of this level tends to indicate a spin of $I^\pi = 3^+,4^+$. $I^\pi = 4^+$ is suggested by the angular distribution analysis of the 1124.8 keV γ-ray and is in agreement with the value obtained from the population characteristics (ESSI).

2413.8 keV level: This level has been established by Coceva et al. [9], who observed that it decays by a 1873.9 keV transition to the 539.5 keV level. In Ref. [6], the evaluator proposes the level energy 2411.8(2) with the same decaying transition; this is a printing error. The application of the Ritz principle on the data from the (n,γ) experiment enables the placement of an additional transition of 1051.5† keV. The decay of this level to two states of spin 2^+ and its feeding by a transition of 7259.9† keV from the capture state indicates an initial spin $I^\pi = 3,4^+$.

2493.0 keV level: This level has been disclosed by Colvin et al. [7]; we observe three of the 4 depopulating transitions assigned to depopulate it, i.e. at 430.3, 612.0 (doublet) and 1266.6 keV. It appears that the fourth γ-ray of 627.8 keV is not originating from this level because, with the quoted intensity, it should be visible in the singles and/or in coincidence with the 1325.6 keV γ-ray (Table 2, 1325 keV gate). The absence of a

[2] γ-rays marked by a † are only seen in the ^{99}Ru(n,γ) experiment.

decay to any states with spin $I^\pi = 2^+$ and the feeding from the neutron capture state by a transition of 7180.3† imply a spin $I^\pi = 4^-$ for this level.

2527.3 keV level: This level was observed for the first time by Lederer et al. [13], who proposed two decaying transitions of 464.9 and 1301.2 keV. Using the same nuclear reaction, we have not observed the first γ-ray, which, with the reported intensity, should have been far above our sensitivity threshold. De Voigt et al. [29] observed only the second transition with an energy of 1301.6(3) keV; their energy calibration was not very accurate, resulting in an overestimation for a large set of transitions. One may observe the discrepancy between our energies and those from de Voigt et al. [29] marked by ^{m} in Table 4.

Our experiments show that the level is depopulated by two additional transitions of 175.8 and 360.3 keV. The last one is a stretched E2 transition decaying to the 3_1^- level, implying a spin and parity $I^\pi = 5^-$.

2543.6 keV level: The direct population by a primary transition and the presence of a ground-state transition favor $I = 1,2$. The excitation slope selects $I^\pi = 2$.

2569.9 keV level: This level is known to decay by transitions of 403.0, 470.8†, 1207.7, 1343.4, and 2030.3† keV. All but the 1343.4 keV transition were observed in the present experiments; the placement of the latter in the level scheme is doubtful since from its reported intensity in ^{100}Rh ϵ decay [10], it should have been seen in our experiments. Lederer et al. [13] place the 403.3 keV in the decay of the 3354 level; the strong coincidence signal of this γ-ray with the 148.7 and 1627.5 keV (see Table 2, 148 keV and 1627 keV gates) proves that it has a complex structure and supports this double placement.

The relatively weak intensities of the decaying transitions in $(\alpha,2n)$ experiments neither enable a reliable angular distribution analysis nor may statistical methods be applied. However, the direct population in (n,γ) experiments by a very strong primary transition indicates a negative parity for this state. The decay of this state to levels of spin $2^+,3^\pm,4^+$ determines $I^\pi = 3^-$.

2576.9 keV level: This new level decays by two transitions of 695.8 and 1350.4 keV (see Fig. 10). Both of them give clear coincidence signals (see e.g. Table 2, 695 keV gate). The stretched E2 multipole character of the 695.8 keV transition implies a spin and parity $I^\pi = 5^+$. This spin-value is also favoured by the angular distribution analysis of the 1350.4 keV γ-rays, the side-feeding intensity and the slope.

2591.9 keV level: This level was observed previously in (n,γ) experiments [7,9]. It was assigned as $I^\pi = 2^+,3^-$. Solely the three strongest transitions, out of the six proposed, were observed in the present $(\alpha,2n)$ experiments (see Fig. 11). The analysis of the angular distribution of the three γ-rays indicates that this level has a spin $I = 4$. The absence of decay to any levels of spin 2^+ and the feeding by a moderately strong primary γ-ray determine a negative parity.

2705.6 keV level: A level at 2695(10) keV was disclosed by Seltz et al. [26] using transfer reactions. It decays by four transitions of 128.3, 629.8, 642.8 and 1479.1 keV. The latest two give clear coincidence signals (see Table 2, 1479 keV and 642 keV gates) and show a stretched E2 multipole character which implies an initial spin and parity $I^\pi = 6^+$.

2747.5 keV level: This level is reported in Refs. [7,9] to decay by one transition of 1520.6 keV. The present coincidence data allow the placement of three additional γ-rays

of 155.7, 580.6 and 866.3 keV. Due to the relatively low intensity of these transitions, their A_2 coefficients are not reliable, and thus no angular distribution analysis was possible. But the spin and parity of the final levels, namely $I = 3^{\pm},4^{\pm}$, restrict the spin-value range for the initial level to $I = 3,4$. The side-feeding intensity and the slope both select $I = 4$ and the absence of any transition to 2^+ states makes a positive parity improbable. The experiments determine consequently $I^{\pi} = 4^{(-)}$.

2775.2 keV level: This level is reported to decay by one transition of 1548.7 keV to the 4_1^+ level and to be fed by a primary γ from the neutron capture state. Two additional transitions of 247.9 and 712.8 keV can be placed which feed spin 5^- and 4^+ levels, respectively. The angular distribution analysis indicates an initial spin $I^{\pi} = 5^-$; this value is well supported by the side-feeding intensity and the slope.

3369.0 keV level: This new level decays by three transitions of 229.9, 417.4 and 593.9 keV. The first two give clear coincidence signals (see Table 2, 229 keV gate). The angular distribution analysis of the three γ-rays select $I = 7$. This result is confirmed by the slope and side-feeding intensity. The δ-value of the 417.4 keV transition is different from zero (see Table 1), which implies a mixed $M1/E2$ multipole character and consequently a negative parity of the initial state.

3576.5 keV level: This new level is observed to decay by four transitions of 129.9, 312.6, 871.0 and 999.5 keV. The angular distribution of the 999.5 keV line can be fitted either as quadrupole (implying thus $I^{\pi} = 7^+$) or as dipole (leading to $I = 5$). The 312.6 keV transition to a 8^+ state forbids an initial spin-value of 5; the slope and the side-feeding intensity favor $I = 7,(8)$. The experiments determine therefore $I^{\pi} = 7^+$.

3599.3 keV level: This new level is depopulated by four transitions of 244.4, 381.2, 460.0 and 647.8 keV. The angular distribution analysis of the last two γ-rays leads to an initial spin $I = 8$. This result is confirmed unambiguously by the slope and side-feeding intensity. Since the observed δ-value of the 647.8 keV line is different from zero (see Table 1), implying a mixed $M1/E2$ multipole character, the parity of the level is negative.

3960.4 keV level: This new level is de-excited by two transitions of 605.7 and 742.3 keV which both populate $I^{\pi} = 8^-$ states. From the analysis of the angular distribution, the three solutions $I = 7,8,9$ are acceptable. The side-feeding and the slope indicates 9^- (or possible 8^-).

4097.5 keV level: This new level decays by two transitions of 521.9 and 728.5 keV. The angular distribution analysis indicates that the two values $I = 8,9$ are possible. The slope and side-feeding intensity favour the upper spin value. Since the observed δ-value of the 521.9 keV γ-ray is not compatible with zero (see Table 1), the parity of the initial state must be the same as the final state; consequently $I^{\pi} = 9^-$.

4235.89 and 4235.90 keV levels: These new levels are very close in energy. Nevertheless, they can be resolved due to different coincidence relations involving the depopulating transitions (see Table 2, 583 keV and 830 keV gate).

The *gamma*-rays 636.5, 660.3 and 732.5 keV depopulate the 4235.89 keV level. The angular distribution analysis of the largest energy γ-ray determine $I^{\pi} = 10^-$. This value is well supported by the side-feeding intensity and the slope.

The other state is observed to decay by three transitions of 152.6, 972.1 and 1175.8 keV. The analysis of the angular distribution selects $I^{\pi} = 9,10^+$. The ambiguity is removed by the slope and side-feeding intensity which determine $I^{\pi} = 10^+$.

† γ-ray only seen in the ^{99}Ru(n,γ) experiment.

4. Interpretation of the results

4.1. Pure U(5) dynamical symmetry

^{100}Ru is one of the nuclei selected in a survey searching for nuclei exhibiting the U(5) dynamical symmetry [3]. The Hamiltonian in this limit of the IBM is written

$$\hat{H} = \epsilon \hat{C}_1[U(5)] + \alpha \hat{C}_2[U(5)] + \beta \hat{C}_2[O(5)] + \gamma \hat{C}_2[O(3)], \qquad (3)$$

where $\hat{C}_i (i = 1,2)$ are the Casimir operators of the ith order of each group forming the U(5) limit. The eigenvalues of the operator (3) are given by the following analytical expression:

$$E = \epsilon n_d + \alpha n_d(n_d + 4) + \beta\nu(\nu + 3) + \gamma L(L + 1), \qquad (4)$$

where the quantum numbers n_d and ν are the number of d-bosons and the d-boson seniority, respectively. L represents the total angular momentum of the state. To adjust the free parameters $\epsilon, \alpha, \beta, \gamma$, a least-squares fit, using the expression (4), to the experimental excitation energies was performed. The solution yields the four parameters $\epsilon = 602.0$ keV, $\alpha = 0.5$ keV, $\beta = -4.3$ keV and $\gamma = 10.8$ keV. The comparison of the resulting fit denoted by Th. I with the experimental levels pertaining to the normal configuration is shown in Fig. 15. The levels connected with thin lines were used for the least-squares fit calculation. At this stage the following observations can be made:

- The agreement between the theoretical and experimental excited levels belonging to the normal configuration is impressive, the average absolute deviation is $\Delta_{U(5)} = 61$ keV. From this point of view, the ^{100}Ru is well described by the U(5) dynamical symmetry.
- The 1- and 2-phonon states have not been included in the least-squares procedure; it is worth noting that the inclusion of these four states in the fit does not modify substantially the fit but reduces the global agreement. This should be related to the 2_1^+ anomaly discussed in Ref. [30], which is here observed for the first time in a nucleus having an ''intruder-free'' two-phonon triplet.

It is clear that not all observed states are described within the restricted model space. However, up to 2 MeV there is a one-to-one correspondence between theory and experiment. This is in contrast with some of the Cd isotopes where intruder states appear near the 2-phonon levels.

A problem of assignment arises for levels at an excitation energy close to the 3-phonon quintuplet. Indeed two extra levels, the 0_4^+ at 2051.6 keV and 2_4^+ at 2099.1 keV, lie in this energy region. Stachel et al. [31] suggested that levels not pertaining to the normal configuration in even Ru isotopes are intruders. Such states can occur in even–even nuclei, when two-particle–two-hole (2p2h) excitations across the $Z = 50$ closed shell are lowered by the residual p–n interaction. In the framework of the *sd*-IBA-1 model, they appear to exhibit a O(6) dynamical symmetry and to form a kind of rotational band. For ^{100}Ru, proton or neutron intruder states should be analog to the normal states in ^{96}Zr or ^{104}Ru, respectively [32]. If the two extra levels lying in the three-phonon energy region are intruder states, they must resemble the ground-state band of one of these isotopes. This is the case for the 0_3^+ and 2_4^+ states at 1741.0 keV and 2099.1 keV, respectively, for which the energy difference differ by less than 1 keV with

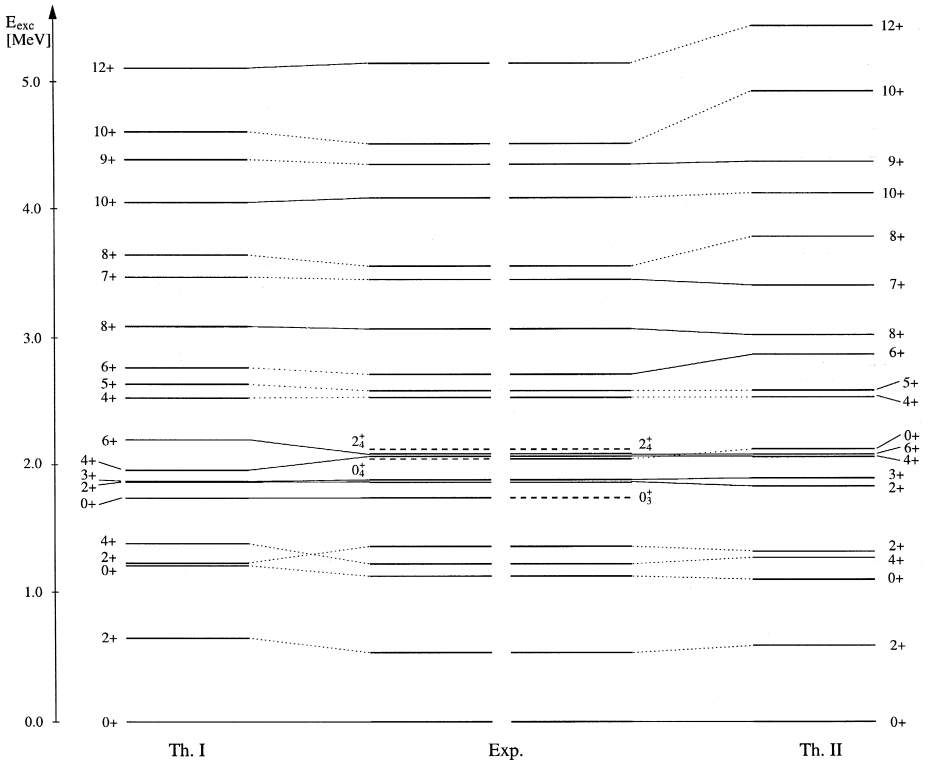

Fig. 15. Comparison between experimental and theoretical excited states belonging to the normal configuration. The calculations were obtained in the pure (Th. I) and perturbed (Th. II) U(5) dynamical symmetry (see Section 4.3). Levels connected with solid lines were used for the least-squares fits.

the corresponding states of ^{104}Ru. However, it was not possible to extend this band to higher spins, which argues against an intruder interpretation of the 0_3^+ and 2_4^+. An additional argument in favour of a 3 phonon interpretation of the 0_3^+ concerns the ratio $R_i = B(\mathrm{E2};0_i^+ \to 2_2^+)/B(\mathrm{E2};0_i^+ \to 2_1^+)$, which yields $R_4 = 8$ and $R_3 = 220$ [6]. However, without the knowledge of the absolute electromagnetic properties of the transitions depopulating the levels in question, the assignment of the 0_3^+ state as three phonon state is only tentative.

Giannatiempo et al. [28,33] concluded that to reproduce the properties of the levels correctly ''it is necessary to take into account the presence of mixed-symmetry states, the lowest ones being the 2_3^+ and 3_1^+ levels (at 1865.1 keV and 1881.1 keV, respectively)''. The mixed-symmetry (MS) states are levels not completely symmetric upon a neutron–proton boson exchange. These levels can be described only within the IBA-2 model [1] which distinguishes explicitly between proton and neutron bosons. Their excitation energy is determined by the so-called Majorana interaction appearing in the IBA-2 Hamiltonian. Because the Majorana operator only affects the MS states, the identification of these states has to be substantiated using properties other than excitation energies. In absence of known absolute electromagnetic properties above 1.4 MeV in ^{100}Ru, the conclusion of Giannatiempo et al. in Ref. [28] seems premature. Moreover,

the presence of an extra 3^+ state in the three phonon multiplet is not at all definite since one of the levels in question is the 2131(10) keV level whose spin is restricted only to the values $J^\pi = 2^+, 3^+$ (not seen in our experiments and not adopted for the reasons given in Section 3.4). More importantly, this MS interpretation cannot explain the presence of the additional 0^+ state at 2051.5 keV, more than 400 keV below the predicted $0^+_{1\mathrm{MS}}$. This state shows no electromagnetic transition to the supposed first 2^+ mixed-symmetry state which is in disagreement with the proposed disintegration pattern for mixed-symmetry states (see Ref. [34]).

At least two states in the three-phonon region are not described by the *sd*-IBA-1 model; we saw that two different interpretations (intruder or mixed-symmetry states) have been attempted to explain their presence at this excitation energy. At the present time, it is not possible to conclude on the nature of these levels.

4.2. Negative-parity states

The IBA-1 model in its original version does not describe states of negative parity. A natural extension of the model consists in the addition p and f bosons with angular momentum and parity 1^- and 3^-, respectively [35], to the *sd* bosons. In the *spdf*-IBA-1 model, the negative-parity states are obtained by coupling a p or a f boson to $N-1$ *sd* bosons in the U(5) limit. This extension of the IBA can account for levels described as octupole and quadrupole–octupole vibrations in the Bohr–Mottelson model.

An octupole vibration around a spherical shape creates an excited state with $I^\pi = 3^-$; this is the lowest negative-parity level in vibrational nuclei. Its coupling with the 2^+_1 state, known as quadrupole–octupole coupling (QOC), leads to a quintuplet of excited levels with spins ranging from 1^- to 5^- and located approximately at an excitation energy close to the sum of the energies of the 2^+_1 and 3^-_1 states. Only recently these states have been studied in detail in vibrational nuclei [36,37].

The spdf Hamiltonian used for the combined positive and negative-parity states is [35]

$$\hat{H}_{\mathrm{tot}} = \hat{H}_{\mathrm{sd}} + \epsilon_p \hat{n}_p + \epsilon_f \hat{n}_f + 2\xi \hat{Q}^{(2)}_{\mathrm{sd}} \cdot \hat{Q}^{(2)}_{\mathrm{pf}} + \xi' \hat{L}^{(1)}_{\mathrm{sd}} \cdot \hat{L}^{(1)}_{\mathrm{pf}}, \tag{5}$$

where $\hat{H}_{\mathrm{sd}}$ is the standard Hamiltonian of the U(5) limit (3), the expressions $\hat{n}_p = \sqrt{3}[p^\dagger \tilde{p}]^{(0)}$ and $\hat{n}_f = \sqrt{7}[f^\dagger \tilde{f}]^{(0)}$ are the p and f particle-number operators, respectively. The other terms appearing in (5) are written explicitly as

$$\hat{Q}^{(2)}_{\mathrm{sd}} = [s^\dagger \tilde{d} + d^\dagger s]^{(2)} - \tfrac{1}{2}\sqrt{7}[d^\dagger \tilde{d}]^{(2)}, \tag{6}$$

$$\hat{Q}^{(2)}_{\mathrm{pf}} = \tfrac{3}{5}\sqrt{7}\left[p^\dagger \tilde{f} + f^\dagger \tilde{p}\right]^{(2)} - \tfrac{9}{10}\sqrt{3}\left[p^\dagger \tilde{p}\right]^{(2)} - \tfrac{3}{10}\sqrt{42}\left[f^\dagger \tilde{f}\right]^{(2)}, \tag{7}$$

$$\hat{L}^{(1)}_{\mathrm{sd}} = \sqrt{10}[d^\dagger \tilde{d}]^{(1)}, \tag{8}$$

$$\hat{L}^{(1)}_{\mathrm{pf}} = \sqrt{2}\left[p^\dagger \tilde{p}\right]^{(1)} + 2\sqrt{7}\left[f^\dagger \tilde{f}\right]^{(1)}. \tag{9}$$

The values of the different parameters were adjusted to reproduce the experimental excitation energies of the octupole band. A good agreement was obtained with the following values: $\xi = -0.04$ MeV, $\xi' = -0.03$ MeV and $\epsilon_f = 2.25$ MeV. The ϵ_p parameter can be adjusted, in principle, to reproduce the excitation energy of the 1^-_1. As this level has not been observed, we have not considered in the following the possible

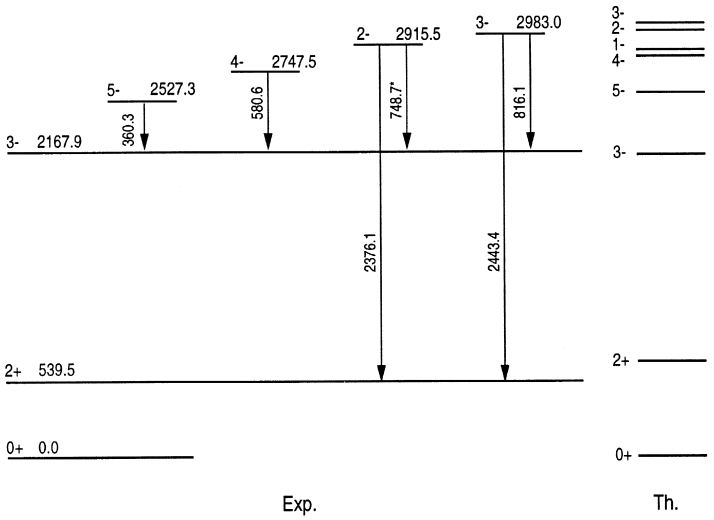

Fig. 16. Proposed QOC states and comparison with theoretical predictions. Only transitions connecting the levels to the 2_1^+ and 3_1^- are presented. The transition indicated with an asterisk has only been observed in the ^{100}Rh ϵ [10].

influence of the p-boson and consequently a very large value of ϵ_p was set in the program. The identification of the QOC states has been done on the basis of their excitation energy. It is clear that this criterion is not sufficient to identify reliably the nuclear levels. In the absence of known lifetimes, one is not able to analyse the collectivity of the electromagnetic properties of the γ transitions depopulating the levels in question. For the present study we have considered the $2_2^-,3_3^-,4_2^-,5_1^-$ as members of the quadrupole–octupole coupled states (see Fig. 16). This is only a tentative assignment because more information is needed to confirm the nature of these levels.

To investigate the effects of the different quadrupole–octupole operators on the nuclear states, it is instructive to calculate analytically the approximate energy eigenvalues of the Hamiltonian (5) applied to the quadrupole–octupole coupled states $|2_1^+ \otimes 3_1^-;L\rangle$ $(L=1^-,2^-,3^-,4^-,5^-)$. This problem can be simplified by reducing the Eq. (5) to a $\hat{H}_{\mathrm{sdf}}$ Hamiltonian, since the p boson only affects slightly the properties of the observed states (see above). The eigenvalue equation for the reduced Hamiltonian can be written as

$$\hat{E}(L) = E_{2_1}^+ + E_{3_1}^- + E_{\mathrm{QOC}}(L) + \left(O(\lambda^2)\right), \tag{10}$$

where $E_{\mathrm{QOC}}(L)$ is the first order energy perturbation on the quintuplet. Denoting the wavefunctions by $\langle [N]n_d(\nu)L' \times 1_f;L\rangle$ with N,n_d,ν,L' defined in Eq. (4) and 1_f representing the f-boson,

$$\begin{aligned} E_{\mathrm{QOC}}(L) &= \left(\tfrac{21}{10}\sqrt{6}\ \xi\langle [6]1(1)2\times 1_f;L \,|\, \left(d^\dagger\tilde{d}\right)^{(2)}\cdot\left(f^\dagger\tilde{f}\right)^{(2)} \,|\, [6]1(1)2\times 1_f;L\rangle \right. \\ &\quad \left. + \left(2\sqrt{70}\ \xi'\langle [6]1(1)2\times 1_f;L \,|\, \left(d^\dagger\tilde{d}\right)^{(1)}\cdot\left(f^\dagger\tilde{f}\right)^{(1)} \,|\, [6]1(1)2\times 1_f;L\rangle \right. \right. \\ &= \tfrac{1}{40}\xi\left(L^4+2L^3-34L^2-35L+210\right) + \tfrac{1}{2}\xi'\left(L^2+L-18\right). \end{aligned} \tag{11}$$

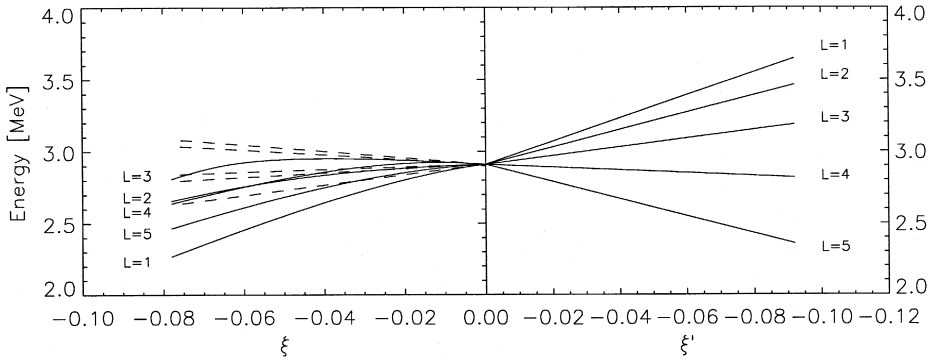

Fig. 17. Breaking of the energy degeneracy of the QOC states by varying independently the parameters ξ, ξ' in Eq. (5). Solid lines represent numerical computations by the program OCTUPOLE [35] while the analytical approximation given by Eq. (11) is represented by dashed lines (note that the lines are superposed on the right part of the figure.

The result (11) is compared graphically in Fig. 17 as a function of the two independent variables ξ, ξ' (dashed lines) with the numerical results of the program OCTUPOLE [35] (solid lines). One can state that the sole analytical calculation of the energy eigenvalues in function of ξ' is exact, whereas the one in function of ξ is valid solely for very small values of this parameter. This is a consequence of the properties of the angular momentum ($\hat{L}$) and quadrupole ($\hat{Q}$) operators. As a matter of fact, the operator $\hat{L}^{(1)}_{\rm sd} \cdot \hat{L}^{(1)}_{\rm pf}$ does not mix the basis states. Consequently the perturbation in orders larger than one in the calculation, which are proportional to the matrix elements connecting different states, are equal to zero. The operator $\hat{Q}^{(1)}_{\rm sd} \cdot \hat{Q}^{(1)}_{\rm pf}$ has a strong mixing effect on the basis states and so the first order approximation is not accurate even for low values of ξ'.

4.3. A more realistic calculation

We have shown in Section 4.1 the good agreement between experimental levels pertaining to the normal configuration and those calculated from Eq. (4). This fact is necessary but not sufficient to assess that ^{100}Ru is a nucleus exhibiting a pure U(5) symmetry. It is important to compare also other properties of the states which can give informations on the structure of the wave functions; this can be done considering the reduced transition probabilities. Due to the limited amount of experimental absolute B(E2)'s, the comparison was done only with the 1- and 2-phonon states for which there are data from Ref. [38] (see Fig. 18). Nevertheless, one can see that the agreement with the U(5) limit (Th. I) of the IBA-1 model is not good; the admixture of a SU(3) perturbation (Th. II) improves the description of the absolute transition rates and gives the correct level sequence of the two-phonon triplet.

The corresponding Hamiltonian is a combination of the Casimir operators of U(5) and SU(3) and it is written as

$$\hat{H} = \epsilon \hat{C}_1[U(5)] + \alpha \hat{C}_2[U(5)] + \beta \hat{C}_2[O(5)] + \kappa \hat{C}_2[SU(3)] + \gamma \hat{C}_2[O(3)] \,. \tag{12}$$

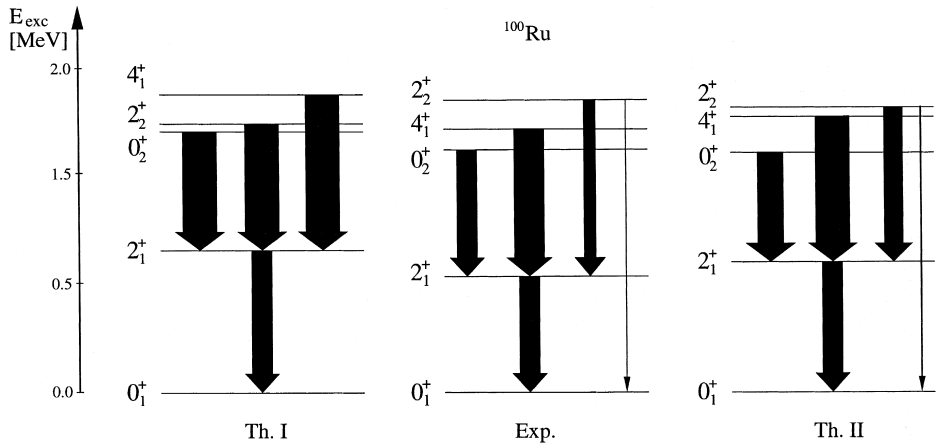

Fig. 18. Comparison between experimental data [38] and theoretical results for the four lowest-lying states and their relevant B(E2) values in ^{100}Ru. The B(E2) values are represented by the thickness of the arrows. The theoretical calculations are the same as presented in Fig. 15. The B(E2) values were normalised to the $2_1^+ \rightarrow 0_1^+$ transition.

Fig. 19 shows the influence of the addition of the quadrupole–quadrupole interaction $\hat{Q} \cdot \hat{Q}$ to the Hamiltonian of the pure U(5) dynamical symmetry (Eq. (3)). One notices the strong effect on the absolute B(E2) values even for small symmetry breaking. The parameter value $\kappa = -0.012$ MeV was chosen in order to reproduce more accurately the 2-phonon triplet. Since the SU(3) symmetry breaking also modifies the theoretical excitation energies of the other states (see Fig. 19), the other four parameters in Eq. (3) have to be readjusted. A direct fit to the experimental excitation energies cannot be performed, as there is no analytical expression which describes the transition regions between the dynamical symmetries. But it is possible to determine good Casimir operators by an iterative least-squares fit using a numerical program; this gives the coefficients $\epsilon = 1.09$ MeV, $\alpha = -0.031$ MeV, $\beta = -0.043$ MeV and $\gamma = 0.028$ MeV, κ being kept fixed at the value -0.012 MeV. The comparison with the experiment and the results from the pure U(5) dynamical symmetry are presented in Figs. 15 and 18. Several observations can be deduced from the comparison between the theoretical and experimental states:

- For the global set of twenty states described, a small symmetry breaking by $Q \cdot Q$ slightly degrades the overall fit quality (the average absolute deviation $\Delta = 81$ keV to compare with $\Delta_{U(5)} = 61$ keV). However, it is worth to note that the average deviation is $\Delta = 50$ keV when one discards the two highest levels from the representation.
- The excitation energies of the 1- and 2-phonon states are predicted almost ideally in the perturbed calculation, whereas there is no such agreement in the pure U(5) limit.
- The 3-phonon states are well described in the two calculations except the 0_3^+ level for which we note a deviation of 368 keV in the perturbed theory. This fact raises again doubts about the nature of the experimental 0_3^+ level at 1741.0 keV. If we consider it as an intruder state, the next 0^+ at 2051.5 keV would be predicted at a correct energy.

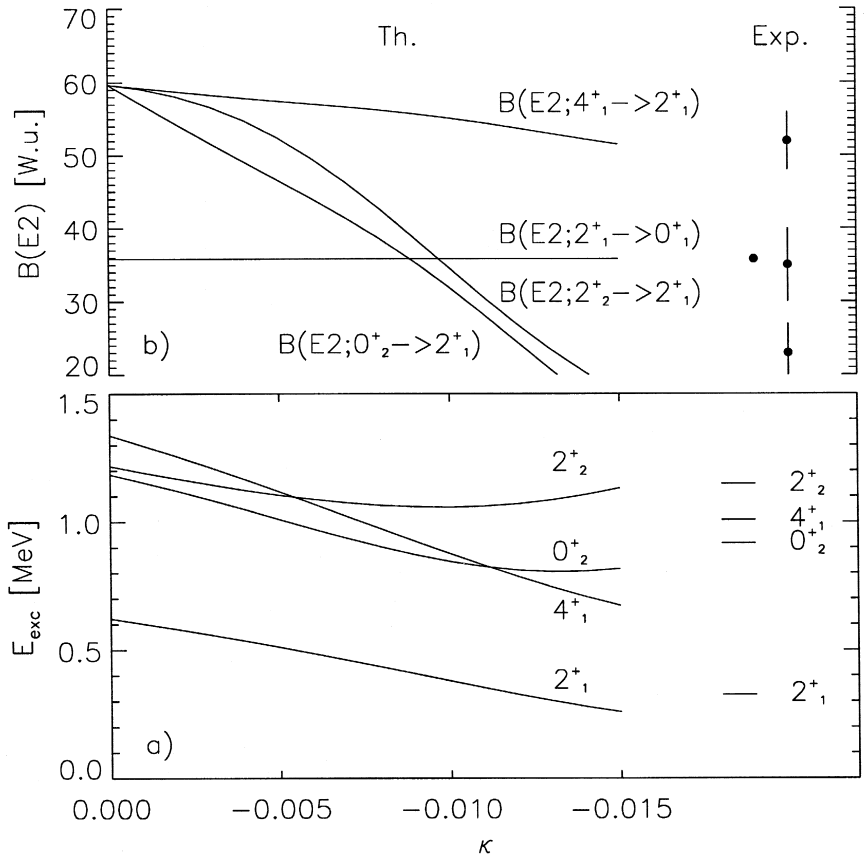

Fig. 19. Effects of a quadrupole–quadrupole perturbation on the first four excited levels (a) and their electromagnetic transition rates (b).

- As expected, the available $B(\mathrm{E2})$ transition probabilities are much better described in the perturbed calculation.

These observations show the necessity to obtain more information about the nature of the wave functions of levels in the region of the 3-phonon.

5. Conclusion

The level structure of ^{100}Ru was investigated by means of the $(\alpha,2n\gamma)$ and (n,γ) reactions. The results of previous studies were extended by 36 new levels. From the combination of angular distributions, the excitation function slopes and the side-feeding intensities it was possible to deduce unambiguously spin and parity for nearly all observed levels populated by the $(\alpha,2n)$ reaction.

The experimental data were interpreted in the framework of the IBM. The exact U(5) dynamical symmetry proved to yield a very good description of nearly all levels up to and including the 3*d*-boson states. Once more an anomaly in the 2_1^+ energy is observed and in this case it cannot be influenced by the presence of low-lying 2p2h intruders, wich do not appear below 1.7 MeV. However, as shown by the presence of two extra states in the 3-phonon quintuplet region, this limit is too restricted to describe the integrality of the level scheme.

We saw that it is necessary to know absolute transition rates to assess reliably the nature of the levels in this region. The comparison of the experimental reduced transition probabilities for the 1 and 2 phonon states with those predicted by the IBA-1 model was improved with the admixture of a SU(3) perturbation to the U(5) limit. The negative parity states pertaining to the octupole band can be described with a *spdf*-IBA-1 Hamiltonian. Members of the quadrupole–octupole excitations are proposed and compared to an analytical perturbation calculation.

Acknowledgements

The authors are grateful to the PSI cyclotron operating crew, especially Dr. P.A. Schmelzbach, for helpful cooperation. We acknowledge support by the Swiss National Science Foundation, PSI and ILL.

References

[1] F. Iachello, A. Arima, The Interacting Boson Model (Cambridge University Press, Cambridge, 1987).
[2] M. Délèze, S. Drissi, J. Jolie, J. Kern, J.P. Vorlet, Nucl. Phys. A 554 (1993) 1.
[3] J. Kern, P.E. Garrett, J. Jolie, H. Lehmann, Nucl. Phys. A 593 (1995) 21.
[4] K. Heyde, J. Jolie, J. Moreau, J. Ryckebush, M. Waroquier, P. van Duppen, M. Huyse, J.L. Wood, Nucl. Phys. A 466 (1987) 189.
[5] J.L. Wood, K. Heyde, W. Nazarewicz, M. Huyse, P. van Duppen, Phys. Rep. 215 (1992) 101.
[6] B. Singh, Nucl. Data Sheets 81 (1997) 86.
[7] G.G. Colvin, S.J. Robinson, F. Hoyler, J. Phys. G 14 (1988) 1411.
[8] M.A. Islam, T.J. Kennet, W.V. Prestwich, Can. J. Phys. 69 (1991) 658.
[9] C. Coceva, P. Giacobbe, Nucl. Phys. A 385 (1982) 301.
[10] G. Kenchian, Thesis, Universidade de Saõ Paulo (1995).
[11] V.V. Babenko, I.N. Vishnevsky, V.A. Zheltonozhsky, V.P. Svyato, V.V. Trishin, Izv. Akad. Nauk SSSR Ser. Fiz. 44 (1980) 1056.
[12] R.J. Peterson, R.A. Emigh, R.E. Anderson, Nucl. Phys. A 348 (1980) 8.
[13] C.M. Lederer, J.M. Jaklevic, J.M. Hollander, Nucl. Phys. A 169 (1971) 449.
[14] A. Arima, F. Iachello, Ann. Phys. 99 (1976) 253.
[15] V.A. Ionescu, J. Kern, C. Nordmann, S. Olbrich, Ch. Rhême, Nucl. Instr. Meth. 163 (1979) 395.
[16] B. Firestone, V.S. Shirley, eds., Table of Isotopes, 8th ed. (Wiley, New York, 1996).
[17] J. Kern, A. Bruder, S. Drissi, V.A. Ionescu, D. Kusnezov, Nucl. Phys. A 512 (1990) 1.
[18] N. Warr, S. Drissi, P.E. Garrett, J. Jolie, J. Kern, S.J. Mannanal, J.L. Schenker, J.P. Vorlet, Nucl. Phys. 620 (1997) 127.
[19] H.R. Koch, H.G. Börner, J.A. Pinston, W.F. Davidson, J. Faudou, R. Roussille, O.W.B. Shlut, Nucl. Instr. 175 (1980) 401.
[20] M. Crittin, J. Kern, J.L. Schenker, Proc. 10th Int. Conf. on Modern Trends in Activation Analysis, Bethesda, Maryland, USA.

[21] T.J. Kennett, W.V. Prestwich, J.S. Tsai, Nucl. Instr. Meth. A 249 (1986) 366.
[22] M.A. Kumakhov, V.A. Sharov, Nature 357 (1992) 390.
[23] P. Taras, B. Haas, Nucl. Instr. Meth 123 (1975) 73.
[24] V.A. Ionescu, J. Kern, C. Nordmann, S. Olbrich, W. Reichart, Nucl. Instr. Meth. 190 (1981) 19.
[25] J. Kern, P. Cejnar, W. Zipper, Nucl. Phys. A 554 (1993) 246.
[26] R. Seltz, N.M. Hintz, Ann. Rept. COO-1265-126 (Univ. Minnesota, 1972) p. 72.
[27] J. Kern, Phys. Lett. B 320 (1994) 7.
[28] A. Giannatiempo, A. Nannini, A. Perego, P. Sona, D. Cutoiu, Phys. Rev C 53 (1996) 2770.
[29] M.J.A. de Voigt, J.F.W. Jansen, F. Bruining, Z. Sujkowsky, Nucl. Phys A 270 (1976) 141.
[30] J. Kern, J. Jolie, Nucl. Phys. A 624 (1997) 415.
[31] J. Stachel, P. Van Isacker, K. Heyde, Phys. Rev. C 25 (1982) 650.
[32] K. Heyde, C. De Coster, J. Jolie, J.L. Wood, Phys. Rev. C 46 (1992) 541.
[33] A. Giannatiempo, A. Nannini, P. Sona, D. Cutoiu, Phys. Rev. C 52 (1995) 2969.
[34] A. Giannatiempo, G. Maino, A. Nannini, P. Sona, Phys. Rev. C 48 (1993) 2657.
[35] D. Kusnezov, PhD. thesis (Princeton University, 1988).
[36] S.J. Robinson, J. Jolie, H.G. Börner, P. Schillebeeckx, S. Ulbig, K.P. Lieb, Phys. Rev. Lett. 73 (1994) 412.
[37] S. Drissi, P.A. Tercier, H.G. Börner, M. Délèze, F. Hoyler, S. Judge, J. Kern, S.J. Mannanal, G. Mouze, K. Schreckenbach, J.P. Vorlet, N. Warr, A. Williams, C. Ythier, Nucl. Phys. A 614 (1997) 137.
[38] S. Landsberger, R. Lecomte, P. Paradis, S. Monaro, Phys. Rev. C 21 (1980) 588.

Characterization of the "three-phonon" region of ^{100}Ru

L. Genilloud [a], T.B. Brown [b], F. Corminboeuf [a], P.E. Garrett [c]
C.D. Hannant [b], J. Jolie [a], N. Warr [b], S.W. Yates [b],

[a] *Institut de Physique, Université de Fribourg, CH-1700 Fribourg, Switzerland*
[b] *University of Kentucky, Lexington, KY 40506-0055 USA*
[c] *Lawrence Livermore National Laboratory, Livermore, CA 94550 USA*

Abstract

Lifetimes of excited states in ^{100}Ru were determined from Doppler-shift attenuation measurements following the ^{100}Ru(n,n$'\gamma$) reaction. Absolute transition rates or limits thereon were extracted for states in the three-phonon region and were compared with an interacting boson model description of this nucleus. Intruder states were identified, and a candidate for the 2^+ mixed-symmetry state is suggested.

PACS: 21.10.Tg,23.20Js,25.40Fq,27.60.+j

Key words: NUCLEAR REACTION: ^{100}Ru(n,n$'\gamma$); Measured $E_\gamma, I_\gamma(\theta)$; DSAM method, deduced lifetime; Comparison with interacting boson model.

Accepted for publication in Nuclear Physics A

1 INTRODUCTION

In a search [1] for nuclei exhibiting the U(5) dynamical symmetry of the interacting boson model (IBM) [2], ^{100}Ru was selected as an excellent candidate. It has been shown recently [3] that for this isotope an admixture of SU(3) breaking terms to the dominant U(5) symmetry enhances the theoretical description of the two-phonon triplet, but definite conclusions could not be drawn because of the lack of knowledge of absolute transition rates of higher-lying states. We have attempted to address this question by measuring lifetimes using the Doppler-shift attenuation method (DSAM) after inelastic neutron scattering (INS) [4]. This (n,n$'\gamma$) experiment yielded the electromagnetic properties of the *three-phonon* part of the level scheme which we compare to those predicted by the IBM.

2 EXPERIMENTAL PROCEDURE

The (n,n$'\gamma$) reaction offers advantages over other nuclear techniques for the study of the low-lying states of nuclei. As neutrons are not electrically charged, there is no Coulomb barrier to penetrate, so the nuclei are produced quite cold. By choosing the energy of the incident neutrons, it is possible to populate low-spin states up to a specific excitation energy. The statistical nature of the INS reaction [5] assures that all states in the spin and energy range are populated. It is, therefore, possible to populate specific states of interest without feeding from higher-lying levels.

2.1 Excitation functions

The experiments reported in this work were performed with pulsed beams from the University of Kentucky accelerator facility. Neutrons from the ^{3}H(p,n)^{3}He reaction bombarded a 4.78 g sample of metallic ruthenium enriched to 95.58% in ^{100}Ru. The γ-ray spectra were measured in 0.1 MeV steps in incident neutron energy from 2.4 MeV to 3.3 MeV using a HPGe detector placed at 90 degrees with respect to the incident neutrons. Compton suppression was performed with an annular BGO shield; time-of-flight gating was employed to reduce events not directly correlated with the reaction. The resolution of this system was 1.9 keV at 1408 keV. The relative efficiency and energy calibrations were determined with ^{133}Ba, ^{152}Eu and ^{226}Ra sources. The γ-ray yields were normalized for each neutron energy according to the number of protons bombarding the tritium gas cell. Fig. 1 shows the γ-ray spectrum measured at $E_n = 2.6$ MeV.

The excitation function measurements give the yield thresholds for the different γ rays. The threshold for a particular γ ray can uniquely lead to the placement of the level from which the transition is issued.

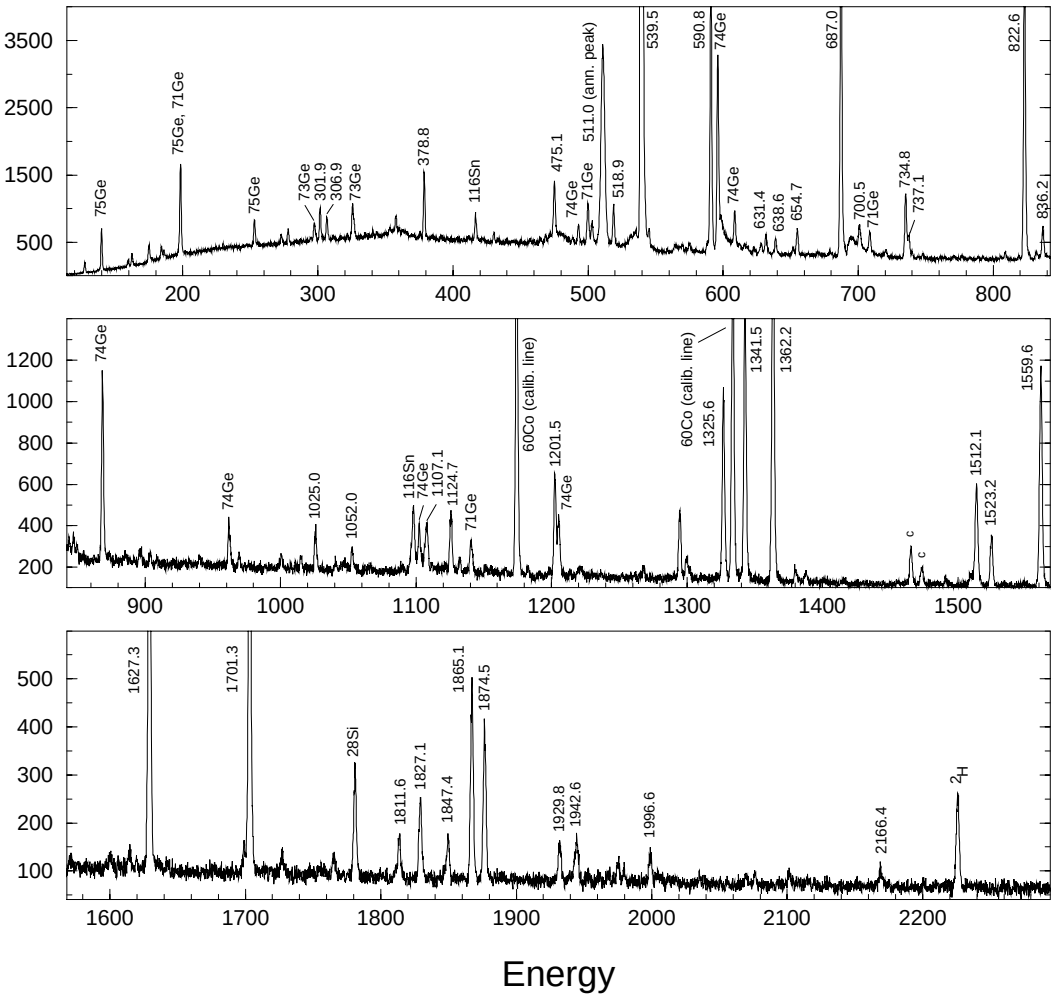

Fig. 1. γ-ray spectrum from the ^{100}Ru(n,n$'\gamma$) reaction with 2.6-MeV neutrons.

2.2 Angular distributions

Angular distributions were performed at incident neutron energies of 2.6 and 3.3 MeV. The spectra were recorded at 11 angles for the first neutron energy and 10 angles for the second. The neutron production method, the sample, and the detector specifications were the same as those given in the preceding section. The γ rays from radioactive ^{60}Co and ^{24}Na sources were recorded simultaneously in order to obtain a precise energy determination of the γ rays produced by the reaction at all angles. Normalization of the spectra was performed using isotropic transitions from 0^+ states.

Following the INS reactions, it is possible to extract lifetimes of excited nuclear levels with DSAM. By measuring the energy of a γ ray at various angles, the experimental attenuation factor $F_{exp}(\tau)$ can be extracted from the relation

$$E_\gamma(\Theta) = E_\gamma(1 + F_{exp}(\tau)\frac{v_{cm}}{c}cos\theta) \quad (1)$$

where E_γ is the unshifted γ-ray energy, v_{cm} is the velocity of the centre of mass in the inelastic neutron scattering with the nucleus, and c is the speed of light. The lifetimes of the states can be determined [4] from the comparison of the measured $F(\tau)$ values with those calculated using the Winterbon formalism [6]. The simultaneous measurement of the γ rays from the (n,n$'\gamma$) reaction and from the radioactive sources makes the determination of reliable Doppler shifts possible, even when they are quite small, i.e., <0.1 keV [7]. The lifetimes for the different levels studied in this work are given in Table 1, column 4; they were extracted using a weighted average $F(\tau)$ value for each level. The Doppler shifts for selected transitions are given in Figure 2. A comparison of our results with previously determined lifetimes [8] is possible only for the level at 1362.2 keV, giving τ(ref. [8])= 1.80(22) ps and τ(this work) = 1.37^{+35}_{-23} ps.

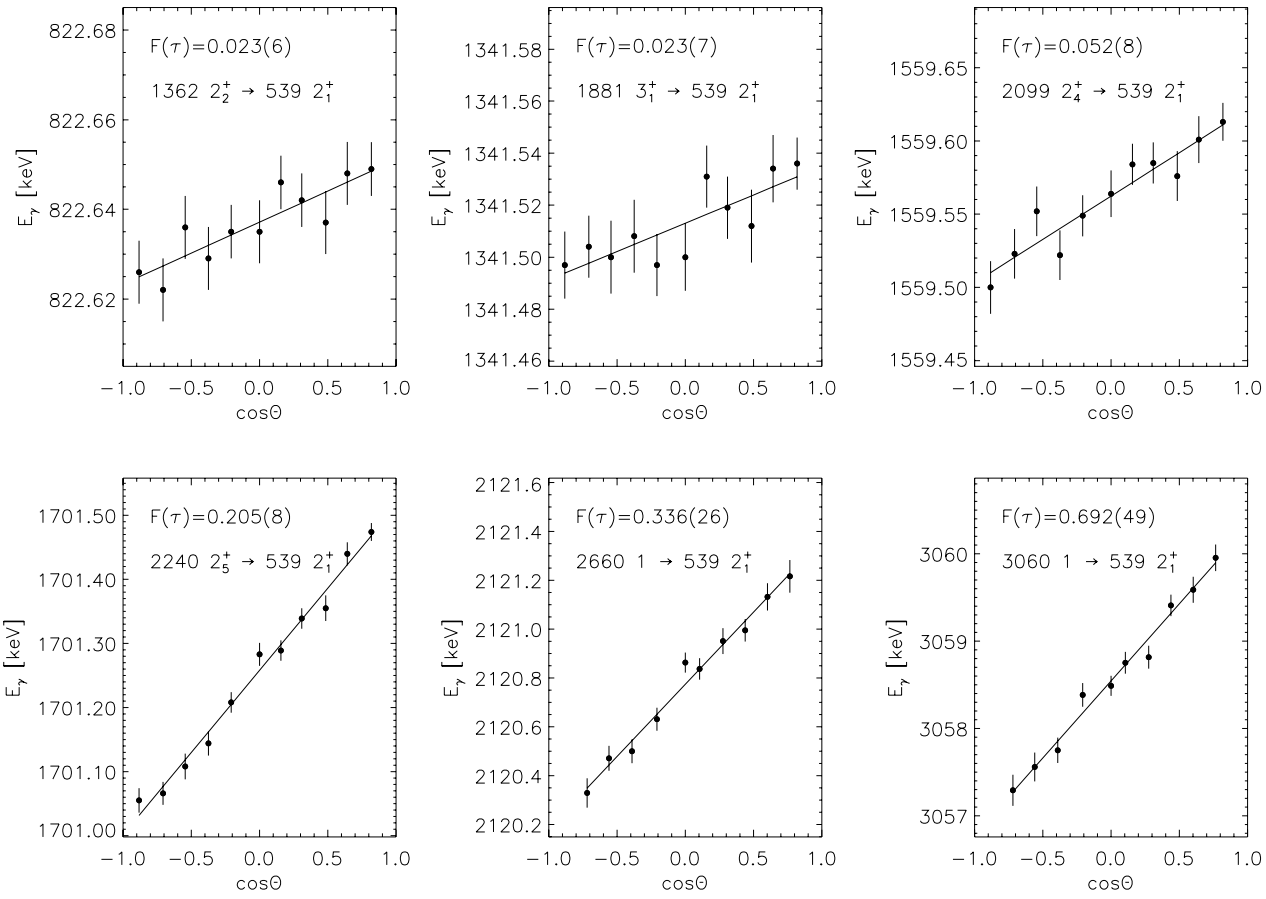

Fig. 2. Measured γ-ray energy as a function of $\cos\theta$ for selected transitions. $F(\tau)$ values determined from a linear fit to the data are indicated.

The experimental angular distributions were fitted using a least-squares procedure on the Legendre polynomial expansion. The use of the program CINDY [10] allowed the extraction of the multipole-mixing ratios δ for several γ-ray transitions. In some cases the analysis of mixed transitions gives two acceptable solutions for δ. Both values are then quoted in Table 1, column 8. Spins and parities were deduced from the angular distribution analysis; column 3 reflects this new information in combination with previous results (column 2).

Table 1
Excited states in ^{100}Ru and their decay properties.

Levels				Transitions							
E [keV]	J^π		τ [fs] [b]	E_γ [keV]	I_γ *rel*	a_2	a_4	multipol.	Mixing ratios [c]		
	prev.[d]	adopt.							this work	literature	adopted
539.5	2^+	2^+		539.506(18)	100.0(13)	0.153(9)	-0.010(5)	E2			
1130.3	0^+	0^+		590.774(20)	100.0(13)			E2			
1226.5	4^+	4^+		686.963(17)	100.0(12)	0.303(6)	-0.047(8)	E2			
1362.2	2^+	2^+	1370^{+350}_{-230}	822.672(16)	57.6(3)	0.086(8)		M1+E2	3.7(3),-0.14(3)	3.7(4)[d]	3.7(3)
				1362.160(21)	42.4(3)	0.231(15)	-0.021(21)	E2			
1741.0	0^+	0^+	> 2000	378.943(28)	42.9(6)			E2			
				1201.543(31)	57.1(6)			E2			
1865.1	2^+	2^+	950^{+290}_{-180}	502.825(55)	4.6(1)						
				638.718(50)	4.3(1)						
				734.810(21)	26.0(2)	0.304(24)	-0.05(3)	E2			
				1325.633(22)	33.2(3)	-0.205(29)		M1+E2	-1.0(3),-2.5(9)	$-1.6^{+1.4}_{-0.7}$[e]	-1.0(3)
				1865.070(56)	32.0(4)	0.294(16)	-0.043(21)	E2			
1881.1	3^+	3^+	1300^{+570}_{-310}	518.816(33)	12.7(3)	0.31(4)	0.21(4)	M1+E2	6.5(14),0.36(8)	0.38(6)[d]	0.37(7)
				654.601(30)	8.6(2)	-0.43(4)	0.09(4)	M1+E2	0.46(7), 3.2(6)	2.1(3)[d]	2.3(5)
				1341.515(22)	78.7(6)	0.276(20)	0.172(26)	M1+E2	6.7(12), 0.37(10)	5.5(5),0.35(2)[d]	5.7(5)
2051.6	0^+	0^+	1380^{+1600}_{-490}	689.456(87)	13.7(9)[f]			(E2)			
				1512.128(38)	86.1(9)[f]			(E2)			
2062.7	4^+	4^+	810^{+1330}_{-320}	700.513(54)	22.6(4)						
				836.238(31)	26.6(1)	0.24(6)	-0.10(7)	M1+E2	-0.13(7), 1.5(3)	1.85(21)[d]	1.73(17)
				1523.080(55)	50.8(7)	0.403(24)	-0.13(3)	E2			
2075.7	6^+	6^+	> 400	849.241(15)	100.0(6)						
2099.2	2^+	2^+	560^{+100}_{-80}	737.147(57)	10.8(6)						
				872.67(16)	1.3(2)						
				968.68(10)	2.6(2)						
				1559.563(34)	81.7(7)			M1+E2		0.72(32)[e]	0.72(32)
				2099.03(15)	3.5(2)						

2166.9	3^-	3^-	> 1400	301.820(29)	10.7(2)	-0.15(4)	0.14(5)	E1	0.04(4)	0.03(6)[d]	0.04(3)
				1627.336(36)	84.7(8)	-0.274(20)		E1	-0.008(24)	0.02(3)[d]	-0.003(20)
				2166.61(21)	4.6(3)	0.60(10)	0.09(12)	(E3)			
2240.8	$(1,2)^+$	2^+	120^{+8}_{-8}	375.729(91)	1.6(3)						
				1701.278(28)	98.4(3)	0.159(24)	0.02(3)	M1+E2	-0.014(50),2.7(3)	$-6^{+4}_{-\infty}$ [e]	-0.014(50)
2351.3	4^+	4^+	600^{+370}_{-170}	1124.771(34)	60.1(11)	0.16(4)	0.05(5)	M1+E2	-0.36(5)		-0.36(5)
				1811.663(84)	39.9(11)	0.36(6)	-0.09(7)	E2			
2366.6	4^+	4^+	1130^{+1100}_{-380}	1139.880(57)	16.5(6)						
				1827.044(59)	83.5(6)	0.42(3)	-0.17(5)	E2			
2387.1	$(0)^+$	0^+	> 750	1024.997(54)	56.6(11)						
				1847.73(11)	43.4(11)						
2414.0	$3,4^+$	(4^+)	126^{+10}_{-8}	1051.964(70)	13.2(4)						
				1874.289(58)	86.8(4)	0.309(20)	-0.02(3)	(E2)			
2469.4	2^-	2^-	630^{+730}_{-230}	588.245(79)	16.6(4)	-0.14(4)		E1	0.14(16)		0.14(16)
				1107.285(49)	45.3(7)	0.21(6)	0.07(7)	E1	-0.10(13), 1.8(3)		-0.10(13)
				1929.802(71)	38.1(7)	0.18(5)	-0.08(7)	E1	-0.8(9), 2.9(8)		-0.8(9)
2493.0	4^-	4^-	> 1200	430.316(60)	27.7(11)	0.62	0.15				
				612.014(53)	11.5(11)						
				1266.66(10)	60.9(12)	0.50(9)		E1	0.4(6)		0.4(6)
2512.4	4^+	4^+	590^{+790}_{-220}	413.28(25)	8.9(4)						
				631.376(26)	54.3(9)	0.25(6)	-0.07(6)	M1+E2	0.41(5)		0.41(5)
				1150.421(95)	7.3(6)						
				1972.854(94)	29.5(7)	0.43(11)	-0.05(11)	E2			
2516.7	$(1,2)^-$	1^-	151^{+62}_{-37}	465.11(15)	8.8(8)						
				651.718(39)	26.9(9)						
				775.95(13)	7.8(5)						
				1154.602(78)	13.1(7)			M1+E2		$0.8^{+1.7}_{-0.5}$ [e]	$0.8^{+1.7}_{-0.5}$
				1386.427(56)	26.8(8)	-0.38(17)					
				1977.18(13)	16.5(6)			M1+E2		$1.3^{+1.8}_{-0.6}$ [e]	$1.3^{+1.8}_{-0.6}$
2527.2	5^-	5^-	860^{+2000}_{-400}	1300.712(37)	100.0(16)	-0.13(9)		E1	0.05(7)	0.004(6)[d]	0.004(6)
2536.2	3^+	3^+	1050^{+1800}_{-480}	1309.94(14)	10.5(5)						
				1996.625(75)	89.5(5)	-0.20(7)		M1(+E2)	0.017(30)	-0.2(3)[d]	0.017(30)

(continued on next page)

Table 1 *(continued)*

Levels				Transitions							
E [keV]	J^π		τ [fs] [b]	E_γ [keV]	I_γ *rel*	a_2	a_4	multipol.	Mixing ratios [c]		
	prev.[d]	adopt.							this work	literature	adopted
2543.7	2	2^+	550^{+710}_{-210}	662.56(25)	5.0(9)						
				678.592(38)	26.0(9)						
				1181.527(39)	40.6(9)				-0.12(9),3.5(12)		-0.12(9)
				2004.20(12)	17.3(7)						
				2543.36(28)	11.1(7)						
2569.8	3^-	3^-	> 430	403.140(39)	42.6(8)	0.37(8)		M1+E2	0.08(8),1.36(20)	1.58(7)[d]	1.58(7)
				1207.775(59)	30.0(9)						
				1343.39(10)	21.8(23)						
				2030.72(31)	5.5(6)						
2576.8	5^+	5^+	> 180	1350.365(70)	100.0(50)						
2591.9	4^-	4^-	370^{+890}_{-170}	424.88(17)	18.4(6)					1.2(3)[d]	1.2(3)
				710.799(32)	44.1(11)	-0.32(15)		E1	0.02(5)	0.05(8)[d]	0.03(5)
				1365.490(91)	37.5(10)					-0.05(12)[d]	-0.05(12)
2606.0	$(2-4)$	2,3	103^{+14}_{-11}	2066.492(91)	100.0(16)	0.22(7)	0.04(7)				
2617.1	$1, 2^+$	(1)	174^{+37}_{-27}	2617.091(88)	100.0(32)						
2660.2	1,2	1	69^{+8}_{-7}	2120.57(11)	82.2(9)						
				2660.22(20)	17.8(9)						
2666.2	(3,4)	2,3	79^{+9}_{-7}	2126.68(11)	100.0(17)	0.19(7)					
2738.7	(3,4)			857.71(23)	100.0(84)						
2745.5	$(1, 2^+)$	1	190^{+60}_{-40}	1615.44(90)	71.0(10)						
				2205.93(19)	29.0(10)						
2764.9	4^-	4^-	> 250	598.29(15)	50.8(16)						
				1538.380(79)	49.2(16)						
2775.3	2^+-4^+		440^{+340}_{-140}	248.109(73)	13.3(5)						
				1413.178(66)	27.8(7)						
				1548.74(10)	15.0(6)						
				2236.09(17)	44.0(11)						

2800.9	3(−)		191^{+69}_{-43}	1438.686(52)	68.8(9)	-0.26(7)		(E1)	0.01(5)		0.01(5)
				1574.24(11)	31.2(9)						
2801.3	3(+) 3+		140^{+24}_{-19}	920.55(26)	16.5(6)						
				2261.88(18)	83.5(6)	0.33(6)		M1+E2	0.42(5),3.9(8)		$^{0.42(5)}_{3.9(8)}$
2837.7	$(0-2)^+$	2^+	167^{+31}_{-24}	1475.67(19)	8.5(5)						
				2298.17(20)	91.5(5)	0.15(6)	-0.04(6)		3.0(5),-0.07(4)		$^{3.0(5)}_{-0.04(6)}$
2862.7			360^{+730}_{-150}	763.33(17)	11.9(24)						
				1500.38(10)	88.1(24)						
2877.2	3^+	3^+		1515.10(19)	100.0(48)						
2878.4		2^+-4^+	202^{+43}_{-31}	779.54(10)	11.1(5)						
				997.412(50)	37.4(7)						
				1651.885(54)	51.5(9)						
2905.0	$3, 4^+$	(4^+)	300^{+120}_{-70}	2365.50(25)	100.0(25)	0.32(9)	-0.04(9)	(E2)			
2915.5	2^-	2^-	500^{+420}_{-160}	446.04(10)	17.1(9)			M1+E2		0.11(3)[e]	0.11(3)
				1553.34(11)	30.6(9)						
				2376.11(27)	52.4(15)						
2951.1			125^{+20}_{-15}	1589.06(34)	7.7(8)						
				1724.622(77)	54.1(12)						
				2411.41(21)	38.2(13)						
2998.9	3,4		260^{+140}_{-70}	2459.39(24)	100.0(33)						
3060.0	$(1, 2^+)$	1	16^{+4}_{-4}	3059.97(24)	100.0(67)						
3064.8	3, 4	4^+	53^{+14}_{-10}	2525.26(17)	100.0(34)	0.18(6)	-0.15(7)	E2			
3069.6	$(1, 2)^-$		> 650	2530.06(18)	100.0(34)						
3072.2	(2^+)	1	290^{+200}_{-90}	1710.00(12)	48.4(18)						
				3071.86(24)	51.6(18)						
3110.7	4	4	> 370	943.79(16)	100.0(89)						
3118.5	$3, 4^+$		53^{+11}_{-8}	1756.21(21)	25.4(16)						
				2579.28(16)	74.6(16)						

[a]) Only levels for which a lifetime has been extracted are listed.
[b]) Weighted average from all observed deexciting transitions.
[c]) Where two values are given, the former has the lower χ^2.
[d]) Taken from Ref. [3].
[e]) Taken from Ref. [9].
[f]) Intensity value taken from Ref. [9].

3 Interpretation of the experimental results

3.1 Level scheme

To be able to make a comparison of the experimental level structure at low excitation energy with that predicted by the theory, it is essential that no levels are missed and no spurious levels are included.

In a recent paper [3], ^{100}Ru was extensively studied through the ^{98}Mo(α,2nγ) and ^{99}Ru(n,γ) reactions. In this article, the authors considered the existence of the previously proposed levels at 2131, 2268 and 2438 keV as doubtful and those at 2075.1, 2313.5 and 2324.6 keV as spurious. The statistical nature of the INS reaction used for the present study ensures that all low-spin levels noindent below a determined excitation energy will be populated. No transitions were found in our data feeding the low-lying levels from any of these questoniable levels. In his study of ^{100}Rh decay, Kenchian [9] did not find any evidence for these transitions, in spite of the good sensitivity for low-spin levels provided by the decay of the 1^- ^{100}Rh parent and the use of a $\gamma\gamma$-coincidence system. From all of these recent data, we conclude that these levels are spurious and we have eliminated them from the ^{100}Ru level scheme.

3.2 Mixed-symmetry states

For vibrational nuclei, the lowest mixed-symmetry (MS) state has $J^\pi = 2^+$ [11]. It should decay to the 2_1^+ state via a transition with a large B(M1) value, and is expected at $\gtrsim$ 2 MeV of excitation [12]. (Note that M1 transitions are completely forbidden between fully symmetric 2^+ states.) Giannatiempo *et al.* [13,14] concluded that to reproduce the properties of the levels in ^{100}Ru correctly "it is necessary to take into account the presence of mixed-symmetry states, the lowest ones being the 2_3^+ and 3_1^+ levels [at 1865.1 keV and 1881.1 keV, respectively]". In Ref. [3] the authors disagreed with the postulate of Giannatiempo *et al.* and suggested the need for obtaining electromagnetic properties of states in the 3-phonon region. Our measured lifetimes and δ values allow the computation of B(M1) values for a few transitions depopulating the low-lying levels (see Table 2).

The IBM-2 prediction [15] in the vibrational U(5) limit for the reduced M1 transition probability is

$$B(M1; 2_{ms}^+ \rightarrow 2_1^+) = \frac{3}{4\pi}(g_p - g_n)^2 6 \frac{N_p N_n}{N^2}. \qquad (2)$$

using the microscopic values of $g_p = 1\mu_N$ and $g_n = 0\mu_N$, this equation gives $B(M1) = 0.36\mu_N^2$ for ^{100}Ru. With the values $g_p = 0.70\mu_N$ and $g_n = 0.05\mu_N$, obtained in Ref. [15] from a fit of the magnetic dipole moment of the first-excited 2^+ states in the whole Ba-Pt region, one gets $B(M1) = 0.15\mu_N^2$. On inspection of Table 2, one notes that no state below 2.2 MeV of excitation

Table 2
Electromagnetic transitions rates for M1 transitions.

Level	Transition		$B(M1; J_i \rightarrow J_f)$ $[\mu_N^2]$
E_{exc} [keV]	$J_i^\pi \rightarrow J_f^\pi$	E_γ [keV]	
1362.2	$2_2^+ \rightarrow 2_1^+$	822.6	0.0029 ± 0.0012
1865.1	$2_3^+ \rightarrow 2_1^+$	1325.6	$0.0043^{+0.0029}_{-0.0018}$
	$2_3^+ \rightarrow 2_2^+$	502.9	< 0.027
1881.1	$3_1^+ \rightarrow 2_1^+$	1341.5	$0.00043^{+0.00025}_{-0.00018}$
	$3_1^+ \rightarrow 4_1^+$	654.7	$0.0021^{+0.0020}_{-0.0.0011}$
	$3_1^+ \rightarrow 2_2^+$	518.9	$0.036^{+0.013}_{-0.012}$
2062.7	$4_2^+ \rightarrow 4_1^+$	836.2	$0.0081^{+0.0073}_{-0.0054}$
2099.2	$2_4^+ \rightarrow 2_1^+$	1559.6	$0.014^{+0.0075}_{-0.0055}$
	$2_4^+ \rightarrow 2_2^+$	737.1	< 0.032
2240.8	$2_5^+ \rightarrow 2_1^+$	1701.3	0.095 ± 0.005

energy can account for such strength. This observation argues against the presence of MS states in this region of the level scheme. However, we notice a $J^\pi = 2^+$ state at 2240.8 keV with a dominant decay branch to the 2_1^+ state via the 1701.3 keV transition which is almost pure M1 in nature. Using the well-determined lifetime of 120 ± 8 fs for this level, the M1 strength is calculated to be $B(M1; 2_5^+ \rightarrow 2_1^+) = 0.095 \pm 0.007 \mu_N^2$. While this value is lower than the two theoretical predictions, it is approximately equal to the summed M1 transition probability of the main fragments of the lowest mixed-symmetry 2^+ state in ^{112}Cd [16].

3.3 Normal configuration and broken U(5) symmetry

As noted earlier, the nucleus ^{100}Ru was selected in a survey of nuclei that might exhibit the U(5) dynamical symmetry [1]. In a recent paper [3], the authors showed that B(E2) transition probabilities for the 1- and 2-phonon states are much better described when the U(5) symmetry is broken by adding a quadrupole-quadrupole perturbation (corresponding to adding a SU(3) operator to the Hamiltonian in the U(5) limit). Moreover, the excitation energies up to the 3-phonon region are better reproduced in the perturbed calculation; the calculation, including comparison of theoretical and experimental level energies, is presented in detail in ref [3]. They concluded by emphasizing the necessity of obtaining more information about the nature of the

wave functions of levels in the 3-phonon region. In order to learn about the wave functions of these states, we must obtain some measure of their collective character. In the present work, we determined the lifetimes of nearly all states in this region of the level scheme, allowing the calculation of absolute transition rates.

The Hamiltonian in the U(5) limit, taking into account a quadrupole-quadrupole perturbation, is a combination of the Casimir operators of U(5) and SU(3) and is written as

$$\hat{H} = \epsilon \hat{C}_1[U(5)] + \alpha \hat{C}_2[U(5)] + \beta \hat{C}_2[O(5)] + \kappa \hat{C}_2[SU(3)] + \gamma \hat{C}_2[O(3)] \qquad (3)$$

The coefficients of the Casimir operator were determined [3] by an iterative least-squares fit using a numerical program, giving $\epsilon = 1.09$ MeV, $\alpha = -0.031$ MeV, $\beta = -0.043$ MeV, $\gamma = 0.028$ MeV and $\kappa = -0.012$ MeV. The E2 transition operator used was $e_B(s^+\tilde{d} + d^+s)^{(2)}$ with the effective charge $e_B = 0.26$ [eb] deduced from the $B(E2; 2_1^+ \rightarrow 0_1^+)$ value. The theoretical predictions for the lowest-lying positive parity states are given in Table 3 and Figure 3, together with the experimental results.

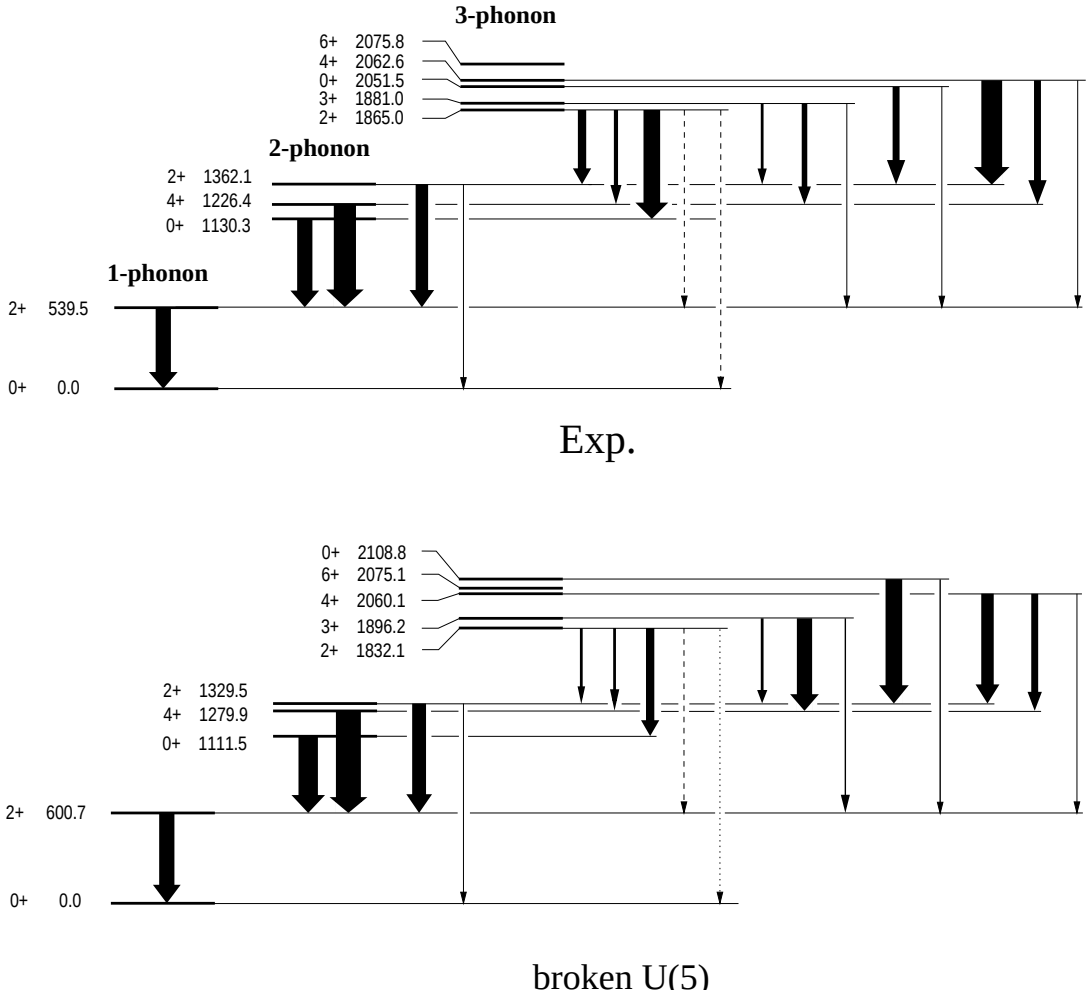

Fig. 3. Comparison between the theoretical and experimental level energies and B(E2) values for the perturbed model.

Table 3
Comparison of experimental and theoretical B(E2) values.

Level	Transition		$B(E2; J_i \to J_f)$ [W.u.]		
E_{exc} [keV]	$J_i^\pi \to J_f^\pi$	E_γ [keV]	Exp.	Theory	
				broken U(5)	U(5)
539.5	$2_1^+ \to 0_1^+$	539.5	35.8 ± 0.4	35.8	35.8
1130.3	$0_2^+ \to 2_1^+$	590.8	$34.8^{+6.0}_{-4.4}$	44.6	59.7
1226.5	$4_1^+ \to 2_1^+$	687.0	$51.6^{+4.3}_{-3.7}$	57.8	59.7
1362.2	$2_2^+ \to 0_1^+$	1362.2	2.0 ± 0.4	4.25	0.0
	$2_2^+ \to 2_1^+$	822.6	30.8 ± 6.6	33.7	59.7
1741.0	$0_3^+ \to 2_1^+$	1201.5	< 3.4	[a]	0.0
	$0_3^+ \to 2_2^+$	378.8	< 815	[a]	71.6
1865.1	$2_3^+ \to 0_1^+$	1865.1	0.44 ± 0.11	0.05	0.0
	$2_3^+ \to 2_1^+$	1325.6	1.3 ± 0.7	0.78	0.0
	$2_3^+ \to 0_2^+$	734.8	37.8 ± 9.0	20.1	33.4
	$2_3^+ \to 4_1^+$	638.6	12.7 ± 3.0	10.0	24.5
	$2_3^+ \to 2_2^+$	502.9	< 20	9.61	13.6
1881.1	$3_1^+ \to 2_1^+$	1341.5	4.0 ± 1.3	5.21	0.0
	$3_1^+ \to 4_1^+$	654.7	$13.7 \pm 5.$	10.4	20.5
	$3_1^+ \to 2_2^+$	518.9	$9.2^{+7.1}_{-4.8}$	36.4	51.1
2051.6	$0_4^+ \to 2_1^+$	1512.1	2.3 ± 1.3	4.7	[a]
	$0_4^+ \to 2_2^+$	689.5	19 ± 10	39.4	[a]
2062.7	$4_2^+ \to 2_1^+$	1523.2	2.3 ± 1.5	3.12	0.0
	$4_2^+ \to 4_1^+$	836.2	18 ± 12	16.1	34.1
	$4_2^+ \to 2_2^+$	700.5	49 ± 31	31.2	37.5
2099.2	$2_4^+ \to 0_1^+$	2099.0	0.046 ± 0.007	[a]	
	$2_4^+ \to 2_1^+$	1559.6	1.6 ± 1.1	[a]	
	$2_4^+ \to 0_2^+$	968.7	1.62 ± 0.25	[a]	
	$2_4^+ \to 4_1^+$	872.7	1.40 ± 0.22	[a]	
	$2_4^+ \to 2_2^+$	737.1	< 26	[a]	
2543.6	$2_5^+ \to 0_1^+$	2543.3	0.056 ± 0.034	0.00098	0.0
	$2_5^+ \to 2_1^+$	2004.2	< 0.46	0.012	0.0
	$2_5^+ \to 2_2^+$	1181.5	$^{8.8\pm5.5}_{<0.64}$ [b]	1.5	0.0
	$2_5^+ \to 2_3^+$	678.5	< 160	23.8	46.0
	$2_5^+ \to 3_1^+$	662.5	< 34	10.0	11.9

[a]) These states are not described in the model (see text).
[b]) Two values of delta were determined for this transition.

While the U(5) limit provides a reasonable picture of ^{100}Ru, the perturbed calculation improves the description of most decays. This is a clear indication that the dynamical symmetry is broken. Two levels with $J^\pi = 0^+, 2^+$ in the three-phonon region are not described at all by the *sd*-IBA-1

model; an examination of the electromagnetic properties helps to disentangle this situation. The decays from the 2_4^+ state to the two-phonon states with $J^\pi = 0^+, 4^+$ are not very collective, their B(E2) values being equal to 1.62 ± 0.25 and 1.40 ± 0.22 W.u., respectively. In contrast, the transitions populating the same levels originating from the 2_3^+ state give $B(E2; 2_3^+ \rightarrow 0_2^+) = 37.8 \pm 9.0$ and $B(E2; 2_3^+ \rightarrow 4_1^+) = 12.7 \pm 3.0$ W.u. making this state the three-phonon 2^+ state. The noncollective 2_4^+ state must be regarded as an intruder state.

The situation with the two 0^+ states is unclear. In fact, only a lower limit was deduced for the lifetime of the 0_3^+ level, giving upper limits for the reduced transitions rates. However, it was shown in Ref. [3], on the basis of their excitation energies that the pure U(5) and perturbed U(5) theories described two different states, the 0_3^+ and 0_4^+ states respectively. In light of the results given in Table 3 for these two levels, we can confirm this point on the basis of the electromagnetic properties. The general comparison of the experimental results shows that the B(E2) transition probabilities are much better described in the perturbed calculation. Consequently we can conclude that the 0_3^+ state is not contained in the restricted U(5) model space. The 0_3^+ and 2_4^+ states are the logical candidates for the beginning of an intruder band, although the latter state likely has some MS character (see Table 2). Based on its decay we can also assign the 4^+ state at 2512.4 keV to belong to this band.

4 Conclusion

The DSAM technique following inelastic neutron scattering has been used to determine the lifetimes of 35 levels in ^{100}Ru. From the angular distribution data it was also possible to make new spin assignments for a few levels (see Table 1).

To study the three-phonon region, the measured transition probabilities were compared to calculations using the pure and perturbed U(5) symmetry of the IBA-1 model. The perturbed calculation improved the description of most decays compared with the pure U(5) limit. Three intruder states in the 3-phonon region were identified on the basis of their absolute decay strengths.

We have shown, on the basis of measured electromagnetic properties, the absence of MS states below 2.2 MeV. The 2_5^+ level at 2240.8 keV decays predominantly to the 2_1^+ state via an almost pure M1 transition; it could be the lowest MS state.

This work was supported by the Swiss National Fund for Scientific Research, by the U.S. National Science Foundation under Grant No. PHY-9863789 and was performed in part under the auspices of the U.S DOE contract No. W-7405-Eng-48. Two of the authors, L.G. and J.J, want to thank the group at the University of Kentucky for their hospitality.

References

[1] J. Kern, P.E. Garrett, J. Jolie, H. Lehmann, Nucl. Phys **A593** (1995) 21.

[2] F. Iachello and A. Arima, *The Interacting Boson Model* (Cambridge University Press, Cambridge, 1987).

[3] L. Genilloud, H.G Börner, F. Corminboeuf, Ch. Doll, S. Drissi, M. Jentschel, J. Jolie, J. Kern, H. Lehmann, N. Warr, Nucl. Phys **A662** (2000) 3, and Erratum Nucl. Phys. **A669** (2000) 407.

[4] T. Belgya, C. Molnár, S.W. Yates, Nucl. Phys. **A607** (1996) 43.

[5] E. Sheldon and D.M. Van Patter, Rev. Mod. Phys. **38** (1966) 143.

[6] K.W. Winterbon, Nucl. Phys **A246** (1975) 293.

[7] F. Corminboeuf, T.B. Brown, L. Genilloud, C.D. Hannant, J. Jolie, J. Kern, N. Warr, and S.W. Yates, submitted to Phys. Rev. C.

[8] S. Landsberger, R. Lecomte, P. Paradis, S. Monaro, Phys. Rev. **C21** (1980) 588.

[9] G. Kenchian, Thesis, Universidade de Saõ Paulo (1995).

[10] E. Sheldon and V.C. Rogers, Comput. Phys. Commun. **6** (1973) 99.

[11] F. Iachello, Phys. Rev. Let. **53** (1984) 1427.

[12] P.O. Lipas, P. von Brentano, and A. Gelberg, Rep. Prog. Phys **53** (1990) 1355.

[13] A. Giannatiempo, A. Nannini, A. Perego, P. Sona, D. Cutoiu, Phys. Rev **C53** (1996) 2770.

[14] A. Giannatiempo, A. Nannini, P. Sona, D. Cutoiu, Phys. Rev **C52** (1995) 2969.

[15] P. van Isacker, K. Heyde, J. Jolie, and A. Sevrin, Ann. Phys. **171** (1986) 253.

[16] P.E. Garrett, H. Lehmann, C.A. McGrath, M. Yeh, and S.W. Yates, Phys. Rev. **C54** (1996) 2259.

PHYSICAL REVIEW C, VOLUME 62, 034313

Lifetimes of negative parity states in ^{168}Er

L. Genilloud and J. Jolie
Institut de Physique, Université de Fribourg, Pérolles, CH-1700 Fribourg, Switzerland

H. G. Börner and H. Lehmann
Institut Laue-Langevin, F-38042 Grenoble Cedex 9, France

F. Bečvář and M. Krtička
Faculty of Mathematics and Physics, Charles University, CZ-180 00 Prague 8, Czech Republic

N. V. Zamfir
WNSL, Yale University, New Haven, Connecticut 06520
and Clark University, Worcester, Massachusetts 01610

R. F. Casten
WNSL, Yale University, New Haven, Connecticut 06520
(Received 3 May 2000; published 21 August 2000)

Using the GRID method the lifetimes of 12 states belonging to four negative parity bands in ^{168}Er were measured at the high flux reactor of the Institut Laue-Langevin (ILL). For $K^\pi=0_1^-$ and $K^\pi=2_1^-$ bands the absolute $E1$ transitions are in agreement with those obtained within the framework of the *sdf* IBA-1 model and their octupole vibrational character is confirmed.

PACS number(s): 21.10.Tg, 21.60.Ev, 27.70.+q, 24.10.Pa

I. INTRODUCTION

A complete set of lifetimes of nuclear excited states below 2.2 MeV in a well-deformed nucleus could form a unique database for the study of nuclear structure. A good candidate for such a nucleus is ^{168}Er, one of the best known deformed nuclei. Davidson *et al.* [1] were able to identify the bandheads of 20 rotational bands by using in a systematic way the different techniques developed for the (n,γ) reaction in combination with transfer reaction data. The development of the γ-ray induced Doppler (GRID) broadening technique afterwards gave access to the lifetimes of states populated after neutron capture [2]. In two previous GRID experiments on ^{168}Er the double gamma vibration [3] and the nature of the $K^\pi=0^+$ bands [4] have been studied. In a continuation of our prior work several low-K bands were investigated. They could be candidates for rotational bands built on the octupole vibration.

Low-lying octupole states in ^{168}Er have been first studied by Neergard and Vogel [5] and next by Cottle and Zamfir [6] who compared excitation energies and $B(E3)$ values with those given in the interacting boson approximation (IBA). Photon scattering experiments [7] provided transition probabilities of $J^\pi=1^\pm$ states, which were compared to the quasiparticle-phonon nuclear model (QPNM) [8]).

II. THE MEASUREMENTS AND THEIR RESULTS

The experiments were performed in two dedicated runs at the high flux reactor of the Institut Laue-Langevin (ILL) in Grenoble. The target consisted of natural erbium in the form of Er_2O_3 powder with its abundance of 23% in ^{167}Er. It was placed at the in-pile position 50 cm away from the reactor core where a neutron flux of 5×10^{14} n cm^{-2} s^{-1} is available. Results obtained during the two earlier experiments [3,4] on negative parity states were also reanalyzed.

A. The GRID technique

After the capture of a thermal neutron coming from the reactor, the newly formed nucleus is in an highly excited state close to the neutron separation energy. This nucleus will deexcite mostly by a cascade of γ rays. The emission of each γ ray induces a small but significant recoil to the nucleus. The subsequently emitted γ rays will be Doppler broadened rather than shifted as the directions of the initial recoils are uniformly distributed. Because the recoils are very small, $v/c<10^{-4}$, extreme precision in the detection of the γ line profile is needed. The sole instruments able to measure such a small broadening are two-axis flat crystal spectrometers like GAMS4 [9].

The experimental data measured by the instrument consist of the line shape of a γ ray. Figure 1 shows the line shape profiles for selected transitions. Two major effects combine to form this line shape, the instrument response and the Doppler broadening. The first is described by the convolution of the line shape following from the dynamical diffraction theory [10] and the small Gaussian spread, called excess width, related to imperfections of the spectrometer. The second depends on the following five effects: the temperature of the target, the decay pattern of the nucleus, the lifetimes of all intermediate levels encountered in the cascades that populate the level of interest, the slowing-down of the recoiling nucleus, and the lifetime τ of the level of interest.

Provided that all phenomena underlying the Doppler broadening are under control [2], it is evident that the life-

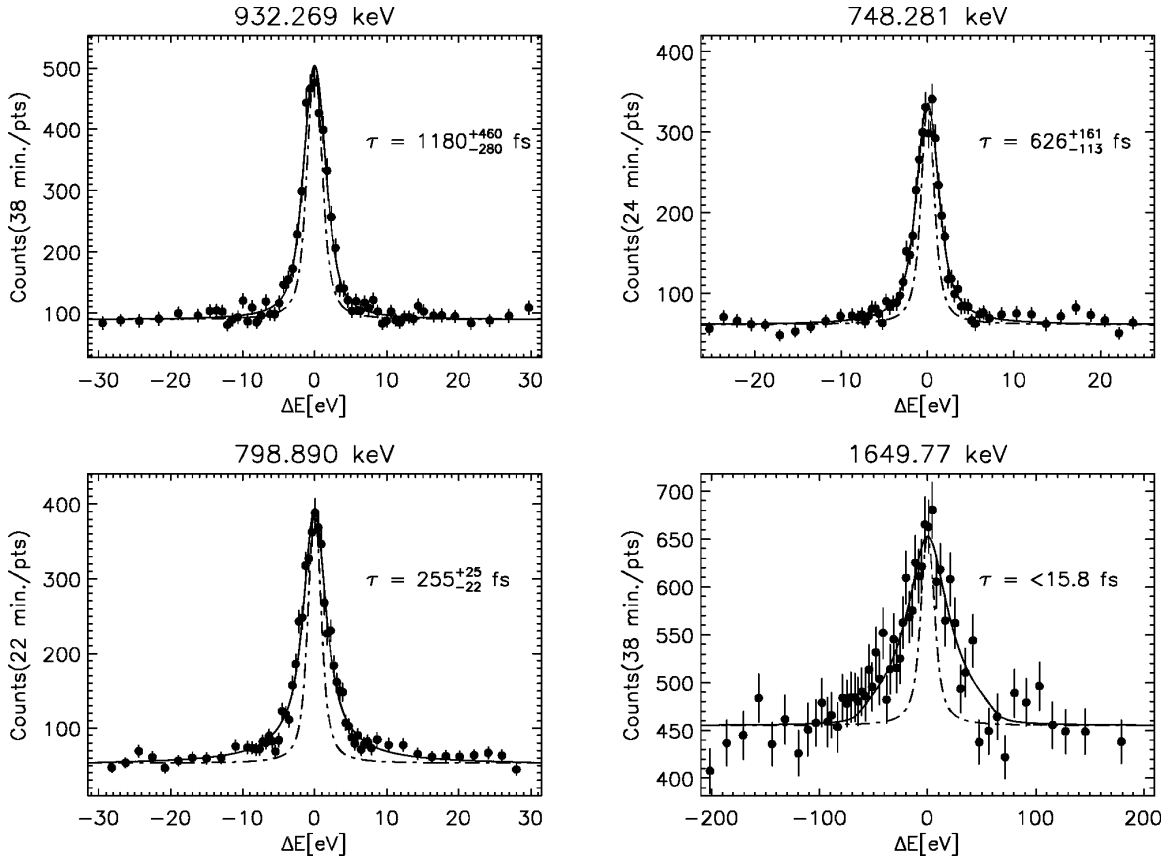

FIG. 1. Line shape of selected transitions measured with the GAMS4 spectrometer. The solid line is the fit of the γ-ray profile, the dash-dotted line corresponds to the instrumental response.

time τ can be extracted from the measured line shape. The major uncertainty in extracting lifetimes is not due directly to the measurement itself, but is related to the quantitative description of these phenomena.

Because the complete γ-decay scheme as well as the lifetimes of intermediate levels are experimentally unknown one has to base the analysis either on extreme feeding assumptions or on a statistical decay calculation. The first approach gives upper and lower limits on τ of the level of interest. To extract these limits from the measured line shape, all known feeding transitions — primaries and usually several distinct secondaries — are taken into account. By inspecting the population-depopulation balance for the level of interest the missing populating intensity is estimated. The upper limit of τ is based on the assumption that the missing intensity comes entirely from the capturing state via a sole primary transition. In this case the decaying nucleus is assumed to receive the highest possible recoil velocity from unobserved transitions. To get the lower limit, the missing intensity is attributed to hypothetical levels situated above the assumed excitation energy where the level scheme is considered to become incomplete as described in Ref. [11]. For extracting both these extreme limits of τ, all levels are assumed to be long lived, including the levels with known level energy and decay pattern. This implies that recoils occurring prior to the depopulation of these specified levels are not assumed to contribute to Doppler broadening of a γ line under the study.

With these assumptions one can predict the nuclear velocity distribution at the moment when the level of interest is populated. Knowing this distribution, the slowing down of the atom is then treated in the framework of mean free-path approach (MFPA) to predict the corresponding line shape as discussed in Ref. [2]. Comparing these line shapes with the observed profile the lower and upper limits are in turn estimated.

B. Statistical simulation of γ-ray cascades

In the second approach the lifetime estimates were deduced with the aid of *joint simulations* of both participating phenomena, specifically γ cascades that are responsible for the nuclear recoils, as well as slowing-down of the deexciting nucleus due to atomic collisions. These simulations were performed to cover the time interval initiated by the emission of a primary γ ray and ending at the moment of the depopulation of the level of interest.

Assuming the validity of the statistical model of the nucleus and the paradigm of the photon strength functions (PSFs) the algorithm DICEBOX [12,13] is used to generate γ cascades by the Monte Carlo method. With this algorithm a

full set of level energies, branching intensities and total radiation widths is generated using the technique of precursors, as explained in Ref. [12]. This set, called hereafter a nuclear realization, characterizes decay properties of a complete level system. It is understood that there exists an infinite number of nuclear realizations, one of them being identical with the real nucleus. Having a fixed nuclear realization, independent cascade decays of the neutron capturing state are repeatedly simulated with the algorithm DICEBOX. Each such trial yields energies of the individual γ rays of a given cascade. Knowing the total radiation widths of the intermediate levels involved, emission times of the individual γ-rays of each cascade are easily calculated. The interval between any pair of successive emissions is considered to be a quantity drawn at random from the corresponding exponential distribution, whose lifetime parameter is uniquely determined by the total radiation width of an encountered intermediate level. In total 20 nuclear realizations have been simulated and for each of them 50 000 cascades were produced.

The semiempirical expression for the PSF of $E1$ radiation proposed in Ref. [14] was adopted for these simulations. In acceptable agreement with the systematics in Ref. [15] values $k_0=3$ and $E_{\gamma 0}=4.5$ MeV for parameters entering this expression were chosen. In the case of $M1$ radiation it was assumed that the photon strength comes from the scissors and spin-flip resonances. In conformity with the NRF data [7] and with the data on the excited-state scissors resonances, see Refs. [16,17], the integrated scissors-resonance strength was taken to be $\Sigma B(M1)\uparrow = 4.1\ \mu_N^2$ for the γ-ray energy interval of 2–4 MeV, while in the case of the spin-flip resonance we assumed a total integrated strength of $\Sigma B(M1)\uparrow = 11.5\ \mu_N^2$. Concerning $E2$ radiation, an energy-independent photon strength of $k_{E2}=1\times 10^{-10}$ MeV^{-5} was postulated. The level density was described by the Bethe formula. As shown in Ref. [13], careful selection of the models for PSFs and the level density is crucial for achieving a minimum bias in estimating lifetimes of short-lived levels with $\tau < 100$ fs.

In the above-mentioned joint simulations the atomic collisions responsible for slowing-down are treated in the framework of the fluctuating free path approach (FFPA) [13]. Most of the assumptions on which the FFPA is based are identical to those of MFPA. The differences between the approaches are as follows: (i) the path between collisions within FFPA is considered to be a random realization of an exponential distribution, whose average is adjusted to the *mean free path* at a given velocity, (ii) in the case of FFPA the thermal motion of atoms in the sample is taken into account during the whole process of γ emission and atomic collisions, affecting in this way the mean free path, while in the case of MFPA the contribution of thermal motion is applied only after the moment when the slowing-down atom reaches the thermal velocity, and (iii) in FFPA the relative energy losses during atomic collisions are considered to be variable. It should be stated that the FFPA yields — in the case of the same feeding pattern — lifetime values are reduced compared to those from statistical calculations using the MFPA, being in agreement with results from other methods (DSAM, RMD), see Ref. [18].

TABLE I. Instrumental response for the different runs.

Run	Date	Excess width [marcsec]	Thermal velocity [m/sec]	Transitions measured [keV]
1	7.1990	6.2(1)	311(11)	1942.7
2	4.1995	13.3(2)	325(24)	1706.4
3	2.1998	9.9(3)	428(25)	798.9,932.7,1279.1,1649.8
4	5.1998	8.4(3)	497(21)	737.7,748.3,790.0 980.0,1892.6,1921.1

C. Experimental results

As has been mentioned above the temperature of the target material contributes also to the broadening of the line profile. This was determined in the usual manner [2] by measuring the broadening of a γ transition depopulating a long-lived state. The instrumental response — given by dynamical diffraction theory folded with a tiny Gaussian spread called excess width — was deduced from nondispersive scans. The values obtained are given in Table I for the different runs. More details concerning these procedures may be inferred from Ref. [2].

The measured line profiles including the contribution from the instrumental response and thermal width are shown in Fig. 1 for selected transitions, while Fig. 2 shows the scans of the χ^2 surface as a function of the lifetime. The resulting lifetime corresponds to the minimum of the function interpolating the curve, whereas the errors are given by the values for τ at $\chi^2_{\min}+1$. When the form of the interpolating function is parabolic the errors are quasisymmetric.

The lifetimes have been extracted with both approaches, MFPA with extreme limit assumptions and FFPA using simulations of the γ-ray cascades; they are given in Table II together with the deduced $B(E1;J_i\rightarrow J_f)$ values. Of the lifetimes measured in this work, one (the 1786.1 keV level) can be compared with the result from another experiment, i.e., the nuclear resonance fluorescence (NRF) measurement. Using the FFPA description a longer lifetime is found. Nevertheless, in view of the relatively large uncertainties these values are not inconsistent.

In addition to the data on the negative-parity bands the data from two previous measurements [3,4] on the $K^\pi=4^+$ double-γ band and $K^\pi=0^+$ bands were reanalyzed (see lines 2 and 3 in Table III) using the FFPA and the DICEBOX simulations. The χ^2 plot for the decay of the $2^+_{K^\pi=0^+_2}$ state is given in Fig. 2.

III. COMPARISON WITH CALCULATIONS

An octupole vibration about a spherical shape creates an excited state with $J^\pi=3^-$. In deformed nuclei this octupole state is split into four intrinsic states with $K^\pi=0^-,1^-,2^-,3^-$, K being the absolute value of the projection of the octupole phonon angular momentum on the symmetry axis of the nucleus. On each of these states, a rotational band is built. The candidates for such a structure in ^{168}Er are shown in Fig. 3. The uncertainties in the assignment of the

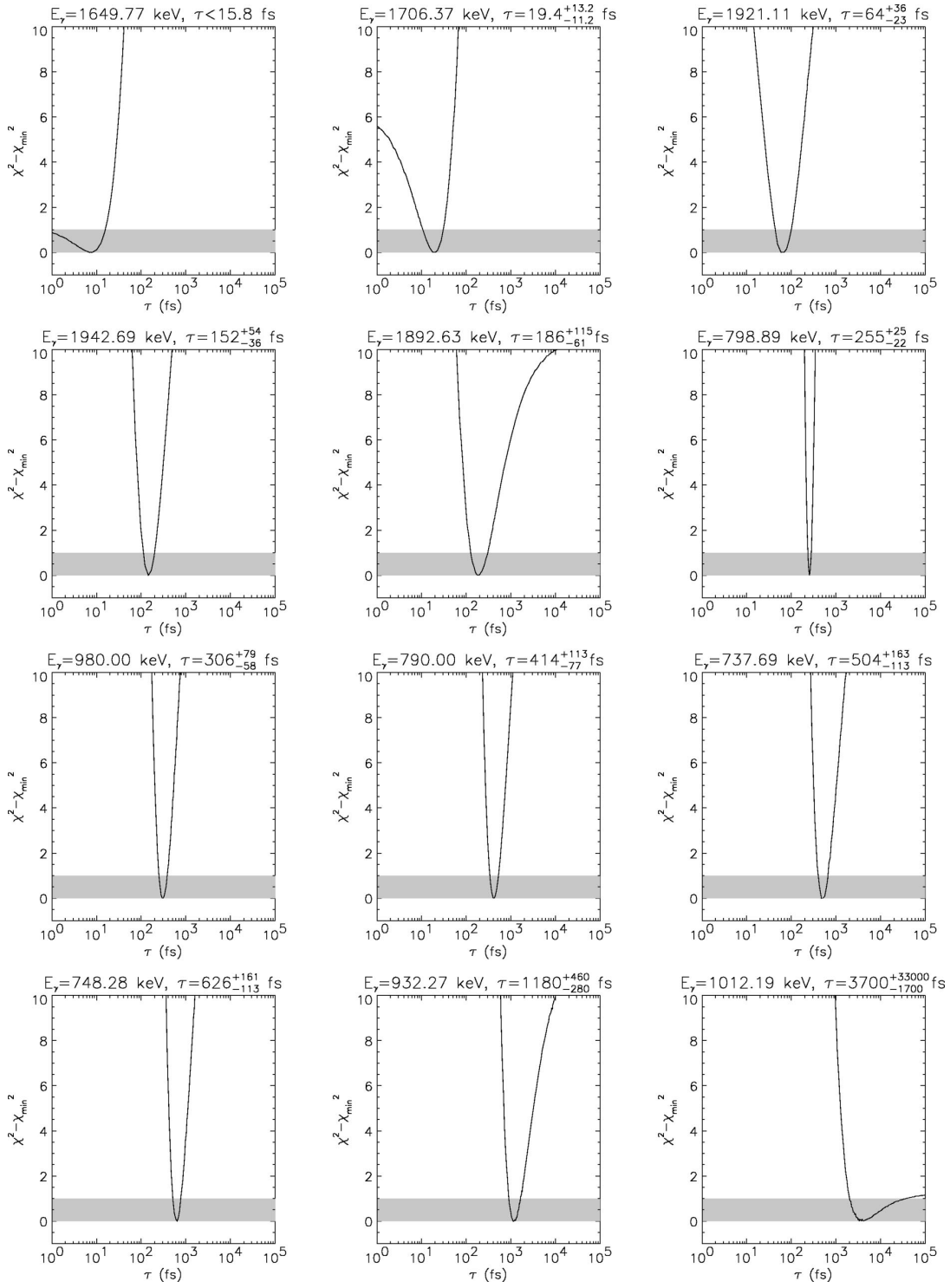

FIG. 2. χ^2 plots for the different measured γ rays as a function of the lifetime τ. The gray areas represent the regions below the one-σ limit.

TABLE II. Experimental and calculated absolute $B(E1)$ strengths.

		Level		Lifetime [fs]				$B(E1;J_i\rightarrow J_f)$ [m W.u.]				
K^π	J_i^π	E_x [keV]	E_γ [keV] [a]	τ_{FFPA} [b]	τ_{ext} [c]	τ_{litt} [e]	J_f^π	Exp. [f]	Calc.		E_{th} [keV]	
									SDF	QPNM [g]	SDF	QPNM [g]
0_1^-	1^-	1786.1	1706.37	$19.4^{+13.2}_{-11.2}$	<137	5.0(6)	0_1^+	1.13^{+150}_{-46}	0.881	2.94	1807	1850
							2_1^+	1.97^{+270}_{-80}	1.645			
	3^-	1913.9	1649.77	<15.8	7–69		2_1^+	0.34–3.3 [d]	1.057		1893	
							4_1^+	0.57–5.6 [d]	1.137			
	5^-	2185.1	1921.11	64^{+36}_{-23}	14–228		4_1^+	0.43^{+24}_{-16}	0.982		2094	
							6_1^+	0.35^{+20}_{-13}	0.698			
1_1^-	1^-	1358.9	1279.127		$\geqslant 7000$		0_1^+	<0.0054	0.013	0.98	1259	1300
							2_1^+	<0.0153	0.067			
							2_2^+	<0.0021	0.035			
	3^-	1431.5				$5.9\cdot 10^4$	2_1^+	0.0011	0.181		1380	
							4_1^+	0.0017	0.282			
							3_1^+	0.0001	0.002			
1_2^-	1^-	1936.6				346(101)	0_1^+	0.108^{+44}_{-24}	0.008	0.233	2178	1920
							2_1^+	0.020^{+8}_{-5}	0.052			
	2^-	1972.3	1892.63	186^{+115}_{-61}	95–570		2_1^+	0.137^{+67}_{-52}	0.006		2218	
							2_2^+	0.134^{+65}_{-51}	0.033			
							3_1^+	0.471^{+230}_{-180}	0.000			
	3^-	2022.3	1942.69	152^{+54}_{-36}	<458		2_1^+	0.215^{+67}_{-56}	0.045		2379	
							4_1^+	0.082^{+25}_{-21}	0.121			
	4^-	2097.6	979.996	306^{+79}_{-58}	<560		4_1^+	0.063^{+15}_{-13}	0.014		2422	
							3_1^+	0.153^{+36}_{-31}	0.054			
							4_2^+	0.047^{+11}_{-9}	0.042			
							5_1^+	0.326^{+76}_{-67}	0.012			
2_1^-	2^-	1569.5	748.281	626^{+161}_{-113}	415–1166		2_1^+	0.0060^{+13}_{-12}	0.010		1616	
							2_2^+	0.815^{+180}_{-170}	0.988			
							3_1^+	0.493^{+110}_{-100}	0.469			
	3^-	1633.5	737.686	504^{+163}_{-113}	239–1181		2_2^+	0.397^{+110}_{-97}	0.339		1700	
							3_1^+	0.631^{+180}_{-150}	0.583			
							4_2^+	0.652^{+190}_{-160}	0.639			
3_1^-	3^-	1541.6				$1.15\cdot 10^4$	2_2^+	0.021			-	
							3_1^+	0.009				
							4_1^+	0.010				
3_2^-	3^-	1828.1	932.269	1180^{+460}_{-280}	750–2890		2_2^+	0.029^{+9}_{-8}				
							3_1^+	0.159^{+50}_{-45}				
							4_2^+	0.140^{+44}_{-39}				
	4^-	1892.9	798.890	255^{+25}_{-22}	47–441		3_1^+	0.0220(20)				
							5_1^+	0.0302(28)				
	5^-	1983.0	790.001	414^{+113}_{-77}	<1069		6_2^+	0.0377^{+86}_{-81}				

[a] Transition measured for the corresponding level.
[b] Lifetime determined using DICEBOX [12] simulations for unknown feeding and FFPA for atomic collisions.
[c] Lifetime determined using extreme assumptions for the unknown feeding [11].
[d] $B(E1)$ values calculated using τ_{ext} because of nonconvergence of τ_{FFPA} in the fit.
[e] Lifetime taken from Ref. [19].
[f] Computed with τ_{FFPA} and branching ratios taken from Ref. [1].
[g] Values calculated in the quasiparticle-phonon nuclear model (QPNM) (Ref. [8]).

$K^\pi=1^-$ and $K^\pi=3^-$ bands as octupole vibrational come from the observation of significant two-quasiparticle strength to the lower levels in single-neutron stripping reactions [20]. In order to settle the question of the structure of these bands, it is necessary to get information of the structure of the wave functions; this can be done considering the electromagnetic transition probabilities.

The negative parity states can be described in the IBA-1 model [21] by adding a single f boson with $L=3$ to the usual sd boson model space [22,23]. The sdf Hamiltonian is

TABLE III. Comparison between lifetimes extracted with FFPA and previous approaches.

J^π_K	E_γ [keV] [a]	$\tau_{\rm stat}$ [fs] [b]	Ref.	$\tau_{\rm FFPA}$ [fs]	$\tau_{\rm litt}$ [fs] [c]
$1^-_{1^-}$	1706.37	$22.7^{+12.5}_{-9.8}$	This work	$19.4^{+13.2}_{-11.2}$	5.0(6)
$2^+_{K^\pi=0^+_2}$	1012.19	2900^{+3100}_{-1000}	[4]	3700^{+33000}_{-1700}	
$4^+_{\gamma\gamma}$	1234.76	440^{+90}_{-70}	[3]	470^{+105}_{-76}	320(16)

[a]Transition measured for the corresponding level.
[b]Statistical model using MFPA to describe the slowing down.
[c]Lifetime taken from Ref. [19].

$$H = H_{sd} + H_f + V_{sdf}, \tag{1}$$

where the different terms were proposed in [6,24]. For the calculation of energies we used the same parameters as those used in Ref. [6]. The results are discussed in the next paragraph. The $E1$ transition rates were calculated using the operator $T^{(E1)}_{sdf}$ defined in Ref. [6] with the same parameters with the exception of the effective charge for which we adopted the value $e_1 = 0.136$ e fm, half the value used in Ref. [6].

The agreement of the calculated $B(E1)$ values with the data is very good (see Table II) for the $K^\pi = 0^-_1$ and $K^\pi = 2^-_1$ bands. This fact is in line with the octupole vibrational interpretation of these 2 bands. In the case of the $K^\pi = 1^-_1$ and $K^\pi = 1^-_2$ bands the overall agreement is rather poor. However, Table II shows that most experimental and calculated $B(E1)$ values from these bands, at least to the ground band, are much smaller than those from the $K^\pi = 0^-_1$ and $K^\pi = 2^-_1$ bands. Therefore, these transitions presumably proceed by noncollective amplitudes and one would not expect good agreement from a collective model such as the IBA. We do note, however, that the $K^\pi = 1^-_2$ band is very well reproduced in the QPNM calculations, both in energy and $B(E1)$ values (see Table II). In order to see the degree of collectivity of different octupole bands, we compare in Table IV the experimental $B(E3; 0_{\rm g.s.} \rightarrow 3^-)$ values from Ref. [25] with the IBA results using the $T(E3)$ operator defined in Ref. [6] ($e3 = 0.076$ $e\,{\rm b}^{3/2}$, $\chi_3 = 0.76$). The calculated $B(E3)$ values agree very well with the data for $K^\pi = 1^-_1, 2^-_1, 0^-_1$. The IBA model predicts a very small value for $B(E3; 0_{\rm g.s.} \rightarrow 3^-_{K^\pi=1^-_2})$, in agreement with the fact that this state was not observed in the inelastic scattering experiment [25]. The very small value predicted by IBA, which is obviously a collective model, indicates that a small $B(E3; 0_{\rm g.s.} \rightarrow 3^-)$ value is not always an argument for lack of collectivity. In the present case, the $K^\pi = 1^-_2$ band and, as will be seen in the next section the $K^\pi = 3^-_1$ band, are octupole excitations based on the γ band and not on the ground state. This situation is reminiscent of the case for the $K^\pi = 0^+_2$ band which, in the IBA, has strong $B(E2)$ values to the γ band but nearly vanishing ones to the ground band: it is a collective band, but collectively related to the γ band not the ground band.

TABLE IV. Comparison between experimental $B(E3; 0^+_{\rm g.s.} \rightarrow 3^-)$ values (from Ref. [25]) with SDF-IBA-1.

K^π	$E_{\rm exc}(J^\pi = 3^-)$ [keV]		$B(E3; 0^+_{\rm g.s.} \rightarrow 3^-)$ [$e^2\,{\rm b}^3$]	
	Exp.	Calc.	Exp.	Calc.
1^-_1	1431	1380	0.046(5)	0.051
2^-_1	1633	1700	0.058(6)	0.035
0^-_1	1913	1893	0.023(3)	0.015
1^-_2	2022	2379		0.003
3^-_1	1541		0.003(1)	
3^-_2	1828		0.007(2)	
3^-_3	1999		0.005(1)	
3^-_4	2323		0.018(2)	
3^-_5	2337 [a]			
3^-		2253		0.000

[a]Taken from Ref. [26].

IV. DISCUSSION

The $B(E1)$ data confirms the results of Refs. [5,6] that the $K^\pi = 0^-_1$ and 2^-_1 bands are octupole vibrational excitations based on the ground state. The $B(E3)$ data show that the $K^\pi = 1^-_1$ band has the same character. The situation with the $K^\pi = 3^-$ bands is more complicated. There are five experimental $K^\pi = 3^-$ bands at 1541, 1828, 1999, 2323, and 2337 keV and the lowest $K^\pi = 3^-$ band predicted by the IBA model is at 2253 keV (see Table IV). For the first three the experimental $B(E3; 0_{\rm g.s.} \rightarrow 3^-)$ values are very small. The IBA model predicts an extremely small $B(E3; 0_{\rm g.s.}$

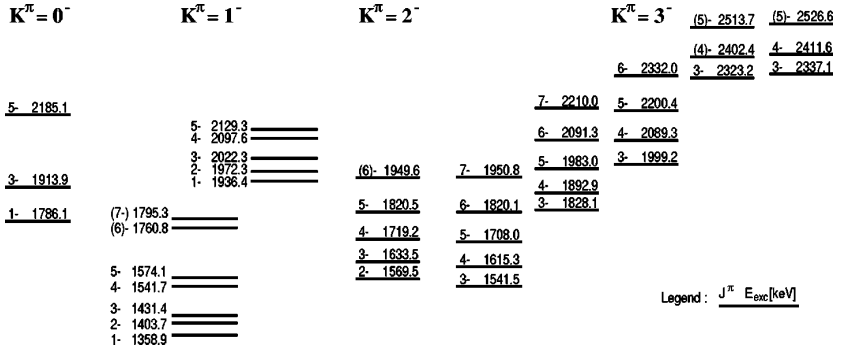

FIG. 3. Candidates for rotational bands built on the octupole vibration.

TABLE V. The IBA $E3$ squared reduced matrix elements.

K^π	$E_{exc}(J^\pi=5^-)$ [keV] (th.)	$M(E3;2_i^+\rightarrow 5^-)^2$ $[e^2b^3]$ 2_1^+ (g.s.)	2_2^+ (γ band)
1_1^-	1598	**0.125**	0.003
2_1^-	1945	**0.047**	0.009
0_1^-	2094	**0.042**	0.001
1_2^-	2698	0.004	**0.025**
3_1^-	2487	0.000	**0.047**

$\rightarrow 3^-_{K^\pi=3_1^-}$) value, as well. However, the existing data do not permit one to identify which experimental $3^-_{K^\pi=3^-}$ state corresponds to $3^-_{K^\pi=3_1^-}$ in the IBA. Moreover, the IBA predictions for the $B(E1)$ values related to the $K^\pi=3_1^-$ band are considerably smaller than the experimental $B(E1)$ values corresponding to the $K^\pi=3_1^-$ and 3_2^- bands. The fact that the IBA predictions do not fit these data suggests a noncollective character of these bands and it is possible that the $K^\pi=3^-$ octupole vibrational band is the $K^\pi=3_3^-$ band or higher, but there are currently no definitive experimental data available. In order to understand better the structure of the $K^\pi=1_2^-$ and 3_1^- bands predicted in the IBA model we compare in Table V the squared reduced matrix elements $M(E3)^2$ calculated for transitions between 2_1^+, 2_2^+, and 5^- states of different bands. The use of the reduced matrix elements is prefered because the statistical factor $2J_i+1$ is removed, allowing a direct comparison with the $B(E3;0^+_{g.s.}\rightarrow 3^-)$ values. The corresponding $B(E3;2_i^+\rightarrow 5^-)$ values are shown in Fig. 4. The squared reduced matrix elements for the transitions from the 2_1^+ state to the 5^- members of the $K^\pi=0_1^-$, 1_1^-, and 2_1^- bands are comparable with the calculated $B(E3)$ values from $0^+_{g.s.}$ to their 3^- members (see Table IV). The reduced matrix elements for the transitions from the 2_2^+ state to the same 5^- states are very small. Thus, these predictions reflect the character of these bands as octupole vibrations built on the ground state. However, in the case of the $K^\pi=1_2^-$ and 3_1^- bands the situation is reversed: these bands are calculated to have large reduced matrix elements to the γ band and not to the ground state, indicating that these two bands are octupole vibrations built on γ vibrations, and hence have a two-phonon (quadrupole-octupole) character.

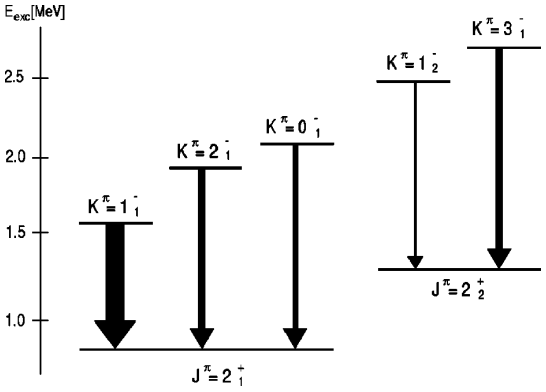

FIG. 4. Largest theoretical $B(E3;5^-\rightarrow 2_i^+)$ strength to the 2_1^+ and 2_2^+ states from various negative parity bands in ^{168}Er in the IBA. In each case, the transition to the other 2^+ state is calculated to be about an order of magnitude weaker.

V. CONCLUSIONS

The lifetimes of 12 states in four negative parity bands ($K^\pi=0_1^-$, 1_1^-, 1_2^-, 2_1^-, and 3_2^-) in ^{168}Er were measured using the GRID method, giving this nucleus one of the best known sets of negative parity states. The IBA model reproduces very well the $B(E1)$ values, the excitation energies and the $B(E3)$ values for the $K^\pi=0_1^-$ and 2_1^- bands. It fails to reproduce the $B(E1)$ values related to the $K^\pi=1_1^-$ and $K^\pi=1_2^-$ bands. However, the excitation energies and the $B(E3)$ values support the octupole vibrational character of these bands, based on ground state and on γ vibration, respectively. The $B(E1)$ values related to the $K^\pi=3_2^-$ band are not reproduced by the model and probably this band does not have a collective character. The IBA calculations indicate that the collective $K^\pi=3^-$ band is located higher in energy and it is a double phonon (quadrupole γ + octupole) excitation, similar to the $K^\pi=1_2^-$ band.

ACKNOWLEDGMENTS

This work was supported by the Swiss National Science Foundation and U.S. DOE under Contract Nos. DE-FG02-91ER40609 and DE-FG02-88ER40417.

[1] W.F. Davidson, D.D. Warner, R.F. Casten, K. Schreckenbach, H.G. Börner, J. Simić, M. Stojanović, M. Bogdanović, S. Koički, W. Gelletly, G.B. Orr, and M.L. Stelts, J. Phys. G **7**, 455 (1981); **7**, 843(E) (1981).
[2] H.G. Börner and J. Jolie, J. Phys. G **19**, 217 (1993).
[3] H.G. Börner, J. Jolie, S.J. Robinson, B. Krusche, R. Piepenbring, R.F. Casten, A. Aprahamian, and J.P. Draayer, Phys. Rev. Lett. **66**, 691 (1991); **66**, 2837(E) (1991).
[4] H. Lehmann, J. Jolie, F. Corminboeuf, H.G. Börner, C. Doll, M. Jentschel, R.F. Casten, and N.V. Zamfir, Phys. Rev. C **57**, 569 (1998).
[5] K. Neergard and P. Vogel, Nucl. Phys. **A145**, 33 (1970).
[6] P.D. Cottle and N.V. Zamfir, Phys. Rev. C **54**, 176 (1996).
[7] H. Maser, S. Lindenstruth, I. Bauske, O. Beck, P. von Brentano, T. Eckert, H. Friedrichs, R.D. Heil, R.-D. Herzberg, A. Jung, U. Kneissl, J. Margraf, N. Pietralla, H.H. Pitz, C. Wesselborg, and A. Zilges, Phys. Rev. C **53**, 2749 (1996).
[8] V.G. Soloviev, A.V. Sushkov, and N.Yu. Shirikova, Phys. Rev. C **56**, 2528 (1997).
[9] E.G. Kessler, G.L. Greene, M.S. Dewey, R.D. Deslattes, H.G.

Börner, and F. Hoyler, J. Phys. G **14**, S167 (1988).
[10] W.H. Zachariasen, *Theory of X-ray Diffraction in Crystals* (Wiley, New York, 1945).
[11] H.G. Börner, M. Jentschel, N.V. Zamfir, R.F. Casten, M. Kritcka, and W. Andrejtscheff, Phys. Rev. C **59**, 2432 (1999).
[12] F. Bečvář, Nucl. Instrum. Methods Phys. Res. A **417**, 434 (1998).
[13] F. Bečvář, M. Krtička, and M. Jentchel, *Applications of High-Precision γ-spectroscopy* (Notre Dame University Press, South Bend, IN 1998).
[14] J. Kopecky, M. Uhl, and R.E. Chrien, Phys. Rev. C **47**, 312 (1993).
[15] J. Kopecky, ''Handbook for calculations of nuclear reaction data,'' Reference input parameter library, IAEA-TECDOC-1034, August, 1998 (unpublished), p. 97.
[16] F. Bečvář, P. Cejnar, J. Honzátko, K. Konečný, I. Tomandl, and R.E. Chrien, Phys. Rev. C **52**, 1278 (1995).
[17] F. Bečvář, M. Krtička, J. Honzátko, I. Tomandl, F. Käppeler, F. Voss and K. Wisshak, in 10th Capture Gamma-Ray Spectroscopy and Related Topics, Santa Fe, 1999 (in press).
[18] J. Keinonen, in *Workshop on Application of High Resolution Gamma Spectroscopy in Studies of Atomic Collisions and Nuclear Lifetimes*, edited by H.G. Börner, J. Jolie, M. Pendlebury, and S. Ulbig (Institut Laue-Langevin, Grenoble 1992), p. 131.
[19] V.S. Shirley, Nucl. Data Sheets **53**, 223 (1988).
[20] D.G. Burke, B.L.W. Maddock, and W.F. Davidson, Nucl. Phys. **A442**, 424 (1985).
[21] F. Iachello and A. Arima, *The Interacting Boson Model* (Cambridge University, Cambridge, 1987).
[22] A. Arima and F. Iachello, Phys. Lett. **57B**, 39 (1975).
[23] A. Arima and F. Iachello, Ann. Phys. (N.Y.) **111**, 201 (1978).
[24] A.F. Barfield, J.L. Wood, and B.R. Barrett, Phys. Rev. C **34**, 2001 (1986); A.F. Barfield, B.R. Barrett, J.L. Wood, and O. Scholten, Ann. Phys. (N.Y.) **182**, 344 (1988).
[25] I.M. Govil, H.W. Fulbright, D. Cline, E. Wesolowski, B. Kotlinski, A. Backlin, and K. Gridnev, Phys. Rev. C **33**, 793 (1986).
[26] W.F. Davidson and W.R. Dixon, J. Phys. G **17**, 1683 (1991).

Part Three

PEGASE

Program **E**valuating **GA**mma-ray **S**pectra for the determination of **E**lemental compositions

Laurent Genilloud

Internal Report IFP-PAN 13

Université de Fribourg

June 2000

1 Introduction

The meaning of the acronym **PEGASE** is: **P**rogram **E**valuating **GA**mma-ray **S**pectra for the determination of **E**lemental compositions.

This software was written at the demand of the Paul-Scherrer Institut (PSI) for the analysis of spectra issued from a Prompt Gamma-ray Activation (PGA). The goals were that any user without knowledge of nuclear physics data analysis should be able to use the PEGASE program running under Windows95/98.

The analysis of the data consists of two main parts: the least-square fit of the whole spectrum and the comparison of the resulting information to a library of neutron capture gamma rays. Finally, the results have to be appreciated *de visu* in order to refine the qualitative and quantitative information.

2 Theory

2.1 Overview of the PGA technique

The analysis with Prompt Gamma-ray Activation (PGA) reaction is an excellent tool to determine the presence and quantity of elements in a sample by irradiating it continuously with neutrons.

In the present paragraph we will present the different advantages of this method. The analysis technique is non-destructive and can so be applied even to rare materials. It is also multi-elementary in the sense that only one measurement is enough to give quantitative information about all observed element. As neutrons penetrate easily into nearly all materials, PGA analyses the entire volume of a sample and not only his surface. Under a continuous flux of neutrons nearly all elements will capture neutrons; the direct consequence is that the PGA technique is sensitive to a vast range of elements. However not all isotopes have the same preponderance to capture neutrons as this depends on the nuclear structure of the atomic nuclei; consequently, the sensitivity of this technique can be very different for elements.

The energy of the prompt γ photons emitted by the excited nuclei following the neutron capture is measured by an anti-Compton spectrometer. The resulting data are a very complex spectrum that has to be analysed by computer in order to extract qualitative and quantitative information about the sample.

2.2 The neutron capture reaction

The SINQ facility at the Paul-Scherrer Institute (Villigen, Switzerland) delivers a cold neutron beam (i.e. neutrons with kinetic energy lower than 0.025 MeV). Neutrons, being not electrically charged, are not affected by the Coulomb

repulsion and so can easily penetrate matter. They are however sensitive to the strong nuclear force and can be captured by an atomic nucleus, leading to the following reaction:

$$^{A}Z + n \rightarrow ^{A+1}Z^{*} \quad (1)$$

where the asterisk means that the formed nucleus is in an excited state. The neutron binding energy (about 8 MeV) is gained by the residual nucleus. This excitation energy has to be released by the emission of γ rays:

$$^{A+1}Z^{*} \rightarrow ^{A+1}Z + \gamma \quad (2)$$

The γ energy is not distributed continuously on the spectrum but in discrete peaks. This radiation is characteristic of the nuclear product ^{A+1}Z, it is therefore possible to know which elements form the sample by identifying their characteristic peaks. In first order of approximation, the number of newly formed nucleus ^{A+1}Z will depend on:

- the concentration of element Z in the sample
- the atomic weight of the element Z
- the flux of neutrons
- the neutron absorption cross-section of the isotope ^{A}Z
- the natural abundance of the isotope ^{A}Z

With these observations, we will demonstrate in the next section how to extract not only qualitatively information about the content of the sample but also absolute concentrations.

PGA should not be confused with the use of the gamma radiation of long-lived radioactive decay products formed after neutron capture for elemental analysis, the well-known neutron activation analysis method (NAA).

2.3 k_0 Method

2.3.1 Theory

As seen in the precedent section, the number of newly formed nucleus depends for one thing on the neutron absorption cross-section. This cross-section is inversely proportional to the speed of the neutrons in the absence of resonance. That means that while the energy of the neutrons is not modified their absorption cross-section for a specified isotope remain the same. But neutron will interact with matter before being captured by an atomic nucleus and consequently their energy will be modified; for example scattering of thermal neutrons in hydrogenous samples can lead to analytical errors of as much as 20%, depending on sample size and shape [1,2]. Neutrons can also gain energy by elastic scattering from a room-temperature sample. Lindstrom [3] notes a 20% higher capture rate in a 1-g sample of organic

material when the sample was freshly cooled with liquid nitrogen, compared with the same sample at room temperature.

One see that an absolute determination of the elemental concentration can lead to large errors when not taking into account the modification of the neutrons' energy. However, we show in a simple way in this section that all these analytical biases disappear if only elemental *ratios* are determined [4]. For a *homogeneous* sample irradiated in a neutron beam with flux density Φ for a time τ, the peak area A of a neutron capture γ ray of energy E_γ from mass m of element x is in general given by [4]:

$$A_{x,E_\gamma} = \frac{m_x N_A \Theta_x I_{\gamma,x}}{M_x} \int_V \int_{E_n=0}^{\infty} \int_{t=0}^{\tau} \sigma_x(E_n)\phi(E_n,t,V)\varepsilon(E_\gamma,V)dtdE_n dV \tag{3}$$

where N_A is Avogadro's number, Θ the abundance of the capturing isotope of the element of interest, I_γ the γ-ray yield in photons per capture, M the atomic weight, ε the apparatus total efficiency and σ the neutron capture cross-section. One can assess that the *shape* of the $\varepsilon(E_\gamma)$ is invariant over the small sample volume *V* [3]; similarly we assume that the neutron spectrum and time parameters are separable [3]:

$$\int_V \varepsilon(E_\gamma,V)dV = \varepsilon(E_\gamma) f(V) \tag{4}$$

$$\phi(E_n,t,V) = \varphi(E_n,V)g(t) \tag{5}$$

Normalizing to the corresponding expression for the peak area of a monitor element s in the *same homogeneous* sample, the space and time factors cancel, giving:

$$\frac{A_{x,E_\gamma}}{A_{s,E_\gamma}} = \frac{\dfrac{m_x \Theta_x I_{\gamma,x}\varepsilon(E_\gamma,x)}{M_x} \displaystyle\int_{E_n=0}^{\infty} \sigma_x(E_n)\phi(E_n)dE_n}{\dfrac{m_s \Theta_s I_{\gamma,s}\varepsilon(E_\gamma,s)}{M_s} \displaystyle\int_{E_n=0}^{\infty} \sigma_s(E_n)\phi(E_n)dE_n} \tag{6}$$

As we said above, the capture cross-section for cold neutrons is inversely proportional to their speed for nearly all atomic nucleus (with well known exceptions as Cd and Gd), so one can write $\sigma = \sigma_0 \cdot v_0 / v$, where σ_0 is the cross-section for thermal neutrons (i.e. neutrons with a velocity $v = v_0 = 2200\,\mathrm{ms}^{-1}$). Consequently, the ratios of the two integrals in expression (6) becomes $\sigma_{0,x} = \sigma_{0,s}$. With these substitutions we then obtain the relation between the ratios of the experimentally measured quantities and the corresponding ratios of tabulated quantities:

$$k_0(x,s) = \frac{A_{x,E_\gamma} \Big/ m_x \varepsilon(E_\gamma, x)}{A_{s,E_\gamma} \Big/ m_s \varepsilon(E_\gamma, s)} = \frac{\Theta_x I_{\gamma,x} \sigma_{0,x} \Big/ M_x}{\Theta_s I_{\gamma,s} \sigma_{0,s} \Big/ M_s} \tag{7}$$

All quantities appearing in the right part of the expression (7) are physical constants; normalizing the k_0 value of the comparator element to 1.000, the expression (7) is written:

$$k_0(x,\gamma) = \frac{\Theta_x I_{\gamma,x} \sigma_{0,x}}{M_x} \tag{8}$$

The k_0 values are used to compute the mass concentrations of the identified elements. For the determination of the absolute masses it is necessary to introduce a correction factor κ. This factor takes into consideration the modification of the neutrons' kinetic energy due to their collisions with different nuclei. Therefore, the κ coefficient depends upon the geometry and the composition of the sample and cannot be determined once for all. Knowing the neutron flux *N*, one computes the masses of the different elements with the following formula.

$$m_x = \frac{A_{x,E_\gamma} \Big/ \varepsilon(E_\gamma, x)}{k_0(x,\gamma)} \cdot \frac{1}{N \cdot \kappa} \tag{9}$$

2.3.2 The k_0 table

The PGAA group of Budapest in collaboration with the National Institute of Standards and Technology (NIST) have determined precise k_0 factors for nearly all stable elements. The table summarizing their result is given in Annex.

For each element, a typical number of three k_0 is given. These data are of a big importance to deduce quantitative information. However, three lines per element is not insufficient to compare with the big amount of fitted γ-ray lines. It is by consequent necessary to add lines for each element in this table. This task was done by Sébastien Baechler (Sebastien.Baechler@unifr.ch); in Table 1 is given an extract of the *k_0 table*.

Table 1: table of k_0

Z	Name	A	Gamma-ray energy	Error	Normalized Gamma-ray intensity	K0	Error
26	Fe	56	7631.050	0.090	100.0000	3.74E-02	1.9
26	Fe	56	7645.490	0.090	86.2069	3.17E-02	2.5
26	Fe	56	6018.420	0.070	34.1379	0.00E+00	0
26	Fe	56	5920.350	0.070	33.1034	0.00E+00	0
26	Fe	56	352.360	0.010	32.7586	1.23E-02	5
26	Fe	56	4217.980	0.110	23.3448	0.00E+00	0
26	Fe	56	1725.290	0.030	21.7241	0.00E+00	0
26	Fe	56	7278.820	0.090	20.6897	0.00E+00	0
26	Fe	56	1612.780	0.020	18.5517	0.00E+00	0
26	Fe	56	692.030	0.020	16.3793	0.00E+00	0
26	Fe	56	136.520	0.020	14.1379	0.00E+00	0
26	Fe	54	9297.900	0.200	11.2567	4.21E-03	3.3
26	Fe	57	810.710	0.030	3.9840	1.49E-03	4
26	Fe	54	412.000	0.100	3.2406	0.00E+00	0
26	Fe	54	8886.400	0.900	2.0978	0.00E+00	0
26	Fe	57	1674.200	0.300	1.0624	0.00E+00	0
26	Fe	57	8369.700	0.900	0.7123	0.00E+00	0

3 *Pegase* program

3.1 Motivation

The use of high-purity semiconductor detectors allows to measure hundreds of γ rays following neutron capture and this with both high energy resolution and high detection efficiency. The analysis of these spectra must be done using automated peak fitting procedures. Next, the precise peaks energies and intensities determined by the fit program have to be compared to a standard; once again the use of an adequate software is necessary.

3.2 Description of the fit program

In the precedent section we saw that the treatment of the data can be separated in two tasks.

- Fit the data
- comparison

The first one requires an automated gamma peak fitting software; such programs exist so that it was not necessary to write a new one. I decided to use a program called GASPAN written by Friedrich Riess (riess@physik.uni-muenchen.de) available for UNIX platforms.

GASPAN can be runned quasi automatically but it was necessary to modify it in order to fulfil the required conditions from the Paul-Scherrer Institute (see Introduction); as a matter of fact it is not a difficult task to analyse gamma-ray spectra with a fit program, but it demands a certain knowledge of the specific procedure. The modifications I brought into GASPAN make that the complete fit procedure is done without any intervention from the user

3.3 *Description of* Pegase

3.3.1 Determination of the peak shape parameters

Ideally, in order do extract precise positions and surfaces for the peaks in a spectrum it is mandatory to determine the different parameters of the gaussian interpolating function (width of the gaussian shape, constant tail, polynomial and exponential tails). Among all these parameters only the first one is essential; as a matter of fact, with high-purity semiconductor devices the peak shape is very close from a gaussian function and the different parameters for the tails can be "zeroed".

The width of the peaks changes smoothly and quasi linearly across the spectrum. To determine this parameter one interpolates the width of the biggest peaks on the whole range of the spectrum.

3.3.2 Energy and efficiency calibrations

A precise energy determination is mandatory for the qualitative determination of the elemental concentration in the sample; a relative error bigger than 0.02% is enough to distort the final results. The energy calibration of the acquisition chain is calibrated frequently but even after several hours its accuracy is not acceptable any more. Consequently, the user has to determine an energy calibration for each analysis.

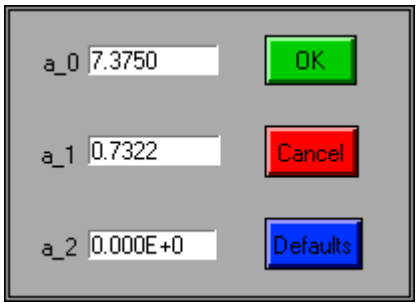

Figure 1: approximate energy calibration

The efficiency calibration of the detectors is very important for the quantitative determination of the elemental concentration. The efficiency calibration of the acquisition chain is only very slightly affected with time so as it is not necessary to determine it frequently.

3.3.3 Fit procedure

The command *Fit Step 1* will launch the MS-DOS executable GASPAN in the background. A new window is displayed on the screen showing the status and remaining time of the peak fitting procedure (see Figure 2). GASPAN firstly determines an interpolating function for the width of the gaussian fit; this is done by considering only the peaks with a big area. Next, it fits accurately the entire spectrum and extract from the result the 10 most intense peaks.

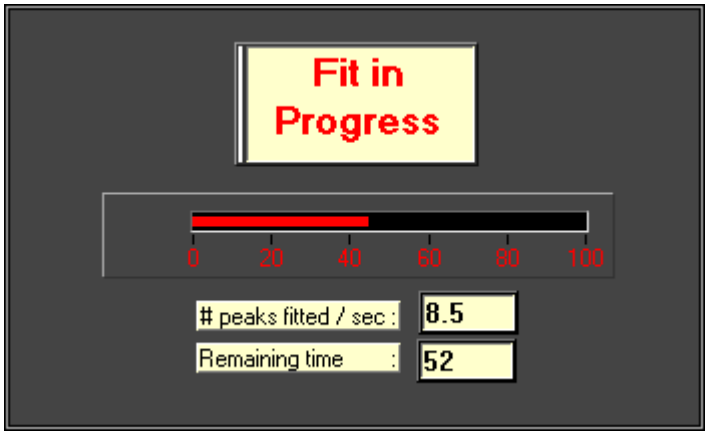

Figure 2: window displaying the fit progress

Once the fit procedure is finished, a new window appears enabling the user to perform an energy calibration. For that purpose the position in channels and approximate energy of the 10 most intense peaks are shown (see Figure 3). In most of the measurements, the user knows some of the major constituents in the sample.

By selecting an element with the appropriate box, its strongest γ-ray lines are displayed in the third column; the precise energy of lines for which a correspondence exists between column two and three are displayed in fourth column. Once at least four correspondences have been found, one can press the OK button.

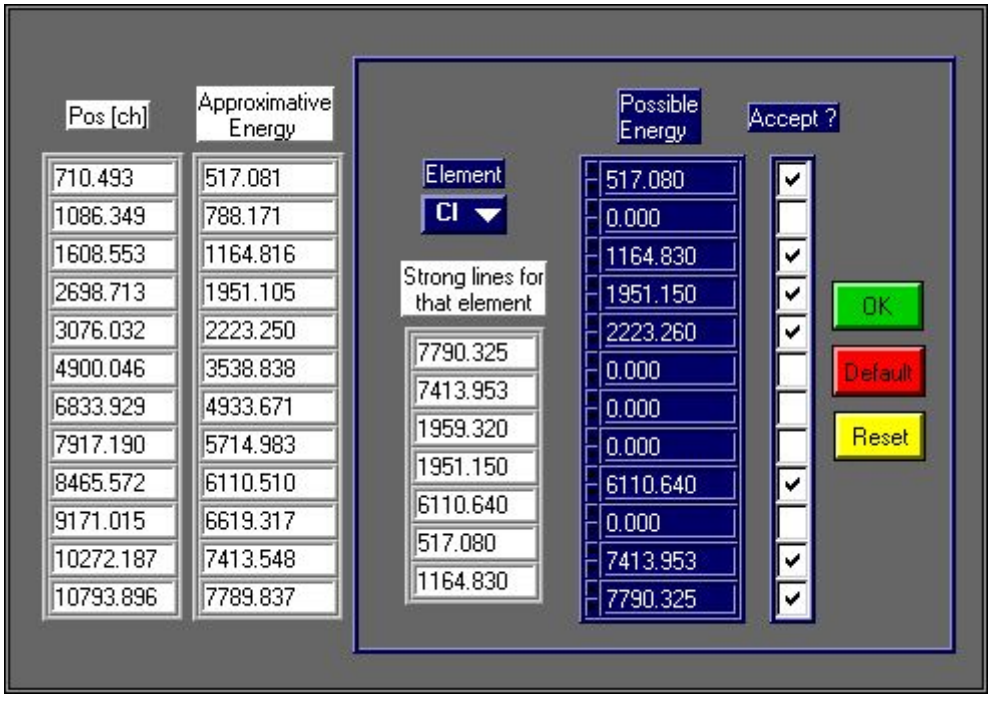

Figure 3: accurate energy calibration process

Next, a new window appears (Figure 4 or Figure 5) showing a graph with the channel position as absiss and the energy as ordinate for all the lines selected in the precedent step; a linear interpolation is done and the residue of this function to the data is displayed in the lower part of the window. If the calibration is satisfactory, one presses the OK button. In the contrary one can return to the precedent step and deselect the lines for which there is a problem (normally, most of the points in the residue graph form a trend, the points which are distant from it are those which can certainly be deleted).

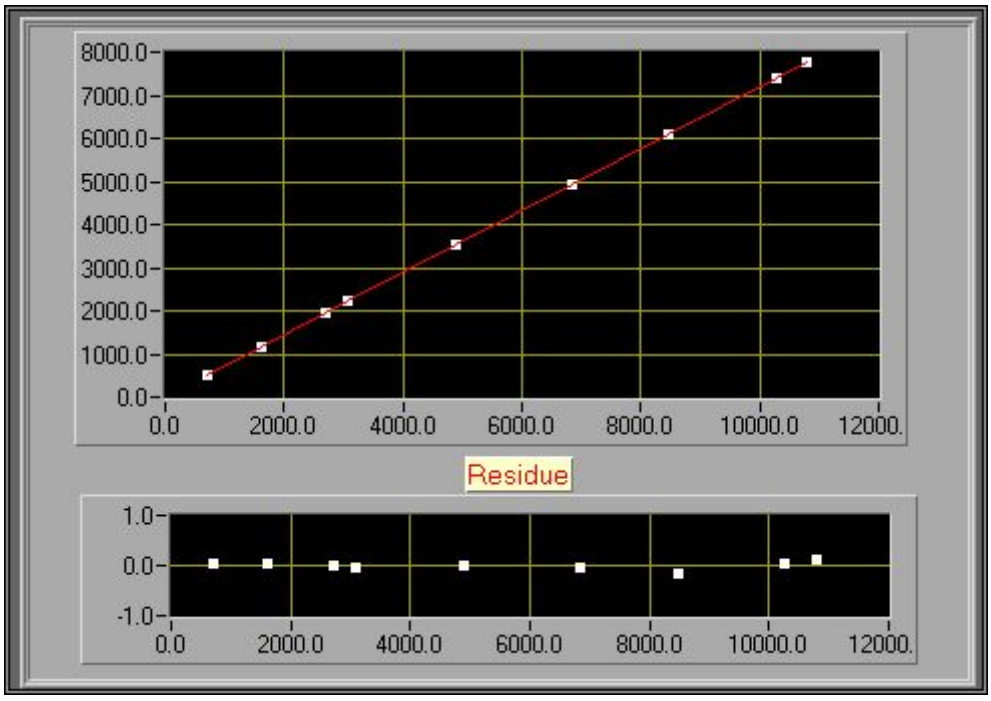

Figure 4: good energy calibration; one sees on the residue plot that the divergence with the trend for the different points is lower than 0.2

Once the energy calibration has been performed, one can launch the *Fit Step 2* procedure. Again, GASPAN is executed in the background; the result will contain the position in channel, energy, area and absolute intensity of every peak detected in the spectrum.

3.4 Description of find_peaks

The problem posed is relatively simple. We have on one side a table containing the most intense transitions γ energies for nearly all elements, and on the other side a list of γ energies resulting from the measurement of the prompt radiation issued by neutron activation of the elements in the sample. By comparing these two lists, one knows the qualitative elemental composition of the sample.

But only a crude comparison of these tables is useless; indeed with the large amount of lines in each of these two tables, the number of chance correspondences will certainly so big as true correspondences. It is consequently

necessary to compare these two tables more accurately. The Labview programming language is not appropriate to such tasks that require a great deal of data manipulation. However, it is possible to write the routine in a conventional programming language, for example *C*, compile the source code and link it to form executable code.

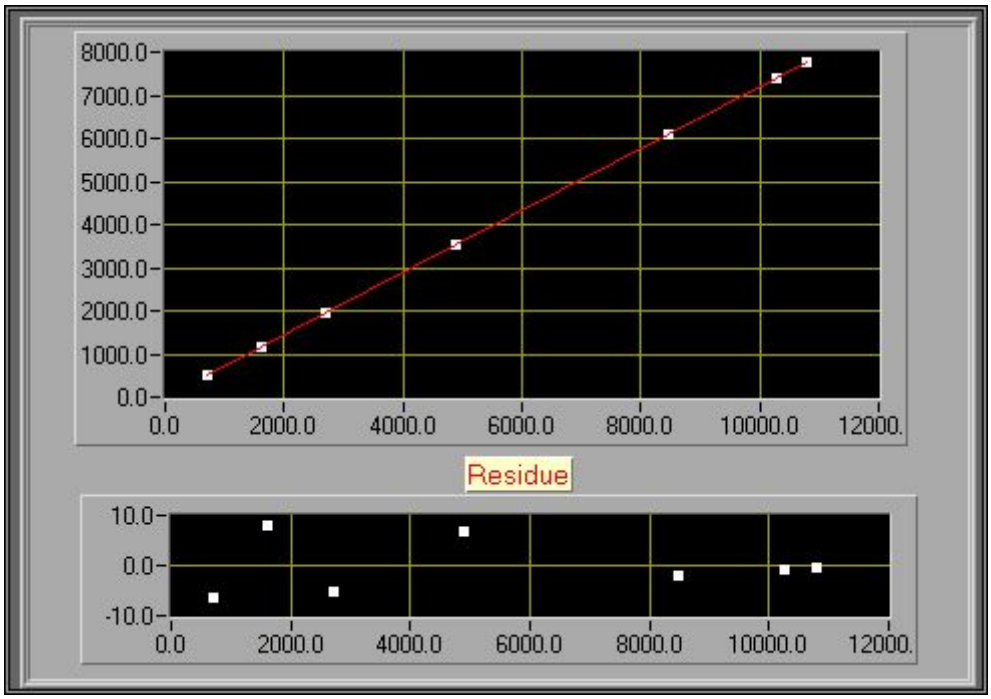

Figure 5: bad energy calibration; on the residue plot one sees that at two points do not fit with the general trend

The routine that effectuates this task is called *find_peaks* and is written in the *C* language; the next paragraphs describe this program.

3.4.1 Initialization and reading of the data

The first subroutine *Initialize* set to zero all variables; the next five subroutines, *Read_k0table*, *Read_fit_file*, *Read_data*, *Read_bck*, *Read_fit* are used to read the different files.

3.4.2 Treat_bore

The ^{10}B has a very high cross section for the (n,α) reaction. After the capture of the neutron, the newly formed nucleus is divided in an α article and a ^{7}Li nucleus. The latter is in an excited state and returns to the ground state by emitting a γ ray of 477. keV. The energy of this transition is Doppler broadened (FWHM=14 keV) due to the high speed of the ^{7}Li nucleus. Due to its particular broadened shape, this peak cannot be fitted with a gaussian function but with another adequate one.

A special treatment to this sole γ ray is motivated by the fact that the ^{10}B isotope, with his very high neutron cross-section, is one of the elements for which the PGAA installation has the highest analytical sensitivity. Consequently, several measurements are planned with the PGAA installation for which the only aim is to detect and measure accurately the quantity of Bore.

The lineshape of a Doppler broadened Lorentzian shaped gamma ray is[5]:

$$I(E) = \frac{A}{2E_0\pi\beta}\left\{\arctan\left[\frac{2}{\Gamma}\left(E - E_0\left(1-\beta\right)\right)\right] - \arctan\left[\frac{2}{\Gamma}\left(E - E_0\left(1+\beta\right)\right)\right]\right\} \quad (9)$$

where E_0 is the peak position, $\beta=v/c$ represents the recoil velocity of the emitting nucleus and Γ is a parameter describing the width of the Lorentzian. Empirically, it has been found that by elevating the parenthesis to the second power one gets a more appropriate function. The fitting function used in the program is:

$$I(E) = A\left\{\arctan\left[c\left(E - E_0\left(1-b\right)\right)\right] - \arctan\left[c\left(E - E_0\left(1+b\right)\right)\right]\right\}^2 \quad (10)$$

This function has been called a *Jolian*, the parameters *A,b,c* do not have anymore a physical signification. The least-square fit of the Jolian to the data consists to find the four parameters E_0,*A,b,c*. For that task, I implemented the subroutine *GRIDLS* and *GRADLS* found in the book of Bevington[6]. An example of the result of this fit is shown in Figure 6.

The initial value of the parameter *b* is given by:

$$b \cong \frac{FWQM}{2 \cdot E_0} \quad (11)$$

where *FWQM* is the full width at 4/15 of the maximum. The value of *FWQM* has been determined to be 14.89 keV.

Another problem with this element is that the reaction $n_{th}(^{10}B,\alpha)$ leads to the emission of a unique transition of 477.6 keV; at energies so low than 500 keV the photon absorption in the target is not anymore negligible.

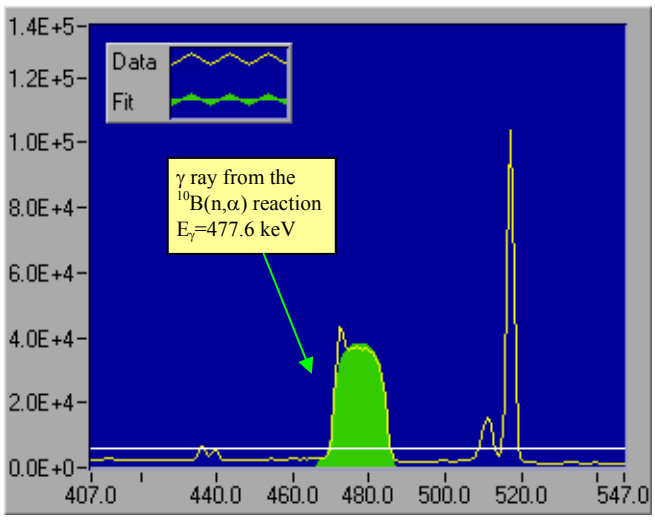

Figure 6: least-square fit to the γ ray from the $^{10}B(n,\alpha)$ reaction

3.4.3 Find_lines

This subroutine is straightforward, one simply searches for each line in the k0 table if there exists a corresponding line in the fit file. When such a correspondence exists we say that a line has been *found*. The number of lines found for each element is returned.

3.4.4 Explain_nofound_lines

A spectrum from a (n,γ) reaction is highly complicated and one can fit up to 600 peaks; but a lot of peaks cannot be detected due to the insufficient statistics, other are drowned in the background and a few are masked by bigger peaks. For a given element contained in the sample in quantity bigger than the detection limit, one cannot ensure that all of its lines in k0 table will be detected. However, by looking at the non-detected lines one can extract qualitative information.

Once at least one line as been found for a given element *E*, it is possible to deduce with the help of this *reference line* and the k0 table the theoretical area and the position in the spectrum of a non-detected peak. We compare then the theoretical intensity, hereafter written t_I, with the total counts in the region of the spectrum near the theoretical position:

1) t_I is lower than $3 \cdot \sqrt{3 \cdot backgrounds\ counts}$ meaning that the detection limit is reached
2) The intensity above the background is bigger than t_I
3) The intensity above the background is 3 times lower than t_I
4) The intensity above the background is situated between $t_I/3$ and t_I.

In cases 1. and 4. one cannot exclude the presence of that line in the spectrum. In case 2. there is an appreciate probability that the line is in the spectrum and we say that it is masked. The implications for the case 3. are more important. Indeed, according to its theoretical intensity, the peak should have been detected and fitted; the only possible reason why t_I is false results from the wrong indication of the *reference line* in the sense that this *reference line* is not correlated to the element *E*. In this case, the information given by the non-detected peak allows to exclude the presence of the element E in the sample[a]. In the interactive analysis (see Section 3.4.8) the line will be labelled as *excluded.*

A crude calculation for the probability to find at least *k* chance peaks[b] for a given element gives P[*k*=1] = 90% and P[*k*=2] = 62%. This points out the necessity to look at *non-found lines* in order to separate chance and true correlations.

(We have seen that the qualitative information deduced from the absence of peaks are of a great importance as one is interested to know not only which elements make up the sample but also the elements which are not)

[a] the word *exclude* used in this report significates that the element in question can be present in the sample, but in quantity less than its detection limit
[b] this calculation has been done for a very complicated spectrum

3.4.5 Summary_results

In this subroutine the results obtained are summarized and written to output files: find_peaks.out and find_peaks.tmp. The file find_peaks.out is intended for debugging only; the other file contains informations that will be passed to the Labview code.

The mass is computed with the use of equation (8).

3.4.6 Create_found_spectrum

The idea in this subroutine is to reconstruct the shape of the different peaks of the spectrum for which a correlation in the k0_table has been found. The surface of one peak for a given element is derived from the average computed element mass and the systems efficiency calibration.

With that tool, it is possible to watch if the reconstructed shape of the peaks for a given element fits to their measured surface; in the contrary one has to exclude the peaks in question in order not to bias the calculation of the average mass.

3.4.7 Show_peaks

The fit program gives for each fitted peak its maximum intensity; this subroutine makes that this data can be displayed in the Labview program.

3.4.8 Interactive Analysis

The straightforward analysis is done by the *find_peaks* routine. Afterwards it is necessary to disentangle these results by doing an interactive analysis.

The command *Analysis* display a new window and executes the routines *find_peaks*; once the execution is finished one can begin the interactive analysis. The list of elements for which lines have been found in the spectrum is divided in two, depending on whether they contains:

- at least one line that is excluded (see definition in Section 3.4.4)[c],
- no line is excluded.

One or the other of these lists can be selected with the button (1) (the numbers between parenthesis refer to those on yellow background in Figure 7). The different elements are selected with the control (2); the lines pertaining to the element selected appear in the table (3).

[c] One has to keep in mind that the results given by the automatic analysis must be checked by *the human eye*; in other words, the user has to control both excluded and non excluded lists.

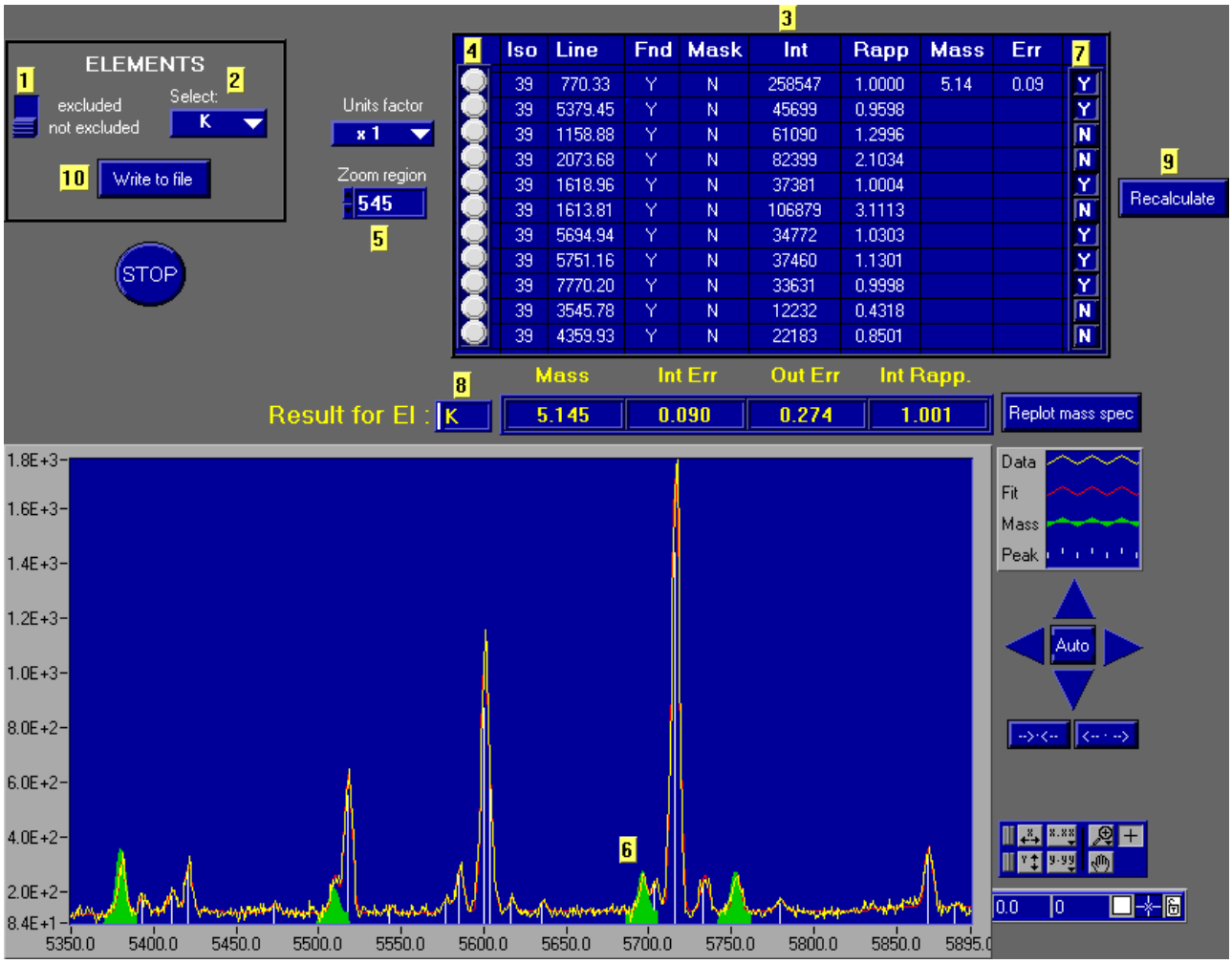

Figure 7: interactive analysis

- **Iso**: atomic mass
- **Line**: energy of the γ ray
- **Fnd**: has the γ ray been found in the spectrum
    - o **Y**: Yes
    - o **N**: No
    - o **Exc**: Excluded, meaning that for the mass computed, the line should be present in the spectrum
- **Mask**: the γ ray in the spectrum is masked by an other relatively strong γ ray
    - o **Y**: Yes
    - o **N**: No
    - o **MB**: Maybe
    - o **DL**: Detection Limit
- **Int**: γ-ray intensity in the spectrum
- **Rapp**: calculated mass for each line normalized to the first line in the table (so the first number in this column is always 1.000)
- **Mass**: calculated mass for each line
- **Err**: error of the precedent number

The user has to appreciate by himself if it is reasonable to keep each line; he is helped in that task by the display of the *computed area* (See Section 3.4.6) draw in green on the spectrum. One zooms on the particular lines in the table by clicking on the button (4); the zoom area can be modified with the control (5). In the centre of the graph lays the zoomed peak (6). If the *computed area* defines relatively well the peak shape, the line in question can be accepted. A line is excluded with a click on the button (7). The computed mass and the internal and external errors on this value are displayed (8). When one excludes one or more peaks from the list, it is useful too recalculate theses values by clicking on the button (9).

Once the treatment for an element is completed, one presses the button (10) to copy the results in the [filename]_report.txt file.

4 References

[1] J.R.D. Copley and C.A. Stone, Nucl. Instrum. Meth. **A281**, 593, (1989).

[2] E.A. Mackey, G.E. Gordon, R.M. Lindstrom and D.L. Anderson, Anal. Chem **63**, 288, (1991).

[3] R.M. Lindstrom and C. Yonezawa, in Prompt Gamma Activation Analysis with Guided Neutron Beams. In Z.B. Alfassi and C. Chung, editors, Prompt Gamma Neutron Activation Analysis, Boca Raton, 1995.

[4] G.L. Molnár, Zs. Révay, R.L. Paul and R.M. Lindstrom, J. Radioanal. Chem, **234**, (1998), 21.

[5] J. Jolie, H.G. Börner, F. Hoyler, S.J. Robinson, M.S. Dewey, Inst. of Phys. Conf. Ser. No88 (1988) pp S586.

[6] P.R. Bevington, *Data Reduction and Error Analysis for the Physical Sciences*, McGraw-Hill Book Company, New York, 1969.

Curriculum Vitae

Name	Genilloud
Forename	Laurent
Date and place of birth	19th September 1972, Fribourg (Switzerland)
Originating from	Villarepos (Fr)
Nationality	Swiss
Civil status	Married

Education

1979-1985 : Primary school in Romont (FR)

1985-1988 : Secondary school at Cycle d'Orientation de Romont (FR)

1988-1989: First year of Maturity at Cycle d'Orientation de Romont (FR)

1989-1992: 2nd to 4th year of Maturity at Collège St-Michel de Fribourg

1992-1997: Diploma in experimental physics at Univesité de Fribourg

1997-2000: Assistant/PhD. student in the Physics Institute of Université de Fribourg.

List of publications

Study of the vibrational nucleus ^{100}Ru by the ^{98}Mo(α,2n) and ^{99}Ru(n,γ) reactions
L. Genilloud, H.G Börner,F, Corminboeuf, Ch. Doll, S. Drissi, M. Jentschel, J. Jolie, J. Kern, H. Lehmann, and N. Warr, Nuclear Physics A662 (2000) 3; Erratum A669 (2000) 407;

Lifetimes of negative parity states in ^{168}Er
L. Genilloud, J. Jolie, H.G. Börner, H. Lehmann, F. Becvár, M. Krticka, N.V. Zamfir, R.F. Casten, Physical Review C62 (2000) 034313.

Study of the double-γ vibration in ^{164}Dy using cold neutron capture
F. Corminboeuf, L. Genilloud, J. Jolie, J. Kern and J.-L. Schenker, in Proceedings of the 10th Int. Symp. On Capture Gamma-Ray Spectroscopy and Related Topics, Editor Stephen Wender, 603 (2000).

Lifetime measurements of three-phonon states in ^{110}Cd
F.Corminboeuf, T.B. Brown, L. Genilloud, J. Jolie, J. Kern,C. D. Hannant, N. Warr, and S.W. Yates, in Proceedings of the 10th Int. Symp. On Capture Gamma-Ray Spectroscopy and Related Topics, Editor Stephen Wender, 606 (2000).

Collectivity of the ''three-phonon'' region in 100Ru
L. Genilloud, T.B. Brown, F. Corminboeuf, P.E. Garrett, C.D. Hannant, J. Jolie, J. Kern, N. Warr, and S.W. Yates, in Proceedings of the 10th Int. Symp. On Capture Gamma-Ray Spectroscopy and Related Topics, Editor Stephen Wender, 651 (2000).

Study of octupole vibration in ^{168}Er
L. Genilloud, J. Jolie, H.G. Börner, H. Lehmann, F. Becvár, M. Krticka, N.V. Zamfir and R.F. Casten, in Proceedings of the 10th Int. Symp. On Capture Gamma-Ray Spectroscopy and Related Topics, Editor Stephen Wender, 654 (2000).

SCODA, acquisition system of coincidence data for capture
γ-ray studies, N. Warr, L. Genilloud, J.-L. Schenker, , in Proceedings of the 10th Int. Symp. On Capture Gamma-Ray Spectroscopy and Related Topics, Editor Stephen Wender, 740 (2000).

Characterization of three-phonon states in ^{110}Cd
F.Corminboeuf, T.B. Brown, L. Genilloud, C.D. Hannant, J. Jolie, J. Kern, N. Warr, S.W. Yates, Physical Review Letters 84 (2000) 4060.

Characterization of the ‘‘three-phonon’’ region of ^{100}Ru
L. Genilloud, F. Corminboeuf, J. Jolie, T.B. Brown, C.D. Hannant, N. Warr, S.W. Yates, and P.E. Garrett, accepted for publication in Nuclear Physics A.

Structures and lifetimes of states in ^{110}Cd
F. Corminboeuf, T.B. Brown, L. Genilloud, C.D. Hannant, J. Jolie, J. Kern, N. Warr and S.W. Yates, submitted to Physical Review C.

Nuclear structure of ^{196}Au - more evidence on its superymmetric structure
J. Gröger, J. Jolie, R. Kru¨cken, C.W. Beausang, M. Caprio, R.F. Casten,,J. Cederkall, J.R. Cooper, F. Corminboeuf, L. Genilloud, G. Graw, C. Günther, M. de Huu, A.I. Levon, A. Metz, J.R. Novak, N. Warr, T. Wendel, Submitted to Physical Review C

Remerciements

En tout premier lieu, je tiens à remercier mes parents qui m'ont donné les ressources morales et financières me permettant de mener à bien toutes mes études.

Un très grand merci va tout naturellement à mon directeur de thèse, le Prof. Jan Jolie, qui par ses compétences, disponibilité, enthousiasme et inépuisable optimisme à été un véritable moteur durant tout mon travail de thèse.

Aux anciens et actuels membres du groupe PAN, je dis merci pour l'aide qu'ils m'ont apportée et pour la bonne ambiance de travail qu'ils ont participé à créer.

Je remercie aussi mon épouse, Catherine, pour son soutien dans mon travail et sa patience lors des expériences qui se sont déroulées à l'extérieur de l'Université.

Je tiens aussi à remercier les chercheurs de l'Institut Laue-Langevin et de l'Université de Kentucky qui ont travaillé sans compter pour mener à bien les expériences.

En dernier lieu, je salue la mémoire du Prof. Jean Kern, grand physicien et grand homme qui à laissé un grand espace non comblé dans le groupe PAN qu'il avait créé. Par son travail, ses pertinentes et nombreuses explications, son humour, il m'a vraiment aidé. Merci.